Reviews in Mineralogy & Geochemistry
Vol. 89 pp. 401-451, 2023

The Lunar Cratering Chronology

H. Hiesinger[1], C.H. van der Bogert[1], G. Michael[2], N. Schmedemann[1], W. Iqbal[1], S.J. Robbins[3], B. Ivanov[4], J.-P. Williams[5], M. Zanetti[6], J. Plescia[7], L. R. Ostrach[8], J.W. Head III[9]

[1]Institut für Planetologie, Westfälische Wilhelms-Universität, Wilhelm-Klemm-Str. 10, 48149 Münster, Germany
[2]Institute of Geological Sciences, Planetary Sciences and Remote Sensing, Freie Universität Berlin, Berlin, Germany
[3]Southwest Research Institute, 1050 Walnut St., Suite 300, Boulder, CO 80302, USA
[4]Institute for Dynamics of Geospheres, Russian Academy of Sciences, Moscow, Russia
[5]Department of Earth, Planetary and Space Sciences, University of California, Los Angeles, CA 90095, USA
[6]Marshall Space Flight Center, Huntsville, Alabama, USA
[7]Johns Hopkins University Applied Physics Laboratory, Laurel, Maryland, USA
[8]U.S. Geological Survey, Astrogeology Science Center, 2255 N. Gemini Dr., Flagstaff, Arizona 86001, USA
[9]Department of Earth, Environmental and Planetary Sciences, Brown University, Providence, Rhode Island, USA

hiesinger@uni-muenster.de; vanderbogert@uni-muenster.de

1. INTRODUCTION

The Moon is a unique body in our Solar System that allows us to groundtruth remote-sensing data (e.g., crater size–frequency distributions, or CSFDs, crater/rock degradation rates, mineralogy, composition) of the Apollo and Luna landing sites with well-characterized samples that have been investigated and dated in terrestrial laboratories (e.g., Hartmann 1966; Greeley and Gault 1970; Papanastassiou and Wasserburg 1971; Soderblom 1972; Husain 1974; Nunes et al. 1974; Schaefer and Husain 1974; Tera and Wasserburg 1974; Tera et al. 1974; Neukum et al. 1975a,b; Boyce 1976; Neukum and Horn 1976; McGill 1977; Neukum 1977a,b; Boyce and Johnson 1978; Maurer et al. 1978; Guggisberg et al. 1979; Ryder and Spudis 1980; BVSP 1981; Taylor et al. 1983; Dasch et al. 1987; Wilhelms et al. 1987; Nyquist and Shih 1992; Neukum and Ivanov 1994; Hiesinger et al. 2000, 2003, 2010, 2011, 2012a,b; Lucey et al. 2000; Nyquist et al. 2001; Gaffney et al. 2008; Haruyama et al. 2009; Marchi et al. 2009; Morota et al. 2009; Ghent et al. 2014; Robbins 2014; Trang et al. 2015; Sato et al. 2017). Calibrations between landing site remote-sensing observations and samples enables us to extrapolate age determinations and compositional analyses to any area on the Moon using remote-sensing data.

One fundamentally important calibration allowed the derivation of the lunar chronology function that links the cumulative CSFD at a reference diameter with the radiometric and exposure ages of lunar samples (e.g., Hartmann 1970a,b; Neukum 1983; Neukum et al. 2001; Stöffler et al. 2006; Robbins 2014). The lunar chronology function is critical for the understanding of at least the inner Solar System, because it is extrapolated to provide not only ages of unsampled regions on the Moon but also of other planetary bodies. Although we have samples from Mars (SNC meteorites) and asteroid Vesta (HED meteorites), we do not know their exact provenance, making it impossible to link their radiometric ages with CSFDs, and thus directly derive chronology functions for these bodies. Consequently, it is fundamental to correctly interpret the available

1529-6466/23/0089-0010$05.00 (print)
1943-2666/23/0089-0010$05.00 (online)
http://dx.doi.org/10.2138/rmg.2023.89.10

lunar samples, their provenances, and their radiometric and exposure ages; as well as the CSFD measurements from the sites from which these samples were collected.

Many lunar missions in the last decade (e.g., Chandrayaan-2, SELENE, Lunar Reconnaissance Orbiter, Chang'E series) carried/carry high-resolution digital cameras with the goal to globally image the Moon, meaning that the database for CSFD measurements has continuously improved. Today global imaging coverage exists at 100 m/pixel for different illumination conditions, and there is widespread coverage down to ~0.5 m/pixel scales (e.g., Robinson et al. 2010), allowing for measurement of highly precise crater statistics at multiple scales and detailed studies of the cratering process (see also Cohen et al. 2023; Osinski et al. 2023, both this volume).

This chapter provides an introduction to CSFD measurements and presents a review of the work performed on dating lunar geological units using CSFDs since the last *New Views of the Moon* volume (2006), including various volcanic and tectonic features, as well as individual impact craters. At the end of the chapter, implications for the new CSFD age determinations for the geologic history and evolution of the Moon are discussed.

2. CRATER SIZE-FREQUENCY DISTRIBUTION MEASUREMENTS

2.1. Historic perspective

Detailed investigations of the lunar surface led to the definition of time-stratigraphic systems, i.e., the pre-Nectarian, Nectarian, Imbrian, Eratosthenian, and Copernican System (e.g., Neukum 1983; Wilhelms et al. 1987; Neukum et al. 2001; Stöffler and Ryder 2001). For example, using the ejecta deposits of impact craters as stratigraphic marker horizons similar to volcanic ash (bentonite) beds on Earth coupled with the relative spatial density of craters on different surfaces, Wilhelms et al. (1987) constructed a moonwide relative stratigraphy by investigating the superposition of ejecta deposits. Application of the superposition approach to mare basalt units (e.g., Head 1976; Whitford-Stark 1979; Whitford-Stark and Head 1980) provided relative ages for the entire lunar surface. The determination of relative ages is one of the most important tools in geologic mapping and the interpretation of geologic processes on the Moon. For example, bright rays and topographic freshness were used as criteria to assign a Copernican age to craters (e.g., Wilhelms 1987). On the basis of their CSFD measurements on bright ray craters, Werner and Medvedev (2010) proposed that the transition between the Eratosthenian and the Copernican systems occurred 750 Ma ago. In addition, bright ray craters were also used to study the cratering rate in the last few hundred million years (Grier et al. 1999). On the basis of Clementine maturity maps, Grier et al. (1999) determined relative ages of rayed craters and concluded that there is no evidence for a change in the cratering rate since Tycho (~109 Ma; Grier et al. 1999) compared to the cratering rate since Copernicus (~810 Ma; Grier et al. 1999). However, Hawke et al. (2004) demonstrated that bright rays can be due to differences in maturity (e.g., Messier), composition (e.g., Lichtenberg), or a combination of both (e.g., Tycho, Olbers A).

Several techniques have been developed to quantitatively extract temporal information from impact craters, including crater degradation and CSFDs. Crater degradation was used to infer relative and absolute ages of geologic units on the Moon (e.g., Pohn and Offield 1970; Trask 1971; Soderblom and Lebofsky 1972; Boyce and Dial 1975; Head 1975; Boyce and Johnson 1978; Fassett 2013; Fassett and Thomson 2014; Ghent et al. 2014; Trang et al. 2015; Basilevsky et al. 2018; Fassett et al. 2018). Data derived from crater degradation stages can give model ages for the lunar surface, but numerous endogenic and exogenic processes can influence the appearance of lunar impact craters, decreasing the certainty of age assignments from that method. In addition, there are some discrepancies between crater degradation-based ages and radiometric ages for specific landing sites. Burgess and Turner (1998), for example,

reported young radiometric ^{40}Ar–^{39}Ar ages (3.2–3.3 Ga) for the Luna 24 landing site, which disagree with ages derived from crater degradation measurements (3.5 ± 0.1 Ga) by Boyce and Johnson (1978). Thus, Burgess and Turner (1998) concluded that crater degradation ages of the Luna 24 landing site have to be reassessed.

Because impact cratering is to a first-order a spatially random process, the number and size of superposed craters on a given geologic unit/surface is directly related to the geologic time since the formation of this surface (e.g., Öpik 1960; Shoemaker 1962; Baldwin 1964; Neukum and Ivanov 1994; Hiesinger et al. 2000, 2003, 2010; Hartmann and Neukum 2001; Ivanov 2001; Neukum et al. 2001; Stöffler and Ryder 2001; Stöffler et al. 2006). Öpik (1960) was among the first to pioneer dating of planetary surfaces with crater spatial densities, yielding relative ages of surface units. After the Apollo and Luna samples became available and were isotopically dated, Hartmann (1970b) linked them with crater spatial densities to derive a lunar chronology that yields absolute model ages (AMAs) of the studied units. Other early studies of the link between isotopic ages and crater spatial densities include those by Hartmann (1970a,b), Baldwin (1971), and Bloch et al. (1971), Neukum and Wilhelms (1972), Neukum et al. (1972, 1975b), and Soderblom and Boyce (1972). Extrapolating the terrestrial cratering record to the Moon, Hartmann (1965) successfully predicted that lunar mare regions should be approximately 3.6 Ga old. This prediction was later confirmed by radiometric ages of the lunar samples. Thus, these studies allowed for the first time the investigation of the geologic evolution of a planetary body with absolute, rather than just relative, time (Werner and Ivanov 2015).

2.1.1. CSFD measurement method. CSFD measurements for the estimation of surface ages involves several parts: (1) measurement of craters in a homogeneous (e.g., morphology, albedo, topography, spectra) region of interest, (2) fitting of the distribution to a production function (PF) to determine a crater spatial density for a reference crater diameter, and (3) solving a chronology function with the reference crater spatial density to get an absolute model age. Detailed descriptions of this technique can be found, for example, in Neukum and Ivanov (1994), Hiesinger et al. (2000, 2003, 2010), Hartmann and Neukum (2001), Ivanov (2001), Neukum et al. (2001), Stöffler and Ryder (2001), Stöffler et al. (2006), Werner and Ivanov (2015), and Robbins et al. (2018).

2.1.2. Measurement of craters. To obtain the age of a photogeologically homogeneous unit, one has to (1) measure the surface area of the unit, and (2) measure the diameters of each primary impact crater within this unit. Traditionally, obtained crater diameters were binned and plotted, for example, as cumulative distributions (e.g., Crater Analysis Techniques Working Group 1979), which give the number of craters larger than or equal to a certain diameter per area measured. Today, computational capabilities allow for an un-binned treatment of crater spatial densities to avoid potential artifacts introduced by data binning (e.g., Michael et al. 2016; Robbins et al. 2018).

2.1.3. Factors affecting CSFDs. Several factors that affect CSFD measurements must be taken into account when deriving absolute model ages (AMAs). These factors can be divided into two different categories: (1) method-specific factors, including image quality, illumination geometry, count area size, and variability of crater detection among researchers, and (2) geology-specific factors, such as an asymmetrical impact rate (e.g., Morota and Furumota 2003; Gallant and Gladman 2006; Gallant et al. 2009; Ito and Malhotra 2010; Werner and Medvedev 2010; Kawamura et al. 2011; Le Feuvre and Wieczorek 2011; Werner and Ivanov 2015), geology-based count area selection (e.g., Hiesinger et al. 2000, 2003, 2011), regional and local slopes (e.g., Basilevsky 1976; Meyer et al. 2016), crater degradation effects (e.g., Soderblom 1970; Schultz et al. 1977; Basilevsky et al. 2014; Fassett and Thomson 2014; Basilevsky 2015; Yasui et al. 2015; Xie et al. 2017; Mahanti et al. 2018; van der Bogert et al. 2018b), layering (e.g., Wünnemann et al. 2012), gravity/strength-scaling effects (e.g., Young 1975; Melosh 1989; Ivanov 2006; Dundas et al. 2010; van der Bogert et al. 2017),

and the occurrence of endogenic, secondary, and/or self-secondary craters (e.g., Shoemaker 1962; König 1977; Neukum 1983; Bierhaus et al. 2005, 2018; Hartmann 2005; McEwen et al. 2005; Malin et al. 2006; McEwen and Bierhaus 2006; Neukum et al. 2006; Werner 2006; Hartmann et al. 2008; Wagner et al. 2010; Speyerer et al. 2016; van der Bogert et al. 2016).

2.1.4. Production function. The CSFD of an area of interest is fit with a lunar production function (PF) to determine the crater density at a given reference diameter, usually 1 or 10 km (e.g., Neukum 1983; Neukum et al. 2001; Ivanov and Hartmann 2007). The PF is a model, either empirical or from first principles, that represents the shape of the CSFD for primary craters. The match or mismatch of a measured CSFD to the shape of the PF gives one test of the quality of the CSFD measurement. The crater spatial density of a geologic unit is directly related to the time the unit was exposed to the meteoroid flux and therefore gives a relative age of this unit. The PF is often assumed to be constant in space and time, although work has been done to understand and correct for a potential asymmetrical impact rate due to the lunar orbit (e.g., Le Feuvre and Wieczorek 2011 and references therein) or temporal changes (Orgel et al. 2018). Linking the CSFD at the lunar sample return landing sites at the selected reference diameter with radiometric and exposure ages of the samples enables derivation of an empirical chronology function (CF) (e.g., Hartmann 1970a,b; Neukum 1983; Neukum and Ivanov 1994; Neukum et al. 2001; Robbins 2014). Once this function is derived, it is possible to estimate AMAs across the entire lunar surface.

A crucial prerequisite for the development of the lunar chronology is a solid understanding of the size–frequency distribution (SFD) of primary impact craters or PF on the Moon (Fig. 1), which describes the expected crater size–frequency measured on a geologic unit at a specific time. Ideally, such a distribution is determined from large, homogeneous surfaces that have not been disturbed by any subsequent geologic process since their formation. However, the derivation of the true crater size distribution is not trivial, because the measurements might be affected by differential crater degradation, resurfacing, secondary craters, target properties, variable impact velocities, impactor properties, as well as inaccurate mapping and crater counting (Robbins 2014; Werner and Ivanov 2015). Due to these complications, several PFs have been developed over the years. For example, Hartmann (1969, 1970a), Neukum et al. (1975a,b), and Neukum (1983) proposed early versions of the PF and these have been summarized by Hartmann et al. (1981). Early results suggested that the PF of lunar craters could be described as power laws of various slopes (e.g., Shoemaker et al. 1970; Baldwin 1971; Hartmann 1971; Hartmann et al. 1981). However, these power laws only worked for specific crater sizes, but not the entire range of crater diameters. Today, the most commonly used PFs are those of Hartmann (1999, 2005) (HPF) and Neukum et al. (2001) (NPF). Thus, we will focus on these two PFs.

2.1.5. Hartmann Production Function (HPF). Hartmann (1999) shows his PF in a log-incremental representation with a $\sqrt{2}$ diameter bin size. To fit the observed crater distribution, Hartmann (1999) applied power laws to three diameter intervals:

$$\log N_{\mathrm{H}} = -2.198 - 2.20 \log D_{\mathrm{L}} \quad \text{for } D_{\mathrm{L}} > 64 \text{ km}$$

$$\log N_{\mathrm{H}} = -2.920 - 1.80 \log D_{\mathrm{L}} \quad \text{for } 1.41 < D_{\mathrm{L}} < 64 \text{ km}$$

$$\log N_{\mathrm{H}} = -2.616 - 3.82 \log D_{\mathrm{L}} \quad \text{for } 0.3 < D_{\mathrm{L}} < 1.41 \text{ km}$$

The physical reasoning behind three power laws comes from collisional physics, where collisions tend to produce fragments with an SFD described by a power law. For the derivation of these power laws for mare units, Hartmann (1999) used the crater catalogs of Arthur (1963) and Arthur et al. (1965a,b, 1966), which includes craters larger than 4 km. Hartmann (1984) proposed that the observed CSFD on such mare units reaches equilibrium for craters of about

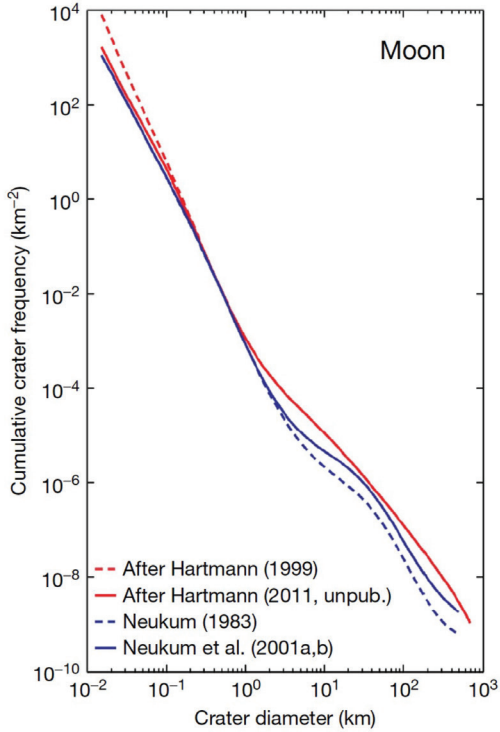

Figure 1. Four different model production functions (Werner and Ivanov 2015).

300 m and smaller, i.e., that any newly formed crater will destroy older craters. According to this PF, the average age of mare units is on the order of 3.4–3.5 Ga (Hartmann and Neukum 2001; Hartmann 2005).

2.1.6. Neukum Production Function (NPF). In several publications, Neukum showed that lunar crater distributions measured on geologic units of different ages and in overlapping crater diameter ranges could be aligned along a complex continuous curve (e.g., Neukum 1983; Neukum and Ivanov 1994; Neukum et al. 2001). The lunar NPF is given by an 11th degree polynomial

$$\log(N_{\text{cum}}) = a_0 + \sum_{k=1}^{11} a_k (\log D)^k \tag{1}$$

where a_0 represents the amount of time during which the unit has been exposed to meteoroid bombardment (Neukum 1983; Neukum and Ivanov 1994; Neukum et al. 2001). N is the number of craters larger or equal to D per square kilometer per billion years. The polynomial representation is mathematical, rather than based on physical principals. Compared to the PF of Neukum (1983), Neukum et al. (2001) slightly reworked their PF for craters <200 km in diameter. This resulted in a new set of coefficients k for equation (1), which are given in Table 1. Because the NPF is a large-degree polynomial function, its validity is constrained to the diameter range of 0.01 km < D < 300 km (Neukum 1983) and to 0.1 km < D < 100 km (Neukum et al. 2001).

Table 1. Coefficients of the lunar production function as defined by Neukum (1983) and Neukum et al. (2001).

a_n	Neukum (1983)	Neukum et al. (2001)
a_0	−3.0768	−3.0876
a_1	−3.6269	−3.557528
a_2	+0.4366	+0.781027
a_3	+0.7935	+1.021521
a_4	+0.0865	−0.156012
a_5	−0.2649	−0.444058
a_6	−0.0664	+0.019977
a_7	+0.0379	−0.086850
a_8	+0.0106	−0.005874
a_9	−0.0022	−0.006809
a_{10}	-5.18×10^{-4}	$+8.25 \times 10^{-4}$
a_{11}	$+3.97 \times 10^{-5}$	$+5.54 \times 10^{-5}$

2.1.7. Discussion of production functions. The overall shapes of the HPF and the NPF are rather similar, although they differ significantly for craters of 1–2 km to 25 km (e.g., Ivanov 2001; Neukum et al. 2001; Werner and Ivanov 2015). Both assume that the SFDs of incoming projectiles remained the same for the last 4 Ga, a view that has been challenged by several authors (Strom and Neukum 1988; Strom et al. 1992, 2005; Bottke et al. 2007; Head et al. 2010; Fassett et al. 2012; Marchi et al. 2012; Morbidelli et al. 2012a,b). Among others, Strom et al. (1992, 2005) proposed that the PF after the emplacement of the lunar mare is different from the PF before 3.8 Ga during the Late Heavy Bombardment, which led them to propose that two separate populations of impactors must be responsible for lunar cratering. However, there is no agreement among these authors concerning the exact timing of this transition. Head et al. (2010) proposed that the transition occurred during the Imbrian System at less than 3.9 Ga, close to the Orientale basin event. In contrast to that study, Fassett et al. (2012) argued for a transition between two impact crater populations before the mid-Nectarian period, before the end of the period of rapid cratering and before the putative lunar cataclysm.

In addition, there appears to be no agreement concerning the number of identified populations. For example, Marchi et al. (2012) suggested a third population, which is different from the early highland-cratering population and the later mare-cratering population. This third population might have been the result of very fast impactors that impacted the Moon at twice the velocity of impactors in the early population. The source of these fast projectiles might have been the ancient E-belt at the inner margin of the asteroid belt postulated by Bottke et al. (2012) and Morbidelli et al. (2012b). This is another inconsistency among the proponents of several impactor populations because Strom et al. (2005), Head et al. (2010), and Fassett et al. (2012) concluded that the Late Heavy Bombardment came from the entire Main Asteroid Belt and not just a specific region, although Ćuk et al. (2010) argued that the Main Asteroid Belt cannot be the source for lunar cataclysm impactors. Provided the lunar PFs did not change with time, this implies that the Moon was bombarded with only one impactor population or several populations that shared the same SFD, whereas a time-variable PF indicates that more than one impactor population is responsible for lunar craters (e.g., O'Brien and Greenberg 2003). Collisional evolution tends to yield similar SFDs with time and, thus, could explain multiple impactor populations with the same SFD (Bottke et al. 2005). For example, investigating impact craters on Mercury larger than 20 km, Neukum and Ivanov (1994) found a striking similarity in the characteristics of the SFDs of both planetary bodies.

Thus, if we assume $D_{Mercury} = 1.6 \times D_{Moon}$ (Neukum and Ivanov 1994), the Moon and Mercury share the same mass–velocity distribution of crater-producing projectiles. Recent dynamical models of the evolution of small Solar System bodies suggest that the velocities and SFDs of projectiles might have varied during the first billion years (e.g., Bottke et al. 2012; Morbidelli et al. 2012b), supporting the hypothesis of more than one impactor population. However, on the basis of an investigation of crater populations of 30 lunar basins (≥ 300 km) with buffered non-sparseness corrected CSFD measurements, Orgel et al. (2018) found that contrary to previous studies (e.g., Strom et al. 1992, 2005; Head et al. 2010; Fassett et al. 2012), the shapes of Pre-Nectarian (including SPA), Nectarian (including Nectaris), and Imbrian (including Imbrium) basins show no statistically significant differences. Thus, on the basis of that study, there is no evidence for changes in the impactor population (Orgel et al. 2018), although it cannot be excluded that there might be multiple populations with the same SFD.

2.2. Saturation equilibrium

Any given inactive surface exposed to meteoroid bombardment accumulates an increasingly large number of craters with time until a point when newly formed craters destroy an equal number of preexisting craters (e.g., Shoemaker 1965; Gault 1970; Woronow 1977; Woronow et al. 1982; Hartmann 1984; Richardson 2009; Hirabayashi et al. 2017). In this case, the crater density reaches an upper limit, known as saturation equilibrium (SEQ). The slope of a CSFD in equilibrium is typically less than that for a CSFD exhibiting crater production (consistent with the PF). Though the specifics of SEQ have been debated, many studies note that SEQ is present in crater populations with relative crater spatial density or R values between 0.1 and 0.3, or 1–10% of a condition called geometric saturation, wherein craters are hexagonally close-packed (Gault 1970; Hartmann 1984; Chapman and McKinnon 1986; Hartmann and Gaskell 1997; Richardson 2009; Kirchoff 2018). Povilaitis et al. (2018) produced maps that show regions of the Moon with $R \geq 0.3$ (>10% geometric saturation or N_{gs}) for several diameter bins. These areas represent candidates for SFDs that may be in SEQ, which are particularly useful for evaluating the ancient cratering history of the Moon (e.g., Xiao and Werner 2015), because older surfaces are expected to exhibit SEQ up to larger crater diameters. This analysis does not preclude other areas with lower relative crater spatial densities from also exhibiting SEQ, for example those exhibiting 1% N_{gs} identified by Xiao and Werner (2015).

A CSFD exhibiting an equilibrium condition cannot be fit with a PF. However, SEQ occurs at different times for craters of different diameters, i.e., smaller craters reach the SEQ state more quickly than larger craters, due to the steeper slopes of a PF versus a population in equilibrium. Thus, if a sufficiently large count area is available, it might be possible to derive an AMA on the basis of larger craters, while smaller craters are in SEQ and do not provide temporal information. The ability to fit ages, although relative crater frequencies exceed some proposed levels for SEQ, is supported by the work by Xiao and Werner (2015), who concluded that arbitrary equilibrium spatial densities are not suitable to evaluate the presence of an equilibrium condition. In their study, Xiao and Werner (2015) observed crater populations that are in equilibrium, although their R values are less than 1% N_{gs}, which has been regarded as the minimum empirical equilibrium density level (Gault 1970). Numerical models (Kirchoff 2018) indicated that crater populations with shallow to moderate cumulative SFD slopes will become more spatially uniform (i.e., more evenly spaced) as they approach and reach SEQ. Richardson (2009) found the shapes of CSFDs for heavily-cratered lunar regions (on all scales) to be consistent with a Main Belt asteroid impactor population. He also found that these regions represent a crater population, which is in equilibrium, but which also continues to reflect, or follow the impactor/production population, which originally produced it (Richardson 2009). Povilaitis et al. (2018) presented CSFDs of large craters that exceed 10% N_{gs}, but still fit the PF. These CSFDs might be linked to potential major impact events that show AMAs of about 4.13, 4.15, 4.19, and 4.28 Ga. In these cases, the relative density of the largest craters approaches equilibrium levels suggested by Woronow (1977) and Woronow et al. (1982). Smaller craters

are subject to several degradational geological processes, including impact swarms, seismic shaking, and regolith processes (e.g., Schultz et al. 1977; Xiao and Werner 2015), whereas the largest basins are more difficult to completely erase. Thus, the size dependency of these processes suggests that SEQ is a size-dependent process, which cannot be easily modeled as a simple power law. In addition, the non-constant slope of the production population could result in equilibrium populations with slopes other than ~–2 (e.g., Woronow 1977; Richardson 2009; Xiao and Werner 2015; Kirchoff 2018).

Richardson (2009) proposed two mechanisms that limit the number of countable craters at or near SEQ. In the first case of a steep PF ($N \sim D^{-n}$, $n > 2$), which is typical for lunar craters smaller than ~1.5 km, small craters can erase larger craters ("sandblast regime"). In this case, the slope of the CSFD is limited to $N \sim D^{-2}$ for all slope indices $n > 2$. In the second case of a shallow PF ($N \sim D^{-n}$, $n \leq 2$), the main mechanism is the episodic resurfacing by the largest crater ("cookie-cutting regime"). In this case, the ejecta deposit of a large crater resurfaces adjacent terrain and the fresh surface again starts accumulating craters, reproducing the primary PF (e.g., Woronow 1978; Chapman and McKinnon 1986; Werner and Ivanov 2015). Hartmann (1984) proposed that craters in SEQ follow a power law of $N \sim D^{-1.83}$ that approximately fits both steep ($n > 2$) and shallow ($n \leq 2$) branches of CSFD.

Craters in SEQ are less randomly distributed than craters outside SEQ (Squyres et al. 1997; Kirchoff 2018). Thus, randomness analyses of the measured CSFD are necessary to identify such a behavior, as well as the effects of secondary cratering, which also tends to produce crater clusters and chains, i.e., a non-random distribution of craters (e.g., Michael et al. 2012). Although efforts to understand the process of equilibrium saturation have been made, there are numerous remaining unsolved problems (Hirabayashi et al. 2017). A new analytical model considers three processes that contribute to SEQ: (1) cookie-cutting (i.e., simple geometric overlap), (2) ejecta deposition, and (3) sandblasting (i.e., diffusive erosion) (Hirabayashi et al. 2017). The results of Hirabayashi et al. (2017) indicate that the power law of the equilibrium slope is independent of that of the PF slope in cases when the slope of the PF is steeper than that of the equilibrium state.

High resolution Narrow Angle Camera Digital Terrain Models (NAC DTMs) allow us to quantitively study small crater degradation fractions in equilibrium—see, e.g., Basilevsky et al. (2014) and Mahanti et al. (2018). Comparing CSFDs for small craters with Neukum et al.'s (2001) chronology (see Eqn. 2 below), we can estimate the time to reach a given degradation state, measured, for example, with the depth/diameter ratio, d/D, derived from high-resolution DTMs. For example, at the Apollo landing sites it takes small craters ($D < 100$ m) ~ 3 to 7 Ma to reach $d/D > 0.06$, using the PF and CF of Neukum et al. (2001) (Ivanov 2018). Mahanti et al. (2018) discussed the difference in degradation rates between Apollo landing sites. On the basis of their study of lunar impact craters (800 m to 5 km) and the application of a topographic diffusion model, Fassett and Thomson (2014) proposed that after 3 Ga the initial depth of a 1 km diameter crater is reduced to about 52%, whereas the depth of a 300 m diameter crater is reduced to about 7%, of its original depth. Smaller craters are degraded beyond recognition (Fassett and Thomson 2014). The model of crater degradation of Xie et al. (2017, 2019) has been used to study the effect of topographic degradation on CSFD measurements and the results suggest that topographic degradation might have significant effects on the shapes of PFs.

2.3. Chronology function

One of the major geologic goals of the Apollo missions was to return lunar samples, which could be dated in the laboratory with radiometric techniques (e.g., Rb–Sr, Sm–Nd, Ar–Ar). Together with CSFD measurements of the landing sites, they are the prerequisites to derive the lunar cratering chronology (e.g., BVSP 1981; Neukum 1983; Strom and Neukum 1988; Neukum and Ivanov 1994; Stöffler and Ryder 2001; Marchi et al. 2009; Robbins 2014).

For this purpose, CSFD measurements for the Apollo 11, 12, 14, 15, 16, 17, and the Luna 16 and 24 landing sites were performed and correlated with the corresponding radiometric ages of these sites (e.g., BVSP 1981; Neukum 1983; Strom and Neukum 1988; Neukum and Ivanov 1994; Stöffler and Ryder 2001; Marchi et al. 2009; Robbins 2014). However, this is not a trivial task and has led to several somewhat different chronologies (e.g., BVSP 1981; Neukum 1983; Neukum and Ivanov 1994; Stöffler and Ryder 2001; Stöffler et al. 2006; Marchi et al. 2009; Robbins 2014 and references therein). It is well known that lunar samples of each landing site show a range of radiometric ages, which is due to an unknown combination of vertical and horizontal mixing (BVSP 1981). Thus, if the investigated sample is a breccia, the individual particles can reflect very different geologic histories and reset ages. For example, for breccia 73215, Jessberger et al. (1977) reported variations in the K–Ar ages of up to 300 Ma, which raises the issue of which radiometric age should be assigned to the corresponding CSFD. In principle, there are two possibilities to correlate CSFDs with radiometric ages, i.e., the correlation with the most frequently measured age (e.g., Neukum et al. 1975a; Neukum 1983; Neukum and Ivanov 1994) or with the youngest age (e.g., Jessberger et al. 1974; BVSP 1981; Wilhelms et al. 1987). Neukum (1983) and Neukum and Ivanov (1994) argued that the "peak age" is the age that most likely reflects the major event/impact that reset the radiometric clocks of most samples, whereas the youngest age might only represent smaller local impacts that occurred after the main impact. The reasoning for adopting the peak age is discussed in greater detail by Neukum and Ivanov (1994).

As mentioned before, over the last few decades several chronology functions (CFs) have been proposed (e.g., BVSP 1981; Neukum 1983; Strom and Neukum 1988; Neukum and Ivanov 1994; Stöffler and Ryder 2001; Marchi et al. 2009; Robbins 2014; Fig. 2). As it is impossible to describe each CF in detail in this chapter, we point the reader to the original publications and focus on the description of the most widely used CF, i.e., the CF of Neukum and co-workers. The empirically derived chronology of Neukum and Ivanov (1994) and Neukum et al. (2001), is given by

$$N_{\mathrm{cum}}(D \geq 1\ \mathrm{km}) = 5.44 \times 10^{-14}\ (\exp(6.93\,t) - 1) + 8.38 \times 10^{-4}\,t \qquad (2)$$

$N_{\mathrm{cum}}(D \geq 1\ \mathrm{km})$ is the cumulative number of craters equal or larger than 1 km; t is the time since the unit has been exposed to the bombardment. Neukum and Wise (1976) and Neukum and Ivanov (1994) compared the impact chronologies of several authors (Baldwin 1971, 1974, 1987; Neukum 1971, 1977b, 1983; Hartmann 1972; Soderblom and Boyce 1972; Soderblom et al. 1974; Neukum and Ivanov 1994) and found that the interpretations of these authors all coincide within a factor of 2 to 3. Since this evaluation of Neukum and Ivanov (1994), new chronologies have been proposed, including those of Marchi et al. (2009) and Robbins (2014). Robbins (2014) reported that his revised chronology changes previously established CSFD-based ages by up to 1 Ga. In particular, Robbins (2014) argued that surfaces younger than ~3.6 Ga and older than ~3.9 Ga derived with the Neukum et al. (2001) chronology are younger and those in between are older in his new system. Some of the Robbins (2014) CSFD measurements were performed on large count areas that might violate the homogeneity criteria, however, he also did tests by dividing the count areas, which showed that the subdivisions resulted in the same CSFDs, within error bars. It remains questionable whether such large areas in fact represent the landings sites, reducing the plausibility of correlating these CSFDs with radiometric ages.

Another approach to derive the chronology was proposed by Marchi et al. (2009), who modeled the incoming impactor flux and converted it to a SFD of resulting craters, instead of directly observing crater sizes and spatial densities on the lunar surface. Marchi PF (MPF) was calibrated with CSFDs from Neukum (1983) for regions with known radiometric ages (Marchi et al. 2009). The Marchi et al. (2009) chronology fits well data points that are older than Copernicus, while it underestimates all younger data points by a factor of 2. Marchi et al. (2009) concluded that this might reflect a non-constant impactor flux over the last 3 Ga. Such a non-constant

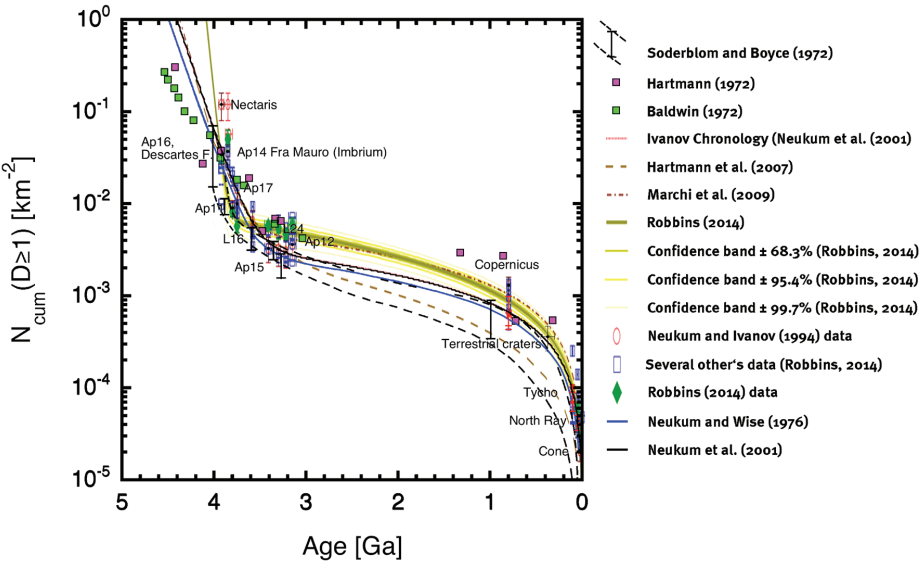

Figure 2. Different chronology functions fit to samples with radiometric and exposure ages.

impactor flux might have been caused by the formation of dynamical families in response to catastrophic asteroid disruptions (Bottke et al. 2007; Nesvorný et al. 2007).

In any case, once a lunar chronology is established, we can derive AMAs for the entire lunar surface from CSFD measurements by solving the function, e.g., Equation (2), for time t for $N_{cum}(D \geq 1$ km) measured on the geologic unit to be dated.

2.4. Radiogenic and exposure ages of samples from the landing sites

Stöffler and Ryder (2001) and Stöffler et al. (2006) provided excellent reviews of the radiometric and exposure ages of samples that best represent a given landing site for the correlation with $N(1)$ or $N(10)$ crater spatial densities. The relevant radiometric ages are shown in Table 2. Since the seminal papers of Stöffler and Ryder (2001) and Stöffler et al. (2006), some of these measurements have been updated and/or augmented, providing new best estimates for landing site surface ages. For example, since 2006, the Ar decay constant has been updated, thus, requiring the recalculation of some of the radiometric ages and updating the chronology function. This is work in progress, and the most widely used Neukum et al. (2001) chronology, as well as the Robbins (2014) chronology, are still based on the radiometric ages published by Stöffler and Ryder (2001) and Stöffler et al. (2006). Further information on lunar sample ages can be found in Cohen et al. (2023), Head et al. (2023) and Shearer et al. (2023), all this volume.

2.5. CSFD $N(1)$ ages of landing sites

Once the radiometric and exposure ages for the samples are established, CSFD measurement areas for their corresponding surface units must be defined. The areas need to be large enough to provide a sufficient statistical crater population. Stöffler and Ryder (2001) and Stöffler et al. (2006) provided a comprehensive review of CSFDs and crater degradation values used for the derivation of the lunar chronology. Since their work, new $N(1)$ values have been derived for some of the landing sites. The new analyses were performed via updated geological mapping and CSFD measurements of the landing regions with image and spectral data from recent lunar missions (Robbins 2014; Iqbal et al. 2019a,b, 2020a,b). Iqbal et al. (2019a,b 2020a,b) also reviewed new and updated radiometric sample ages to check their correlation with the new geological maps and CSFD results.

Table 2. Best estimates of crystallization ages of mare basalt flows and formation ages of geological units at the Apollo and Luna landing sites updated from Stöffler et al. (2006).

Formation	**Age (Ga) Set a1**	**Age (Ga) Set a2**	**Age (Ga) Set b1**	**Age (Ga) Set b2**
Ancient highlands (older crust)	4.3–4.55			4.54 ± 0.027
	4.35 ± 0.10			
SPA				4.293 ± 0.044
Highlands	4.0–4.4			
Nectaris Basin	4.10 ± 0.10	3.92 ± 0.03	3.92 ± 0.03	
			3.85 ± 0.05	
A16/Descartes Fm	3.90 ± 0.10	3.92 ± 0.03	3.92 ± 0.03	
			3.85 ± 0.05	
Crisium Basin		3.89 ± 0.02	3.84 ± 0.04	
Serenitatis Basin	3.98 ± 0.05	3.89 ± 0.01	3.87 ± 0.03	3.934 ± 12
A16/Cayley Fm.		3.85 ± 0.02	3.77 ± 0.02	
Imbrium Apennines	3.91 ± 0.10	3.85 ± 0.02		
A14/Fra Mauro Fm.	3.91 ± 0.10	3.85 ± 0.02	3.77 ± 0.02	3.938 ± 0.005
Imbrium Basin	3.91 ± 0.10	3.85 ± 0.02	3.77 ± 0.02	3.938 ± 0.005
Orientale ejecta blanket		ND	ND	
Orientale Basin		3.72–3.85?	3.72–3.77?	
Oldest Mare (Nubium)		ND		
Mare Nectaris		3.74		
M. Tranq., old (A11)	3.72 ± 0.010	3.80 ± 0.02		3.747 ± 0.003
M. Serenitatis (A17)		3.75 ± 0.01		3.767 ± 0.009
M. Tranq., young (A11)	3.53 ± 0.05	3.58 ± 0.01		3.578 ± 0.009
M. Fecunditatis (L16)	3.40 ± 0.05	3.41 ± 0.04		
M. Imbrium (A15)	3.28 ± 0.10	3.30 ± 0.02		3.285 ± 0.007
M. Crisium (L24)	3.30 ± 0.10	3.22 ± 0.02		
O. Procellarum (A12)	3.18 ± 0.10	3.15 ± 0.04		3.129 ± 0.01– 3.176 ± 0.006
Autolycus		2.1 ± ?		
Copernicus	0.85 ± 0.20	0.8 ± 0.015		0.789 ± 0.013
Tycho, A17	0.109 ± 0.004	0.109 ± 0.004		
Tycho		0.109 ± 0.004		
North Ray Crater	0.05 ± 0.0014	0.053 ± 0.008		
Cone Crater	0.026 ± 0.0008	0.025 ± 0.012		
South Ray Crater		0.002 ± 0.0002		
Terrestrial craters (Phanerozoic)	0.375 ± 0.075	0.375 ± 0.075		

***Note*:** Data compiled from various sources by (a1) Hartmann et al. (1981), Neukum (1983); (a2) Ryder and Spudis (1987), Wilhelms et al. (1987), Stöffler and Ryder (2001); (b1) Jessberger et al. (1977), Spangler et al. (1984), Stöffler et al. (1985), Deutsch and Stöffler (1987), Dalrymple (1991), Stadermann et al. (1991), Nyquist and Shih (1992), Burgess and Turner (1998), Snyder et al. (2000), Stöffler and Ryder (2001) and references therein; (b2) Recently updated ages; Barra et al. (2006), Grange at al. (2009), Fernandes et al. (2013), Merle et al. (2014), Snape et al. (2018, 2019) (see Table 5.10; Stöffler and Ryder 2001).

Table 3. Compilation of cumulative crater densities for reference areas across the Moon and at Apollo landing sites updated from Stöffler et al. (2016).

Formation	$N = 10^{-4}$ craters >1 km/km^2 (1)	$N = 10^{-3}$ craters > 4 km/km^2 (2)	$N = 10^{-4}$ craters > 1 km/km^2 (3)	$N = 10^{-6}$ craters > 10 km/km^2 (3)	$N = 10^{-4}$ craters >1 km/km^2 (4)	$N = 10^{-4}$ craters >1 km/km^2 (5)	$N = 10^{-4}$ craters > 20 km/km^2 (6)
Ancient highland (older crust)		564–677	3600 ± 1100	920	7851.0[a]		
					2018.0[b]		
South Pole–Aitken Basin							254 ± 21
Highlands		132–564					
Nectaris Basin			1200 ±	310	1327.0[a]		172 ± 20
			400		664.8[b]		
A16/Descartes Fm			340 ± 70	87	249.0[a]		
					250.9[b]		
Crisium Basin			570#	145#			114 ± 13
Serenitatis Basin			?	?			334 ± 73
A16/Cayley Fm.		34.7			310[c]	188[f]	
Imbrium Apennines	250–480		?	89	196.8[a]		
					193.1[b]		
A14/Fra Mauro Fm.	250–480	47.7	370 ± 70	94#	259.5[a]	431[e]	
					267.2[b]		
					501[c]		
Imbrium Basin							26
Orientale ejecta blanket	220	ND	220 ± ?				
Orientale Basin							20
Oldest Mare (Nubium)	ND	ND	ND	ND			
Mare Nectaris	ND	ND	ND	ND			
M. Tranq., old (A11)	200	26.2?	90 ± 18	23	183.6[a]		
					183.2[b]		
					81.4[c]		
M. Serenitatis (A17)	90		100 ± 30	26#	157.9[a]	106[d]	
					158.5[b]		
					6.6[c]		
M. Tranq., young (A11)	34	15?	64 ± 20	16	93.00[a]	64.2[a]	
					93.57[b]		
M. Fecunditatis (L16)		15.3	33 ± 10	8.4	32.34[a]		
					32.57[b]		
					58.20[c]		

Formation	$N = 10^{-4}$ craters >1 km/km^2 (1)	$N = 10^{-3}$ craters >4 km/km^2 (2)	$N = 10^{-4}$ craters >1 km/km^2 (3)	$N = 10^{-6}$ craters >10 km/km^2 (3)	$N = 10^{-4}$ craters >1 km/km^2 (4)	$N = 10^{-4}$ craters >1 km/km^2 (5)	$N = 10^{-4}$ craters >20 km/km^2 (6)
M. Imbrium (A15)	26	8.01	32 ± 11	8.2	54.68[a]	29.8[g]	
					55.26[b]		
					55[c]		
M. Crisium (L24)	26	8.17	30 ± 10	7.6	23.35[a]		
					23.77[b]		
					46.60[c]		
Autolycus	ND	ND	ND	ND			
Copernicus		0.06	13 ± 3	3.3	13.21(a.i)	6.67[b]	
					13.37(b.i)	6.53[c]	
					13.48[a.ii]		
					13.43[b.ii]		
Tycho, A17	ND	0.019	0.9 ± 0.18	0.23		0.716[c]	
						0.704[d]	
Tycho					.391[a.iii]	0.712 [c]	
					3.401[b.iii]		
					1.644[a.iv]		
					1.712[b.iv]		
North Ray Crater	ND	ND	0.44 ± 0.11	0.11	1.389[a]	0.39[c]	
					1.421[b]	0.384[c]	
					0.601[c]	0.426[h]	
Cone Crater	ND	ND	0.21 ± 0.05	0.05	0.697[a]	.326[i]	
					0.7131[b]		
					0.336 [c]		
South Ray Crater					0.0123[c]	0.00895[h]	
Terrestrial craters (Phanerozoic)			3.6 ± 1.1	9.2	12.67[a.v]		
					7.655[b.v]		
					3.835[a.vi]		
					2.195[b.vi]		

Note: (1)Wilhelms et al. (1987); (2) Hartmann et al. (1981); (3) Neukum and Ivanov (1994); # from Neukum (1983); (4) (a) Marchi et al. (2009) NEO, (b) Marchi et al. (2009) MBA, (a.i) Copernicus ejecta using NEO, (b.i) Copernicus ejecta using MBA, (a.ii) Copernicus floor using NEO, (b.ii) Copernicus floor using MBA, (a.iii) Counted small craters using NEO (b.iii) Counted small craters using MBA, (a.iv) Counted large craters using NEO, (b.iv) Counted large craters using MBA, (a.v) Terrestrial craters using NEO, (b.v) Terrestrial craters using MBA, (a.vi) Young terrestrial craters using NEO, (b.vi) Young terrestrial craters using MBA; (c) Robbins (2014); (5) (a) Iqbal et al. (2019a), (b) Iqbal et al. (2020a), (c) Hiesinger et al. (2012a), (d) Iqbal et al. (2019b), (e) Borisov et al. (2019), (f) Gebbing et al. (2019), (g) Iqbal et al. (2020b), (h) Gebbing et al. (2020) (i) Hiesinger et al. (2015); (6) Orgel et al. (2018); ave. = average; ND = not determined; A = Apollo; Fm. = Formation; L = Luna; M. = Mare; O. = Oceanus; Tranq. = Tranquillitatis; a: average mare = 1.88 > 10^{-4} craters >4 km/km^2.

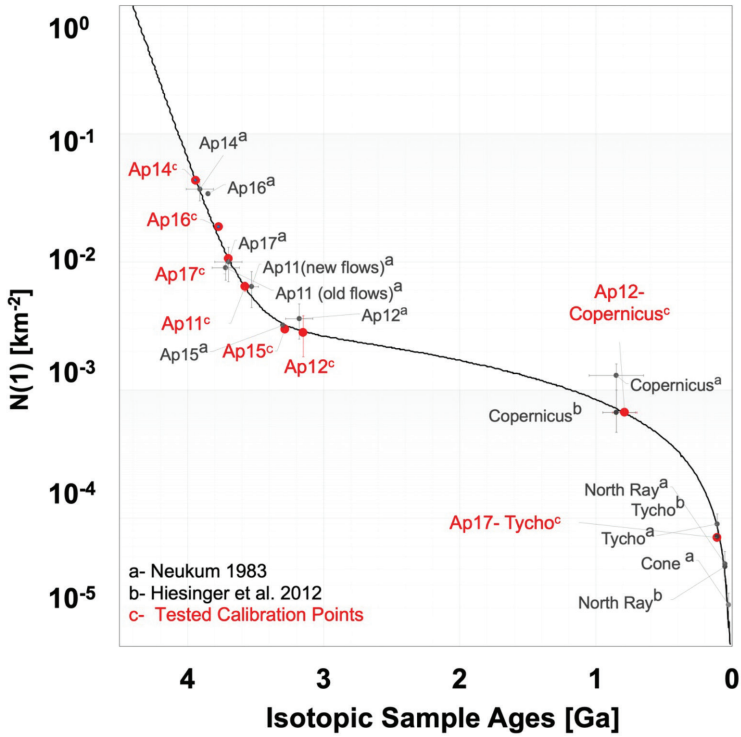

Figure 3. Tested lunar chronology function from Neukum (1983) with three set of data: (a) Neukum (1983), (b) Hiesinger et al. (2012a), and (c) Borisov et al. (2019), Gebbing et al. (2019), Iqbal et al. (2019a,b, 2020a,b).

2.6. Data presentation and estimation of cratering model ages

2.6.1. Crater catalogs. Crater catalogs are a valuable resource to study impact processes on planetary bodies, including Mars (e.g., Salamuniccar et al. 2011), Mercury (e.g., Fassett et al. 2011), Venus (e.g., Herrick et al. 1997), and Ceres (e.g., Hiesinger et al. 2016c). For the Moon, several pre-digital catalogs were produced, but in this section of this chapter, we only address global modern catalogs. Head et al. (2010) used newly available digital topography and image data to analyze the global population of impact craters larger than 20 km. This catalog was expanded to craters larger than 5 km (Povilaitis et al. 2018). Wang et al. (2015) published a global catalog containing more than 100,000 craters as small as 500 m, identified and measured by a hybrid crater detection algorithm. Robbins (2019) also published a global catalog of over 2 million craters, 1.3 million of them ≥ 1 km in diameter. For larger crater and basin diameters, Neumann et al. (2015) and Evans et al. (2016, 2018) employed combinations of GRAIL gravity data (Zuber et al. 2013) and LOLA altimetry data (Smith et al. 2010).

2.6.2. Types of data presentation and binning. Early work on impact crater populations seeded a variety of approaches to the presentation of measurements. Those approaches were fundamentally similar, their aim being to relate crater diameter to frequency of occurrence, yet there was sufficient variation among them to make it difficult to compare results from different authors. A workshop held in 1977 attempted to standardize the presentation, reviewing the forms then in use and recommending two of them, together with suggestions for binning and tabular forms (Crater Analysis Techniques Working Group 1979). Forty years on, four types

of data presentations remain in common use, including cumulative, differential, incremental, and R or "relative". From the earliest studies, it was evident that the crater size–frequency distribution follows a function rather close to a power law with a differential slope of –3. It is possible to make use of this knowledge to remove the general trend from the plotted distribution in differential form. Such a presentation is known as a relative size–frequency distribution plot or R-plot (Fig. 4d), and it enables a better visualization of residual deviations from the –3 differential slope, helping to identify more subtle features in the CSFD.

Frequency distributions are typically represented graphically using a histogram, the construction of which requires a choice of bin width. The optimal choice of bin width depends on the data: if chosen too narrow, the resulting plot is degraded by discretization noise; if too wide, some resolution of the distribution shape is lost. In its simplest form, we may plot the number of craters within a bin against the bin diameter on log–log axes. This has been known as an incremental plot (Fig. 4a) (e.g., Hartmann 1964). A variant of it, known as a differential plot (Fig. 4b), divides the number of craters in each bin by the width of the bin. This gives the benefit that the y-values on the plot are essentially independent of the choice of bin width, enabling easy comparison of datasets plotted with different binnings.

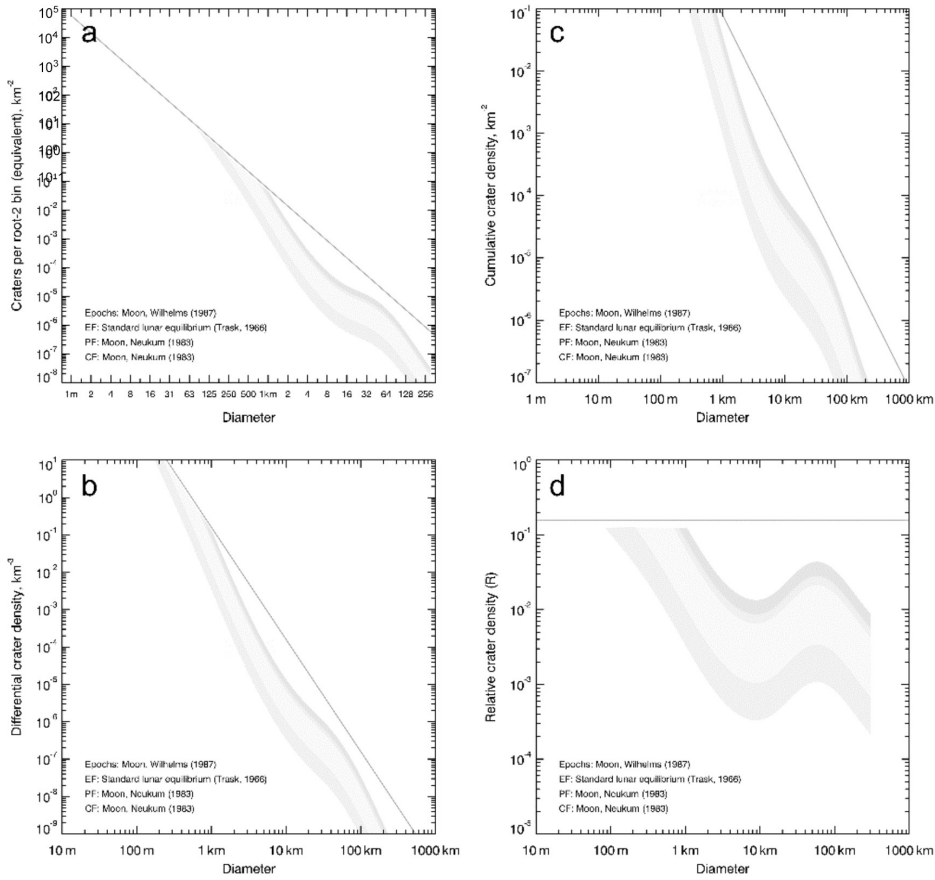

Figure 4. **(a)** Incremental plot showing crater spatial densities for the lunar epochs shown in Figure 5. Bounding line is standard lunar equilibrium (Trask 1966), **(b)** differential plot showing same. **(c)** Cumulative plot showing same. **(d)** Relative or R-plot showing same.

Use of a *cumulative* histogram (Fig. 4c) removes the difficulty of the choice of bin width: the width may be chosen arbitrarily small or the data left unbinned without degrading the plotted distribution shape. No distribution features are lost to the smoothing effect of the binning. Its cumulative nature, however, means that variations in one part of the distribution—whether real features or statistical artefacts—can propagate across the plot. Because of the near power law nature of the CSFD, the magnitude of propagated variations diminishes rapidly, but it remains a complication of interpretation of cumulative plots (e.g., Michael and Neukum 2010).

As for the choice of binning, the 1977 workshop recommended the use of bins no larger than with a $\sqrt{2}$ factor between bin boundaries (the scale is always logarithmic). $\sqrt{2}$ interval systems have been commonly used for incremental and R-plots, which is equivalent to about 6.5 bins/decade (that is 6.5 bins between, e.g., 1 km and 10 km diameter). It is worth noting that, for a 'standard' crater population with a differential size–frequency power law slope of –3, there is a roughly 3:1 frequency ratio between craters of diameters occurring near the opposite edges of a $\sqrt{2}$ bin. In other words, a 1 km crater is expected to form three times more often than a 1.4 km crater. Researchers using cumulative plots have typically used a finer binning of 18 bins/decade.

While the methods from the 1977 workshop have been in use for over four decades, statistics and computers have advanced such that alternative methods might be considered. Robbins et al. (2018) introduced a new technique that treats each crater as a probability distribution (such as a Gaussian) with the mean centered at the measured diameter and the standard deviation estimated from repeatability and replicability studies (e.g., Robbins 2014). The probability distribution from each crater is summed to give the resultant CSFD. By default, this technique produces the differential plot, and it can easily be converted to incremental, cumulative, and relative plots. This method removes the need for binning, though introduction of the standard deviation parameter could be thought of as a form of binning, but it is informed by an actual process (repeatability and replicability of crater diameter measurement) rather than an arbitrary bin width.

2.6.3. Fitting of data. *A*fter a given time of exposure of a surface to the impact flux, we expect to see a crater population corresponding to the PF multiplied by the time of exposure. For each of the types of plots shown in Figure 4, we should expect to plot points corresponding to the PF, shifted further upwards if the surface is older, or further downwards if younger. In Figures 4 and 5, the epoch boundaries defined by Wilhelms et al. (1987) are shown as changes of grey tone. It is possible to pre-plot a sequence of isochrons, e.g., 0.01, 0.1, 1 Ga or the epoch boundaries as shown, and compare the position of superposed data points to these standards to interpret the surface age. Alternatively, we may use a numerical fitting algorithm to find the isochron which best fits a given set of points.

Up to now, the PF has typically been defined in one of two forms: either as an incremental piecewise power law, or as a cumulative polynomial power law. Either of these can be transformed for any of the four styles of plot, but numerical fits using these transformed functions will achieve marginally different results in each case. When the number of craters is large and the population is unmodified, the differences are negligible. In cases where the number of craters is small, the error in fitting will grow. A third approach, which is preferable for small numbers of craters, is to make the calculation analytically using Poisson statistics (Michael et al. 2016).

The Poisson approach yields an age and uncertainty based on the assumption that the observed population formed as a Poisson process with no loss of craters. In practice, this is the same assumption required to fit an isochron to a series of binned data points representing a crater population. We know, however, that real measurements often show population loss effects, which we see as deviations from the production curve. When examining a very small number of craters, it is not possible to observe this type of deviation. The possibility that the population has been modified thus always remains.

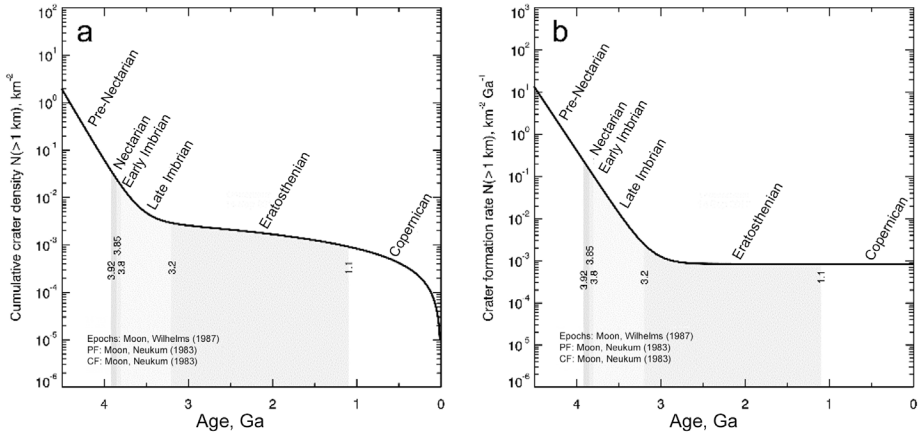

Figure 5. a) Chronology function in cumulative form (Neukum 1983) with lunar epoch system (Wilhelms et al. 1987). **b)** Same function in rate form.

Recent years have seen an increased interest in studying resurfacing ages. Some studied crater populations indicate that there was a loss of craters at smaller scales while larger craters were left unaffected. This leaves a characteristic step signature in the CSFD. Although it is possible to study these features in the cumulative plot form (Michael and Neukum 2010), they are clearer to see in the differential or incremental forms.

2.6.4. Uncertainty. The uncertainty of crater population-derived age measurements is an important issue. Quoted ages result from a cratering chronology model, which is built upon several assumptions and inferences, each of which contributes a degree of uncertainty to the overall measurement. Within the model, the chronology function attempts to relate the radiometrically determined ages of melt components within returned lunar surface samples to accumulated crater spatial densities on the surfaces from which they are inferred to have originated. Naturally, there is uncertainty in the radiometric dating procedure itself, which is quantifiable, and likewise, there are errors on the measured crater density values. Efforts have been made in recent times to improve some of these measurements (Fernandes et al. 2013; Robbins 2014; Iqbal et al. 2019a,b, 2020a,b)

Most significant for the cratering chronology model is the uncertainty of the inference connecting the last heating event of a dated sample component to the surface thought to originate from that event. The inferences are difficult and, in some cases, potentially complicated by the fact that lunar material can be recycled through impacts many times without heating, the majority of material ejected during an impact event being cold. If some of the inferred connections are erroneous—and, at present, there are only 16 of them in total—the shape of the chronology function would be in error in a manner which is not meaningfully quantifiable. In the future, it is reasonable to expect that a broader suite of samples from sites selected specifically for refining the chronology will not only fill in less well-defined time periods (e.g., van der Bogert and Hiesinger 2020), but also bring about a general change of shape of the calibration function. These inferences thus introduce an uncertainty to age measurements, which is both unquantifiable and possibly large compared to other sources of error.

A necessary technique in crater-based dating is to select a portion of the crater distribution which is judged to correspond to the PF. The shape of the distribution is used to assess which part of the population is undisturbed in its accumulation. Given that there is stochastic variation in the population, this procedure itself is subject to error, which increases when fewer craters are present.

Finally, having chosen the crater size range to be analyzed, there is the uncertainty arising from the stochastic nature of the cratering process. This component can be estimated using Poisson statistics.

The combination of quantifiable and unquantifiable components of uncertainty carries through to any ages derived from it. The calculable component can be expressed as errors on the given age, but the unquantifiable component cannot. It has become conventional to emphasize that crater chronology model-derived ages are model ages, or absolute model ages (AMAs), or to denote the unknown error in the calibration function with the symbol μ. A crater model age can be considered a 'best effort' translation of a crater population density into a value representing time. Inasmuch as we understand that a more densely cratered surface is older than one less so, the quoted errors on model ages retain the same relative certainty, the model age placing the density values on a timeline as close to the truth as may currently be achieved.

In the past, the level of uncertainty of the crater retention age of a given count was given by the following equation:

$$\pm\sigma_N = \log\left[\frac{N(1) \pm \sqrt{N(1)}}{A}\right] \quad (3)$$

in which $N(1)$ was the crater retention age calculated for craters ≥ 1 km diameter and A was the size of the counted area. The $\pm\sigma_N$ value gave the upper and lower limits of the error bar of the crater retention age, which were used for estimating the uncertainty of the absolute crater model age from the cratering chronology. Neukum (1983) and Neukum et al. (2001) generally assumed that the cratering chronology is free of errors. Therefore, errors in the AMAs were only caused by errors in the determination of crater frequencies (Neukum 1983). Neukum et al. (1975a) estimated the systematic uncertainty of the standard distribution curve or the measurement to be < 10% for 0.8 km ≤ D ≤ 3 km and up to 25% for 0.8 km ≤ D ≤ 10 km.

However, this error calculation resulted in relatively small errors that have always drawn considerable criticism (e.g., Chapman 2015). Thus, Michael et al. (2016) and Robbins et al. (2018) proposed new algorithms for the calculation of errors, which are now commonly used, e.g., Poisson fitting (Michael et al. 2016).

2.6.5. Spatial randomness testing. Accurate crater-based dating requires a confidence that the population being examined accumulated without alteration from the time of the event of interest, and that craters from any previous time can be reliably eliminated from the counts. There are many possible geological processes that may frustrate this requirement either by eroding craters or covering them. Often, the occurrence of such processes may be revealed by studying the spatial distribution of the crater population. Primary crater formation is spatially random: the flux of bodies impacting a planet has no (or very little) dependence on surface location. Geologic processes, however, are often inhomogeneous in the extent of their effect.

A spatial randomness test may be used to verify that the population under study has a spatial configuration consistent with being random (e.g., Michael et al. 2012). A deviation from randomness to a certain confidence level is likely an indicator that the population has been disturbed, or has been overprinted by secondary craters that can be more clustered than a random distribution (e.g., Williams et al. 2018a).

It is useful to test for spatial randomness of craters of different sizes. Because different geological processes act at different scales, it is often seen that a population is non-random at some scale but not at others. This information can be used to determine which part of a population is not useable for dating, but it is often also helpful in understanding the nature of the disturbance. Knowing the scale of craters affected reveals the depth of material affected, which is a clue to which type of surface features were caused by the event.

3. RECENT LUNAR AGE DETERMINATIONS

The new global high-resolution imagery (e.g., Lunar Reconnaissance Orbiter Camera (LROC) and Kaguya Terrain Camera (TC)), spectral information (e.g., M^3), and topography data (e.g., LOLA) have significantly improved our capability to date regions of the Moon, from global inventories of craters >20 km, >5 km, and >1 km (e.g., Head et al. 2010; Povilaitis et al. 2018; Robbins et al. 2018) to small surface-area counts to the limit of resolution of LROC-NAC imagery. Complementary remote-sensing datasets such as Diviner and Mini-RF provide additional means for deriving relative and absolute model ages (e.g., Ghent et al. 2014; Mazrouei et al. 2019). The tremendous amount of data provides opportunities to constrain the formation times of individual events (e.g., irregular mare patches (IMPs), crater formation), correlate units over large distances (e.g., Tycho antipodal melt ponds), and date never-before seen areas (e.g., permanently shaded regions (PSR) at the poles). These new data and investigations shed new light on old problems, but have also raised new questions.

3.1. Major terranes

3.1.1. Highlands. Based of their catalog of craters >5 km, Povilaitis et al. (2018) found that 57–160 km diameter craters across most of the highlands are at or exceed crater densities of 10% geometric saturation, but nonetheless fit the lunar PF of Neukum et al. (2001). Combining this with the observation that small craters on old surfaces can reach saturation equilibrium at 1% geometric saturation (Xiao and Werner 2015), Povilaitis et al. (2018) proposed that saturation equilibrium is a size-dependent process, where large craters persist because of their resistance to destruction, degradation, and resurfacing. Werner (2014) compared basin-forming events on Mars, Mercury, and the Moon and found that the Moon holds the oldest surface record.

In high resolution LRO NAC images, Robinson et al. (2016) discovered an unusual group of smooth, flat, pond-like deposits on the lunar farside. They investigated four possible formation mechanisms, i.e., basin ejecta, pyroclastic volcanism, effusive volcanism, and ballistically emplaced impact melt (Robinson et al. 2016). They concluded that an origin as volcanism or basin ejecta is inconsistent with the observed morphology and favored an origin related to ballistically-emplaced impact melt, although specific source craters could not be identified. Using Diviner data, Bandfield et al. (2017) showed that the rock distributions in these regions favor certain slope azimuths, indicating a directional component consistent with a Tycho ejecta origin. However, the maximum summed AMA for these deposits is ~26 Ma, with individual ponds exhibiting AMAs from 10 to 42 Ma (Robinson et al. 2016), thus being much younger than the canonical age of Tycho of 109 Ma (Drozd et al. 1977). These AMAs are, however, consistent with those measured on the Tycho melt sheet (Krüger et al. 2016).

3.1.2. Mare basalts. In the past decades, significant progress has been made on the dating of mare basalt surfaces (e.g., Hiesinger et al. 2000, 2003, 2006, 2011; Bugiolacchi et al. 2006; Bugiolacchi and Guest 2008; Haruyama et al. 2009; Morota et al. 2011a,b; Thaisen et al. 2011; Whitten et al. 2011; Cho et al. 2012; Pasckert et al. 2015, 2018; Qian et al. 2018, 2021a,b).

Early CSFD measurements revealed that lunar mare volcanism ceased at about 1.2 Ga ago on the lunar nearside (Hiesinger et al. 2000, 2003, 2011; Morota et al. 2011a,b), whereas volcanism on the farside ended ~2.5–3.0 Ga ago (Haruyama et al. 2009). In particular, mare basalt deposits on the northern lunar farside, i.e., Lacus Luxuriae, Buys-Ballot, Campbell, and Kohlschutter, range in age from 2.7 to 3.7 Ga (Morota et al. 2011b), the basalts in Mare Moscoviense exhibit AMAs of 2.5–3.5 Ga (Haruyama et al. 2009), and those in Mare Australe show ages of 3.0–3.9 Ga (Hiesinger et al. 2000). Mare basalts in the Moscoviense basin were also dated by Morota et al. (2009) and Thaisen et al. (2011). There, unit Im (Imbrian low-Fe, low-Ti) exhibits an AMA of 3.9 Ga, unit Iltm (Imbrian low-Ti) is 3.5 Ga old, unit Ikm (Imbrian mare associated with Komarov crater) was dated as being 3.3–3.5 Ga old, and unit Ihtm (Imbrian high-Ti) is 2.6 Ga old (Morota et al. 2009; Thaisen et al. 2011).

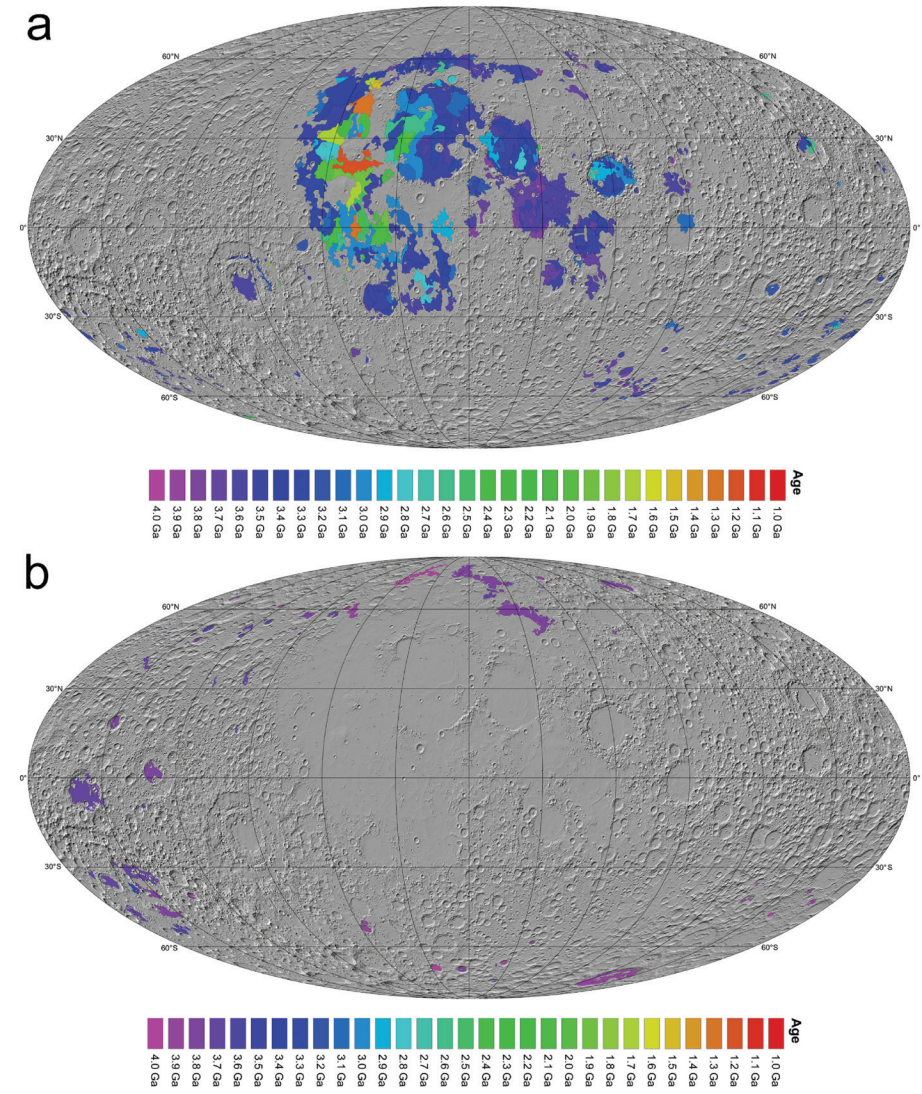

Figure 6. CSFD ages of lunar mare basalts **(a)** and light plains **(b)**. See text for references.

In their comprehensive study of 101 mare basalts on the farside, Pasckert et al. (2018) showed that volcanism lasted until ~2.2 Ga. Their investigation indicated a major peak in volcanic activity between 3.2 Ga and 3.6 Ga, which is a similar time range as the major volcanic activity on the nearside, and the rest of the farside (Hiesinger et al. 2000, 2003, 2011; Haruyama et al. 2009; Morota et al. 2009; Whitten et al. 2011; Paskert et al. 2015) (Fig. 11). Even younger mare basalts were identified in Roseland crater, ranging from 1.5 to 2.9 Ga (Pasckert et al. 2015). Sruthi and Senthil Kumar (2014) also reported very young AMAs of ~1.6 Ga for basalts in Antoniadi crater and, thus, from the interior of the South Pole–Aitken basin (SPA). However, Pasckert et al. (2018) found a somewhat older model age of 2.2 Ga for the basaltic deposits in Antoniadi. These ages are drastically younger than previously derived ages of mare basalts within SPA, which are ~2.5–3.9 Ga old (Haruyama et al. 2009).

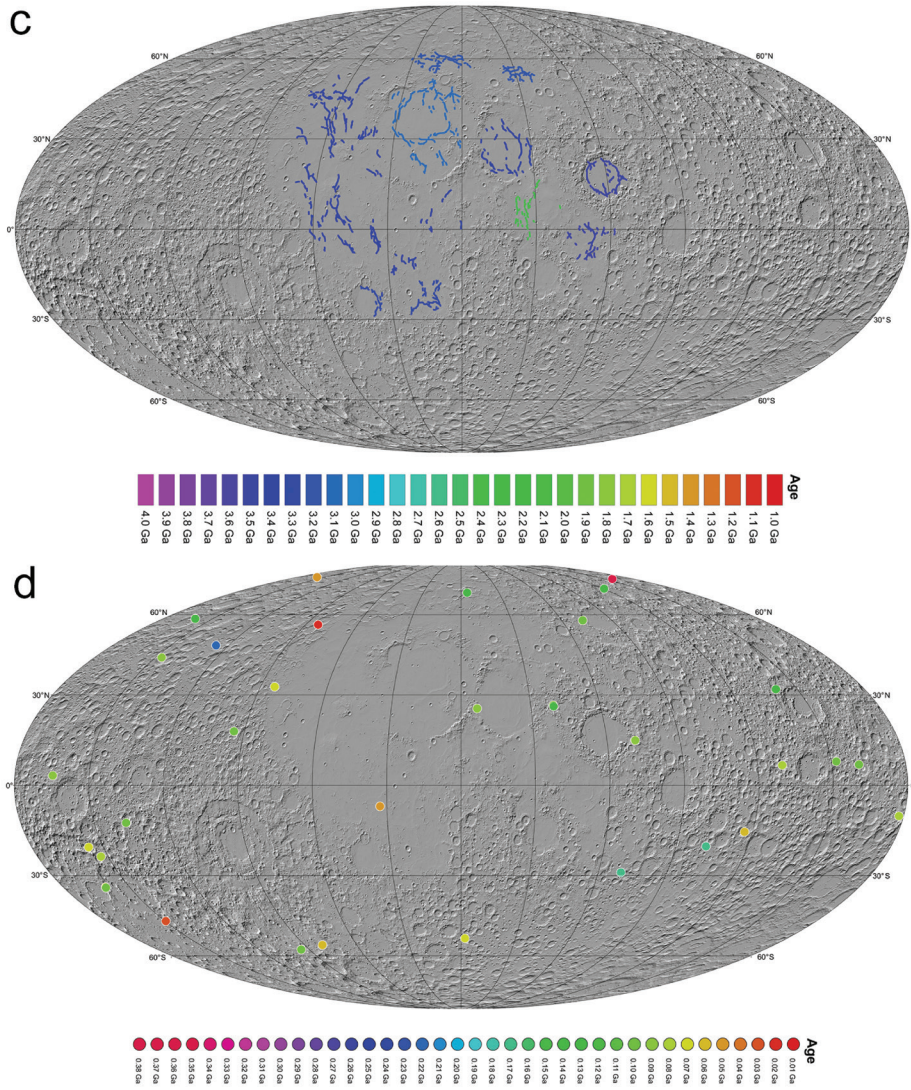

Figure 6 (cont'd). CSFD ages of wrinkle ridges **(c)** and lunar scarps **(d)**. See text for references.

Whitten et al. (2011) showed that the range of ages of basalts in the western limb Orientale impact basin interior (1.66–3.7 Ga) was similar to the range seen on the lunar nearside, but that the abundances were considerably smaller.

Hiesinger et al. (2000) concluded that eruptions of basalts, lasting for hundreds of million years within an individual basin are most likely unrelated to the impact heat of the basin-forming event. Support for this conclusion comes from thermophysical modeling that suggests that thermal and heat flux anomalies associated with a basin will fade within ~100 Ma (Rolf et al. 2017). Additional support comes from the analysis of post-Orientale basin mare basalt deposits, which range over more than 2 Ga (3.7–1.66 Ga), and began about 60–100 Ma later than the formation of the basin itself (Whitten et al. 2011). In contrast to the lunar farside and western limb,

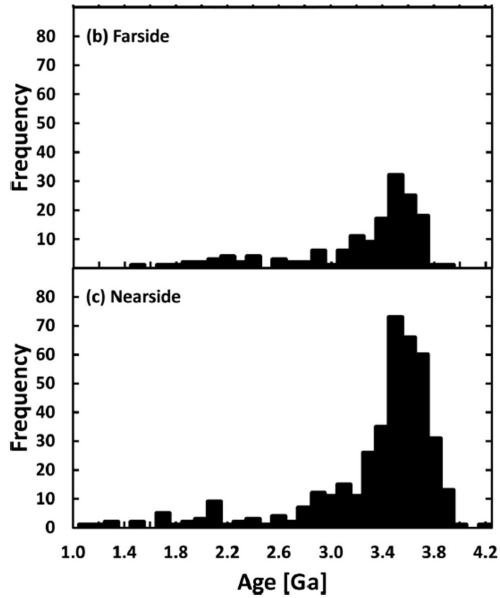

Figure 7. Histograms of **(a)** AMAs of all investigated mare basalts on the lunar farside, including model ages of Haruyama et al. (2009), Morota et al. (2009, 2011a,b), Pasckert et al. (2015, 2018), and **(b)** nearside mare basalt ages of Hiesinger et al. (2011).

on the nearside, the youngest basalts occur in the Procellarum KREEP Terrane (PKT), which is characterized by elevated Th abundances. The radioactive decay is interpreted to have kept the Moon warmer for longer, allowing for continued eruption of basalts in this region (e.g., Wieczorek and Phillips 2000; Laneuville et al. 2013), whereas volcanism ceased earlier in "colder" regions. Unit P60 of Hiesinger et al. (2003) is located in this area and was found to be the youngest mare deposit dated, i.e., about 1.2 Ga old. More recently, Stadermann et al. (2018) reinvestigated the age of this unit with independent CSFD measurements and confirmed this young age. On the basis of their CSFDs, they proposed volcanic flooding from east to west over 1.5 Ga.

Cho et al. (2012) performed CSFD measurements and derived very young basalt model ages of ~2.9 Ga for the eastern parts of Mare Orientale and even younger AMAs of ~1.8–2.2 Ga for basalts in Lacus Veris, Lacus Autumni, and mare patches along the northeastern basin rings. Previous studies yielded ages of ~3.45–3.58 Ga for the emplacement of Mare Orientale basalts (Wilhelms et al. 1987; Greeley et al. 1993; Kadel et al. 1993; Whitten et al. 2011), thus being significantly older than the ages of Cho et al. (2012). For Lacus Veris, Kadel et al. (1993) reported AMAs of ~2.29 Ga, and Greeley et al. (1993) found AMAs of ~2.85 Ga of basalts in Lacus Autumni. An even younger age of ~1.65 Ga for Lacus Autumni basalts was published by Whitten et al. (2011). Interestingly, the young mare basalt ages of Cho et al. (2012), particularly near the basin rim (Lacus Autumni, Lacus Veris) coincide with the peak of volcanic activity elsewhere on the Moon (Hiesinger et al. 2011; Pasckert et al. 2018).

A global study of 261 mare units revealed that younger basalts in Oceanus Procellarum appear to be more titanium rich, and this was interpreted as evidence for a changing magma source at about 2.3 Ga ago (Kato et al. 2017). Interestingly, the ages of the higher TiO_2 basalts correlate with the secondary peak of volcanic activity at ~2 Ga, identified by Hiesinger et al. (2003, 2011) and Morota et al. (2011a). Rajmon and Spudis (2004) argued that in Mare Tranquillitatis and Mare Fecunditatis, volcanic activity began with low-titanium eruptions that evolved into medium- and high-titanium basalts, similar to the observations of Staid

et al. (1996) for Mare Tranquillitatis basalts. Kodama and Yamaguchi (2003) also found such an evolution from low to high titanium basalts, although they noted a decrease in TiO_2 abundances from high to low titanium in young basalts in northeastern Mare Tranquillitatis and Mare Fecunditatis. Rajmon and Spudis (2004) also reported that some high-TiO_2 basalts in Mare Tranquillitatis erupted contemporaneously with low- and medium-TiO_2 basalts. For Mare Fecunditatis, Rajmon and Spudis (2004) found decreasing basalt eruption volumes with increasing titanium abundance. Bugiolacchi et al. (2006) investigated the stratigraphy of basalt flows in Mare Nubium and Mare Cognitum and identified three major phases of eruptions, each lasting for about 300 Ma. The oldest exposed flows are Late Imbrian (~3.4 ± 0.1 Ga) low titanium (2-3 wt%) basalts, followed by early Eratosthenian (~3.2 ± 0.1 Ga) more titanium-rich (3–4 wt%) basalts and even more titanium-rich basalts (4–5 wt%) that erupted until the Late Eratosthenian Period (~2.7 ± 0.4 Ga). Similarly, Bugiolacchi and Guest (2008) argued for a correlation between AMAs and TiO_2 abundances of mare basalts in Mare Imbrium. According to their work, eastern flows are characterized by lower TiO_2 contents and were erupted between 3.0 and 3.5 Ga ago, whereas Eratosthenian, western basalts show higher titanium and iron contents. Although it seems that AMAs are correlated with TiO_2 abundances in the data of Bugiolacchi et al. (2006), a comprehensive global study did not show such a correlation (Sato et al. 2017), thus being consistent with Hiesinger et al. (2001). Specifically, Sato et al. (2017) found a large variability of TiO_2 abundances (0–10 wt%) for early basalts (>2.6 Ga) whereas younger basalts only show medium to high TiO_2 abundances (average = 6.8 wt%, minimum = 4.5 wt%). Further support for this conclusion comes from work by Hackwill (2010), who studied 14 basalt units in Mare Serenitatis and concluded that there is no trend in the iron and titanium abundances of the studied basalts with time although the variability in FeO and TiO_2 abundances of younger basalt flows is much larger.

CSFD measurements for five mare basalt units in Sinus Iridum revealed AMAs of 2.50 to 3.32 Ga (Qiao et al. 2014). Those ages were found to be consistent with AMAs of Hiesinger et al. (2000) to within less than 500 Ma. Morota et al. (2011a) and Zhao et al. (2013) also reported similar ages, whereas the AMAs of Bugiolacchi and Guest (2008) are mostly significantly younger than the AMAs of the other authors (i.e., Hiesinger et al. 2000; Morota et al. 2011a,b; Zhao et al. 2013; Qiao et al. 2014). Zhao et al. (2013) reported AMAs of 2.60–3.33 Ga for the Iridum basalts, whereas Bugiolacchi and Guest (2008) found ages ranging from 2.22 to 3.31 Ga. Fa et al. (2014) reported that there are significant variations in regolith thickness and that regolith thicknesses correlate well with AMAs of the basalts, i.e., older units exhibit thicker regolith layers. They also determined that the regolith growth rate is larger for younger surfaces compared to older surfaces.

In 2020, the Chang'E 5 mission landed NE of Mons Rümker and returned samples that provide a new data point for the lunar chronology. To properly understand the provenance of the samples several studies have been carried out (e.g., Zhao et al. 2017; Qian et al. 2018, 2021a,b, Wu et al. 2018). Results of Qian et al. (2021b) indicate that the basalts in the vicinity of the landing site vary in age between 1.43 and 1.71 Ga. The landing site itself was dated to be 1.53 Ga old, thus, being somewhat older than the age of 1.33 Ga determined by Hiesinger et al. (2003, 2011). Qian et al. (2018) found an AMA of 1.21 Ga and Wu et al. (2018) determined an AMA of 1.49 Ga. Slightly older AMAs were published by Morota et al. (2011a; 1.91/2.20 Ga) and Jia et al. (2020; 2.07 Ga). All these AMAs and the corresponding N(1) fall into a range in which the lunar chronology is poorly constrained. Thus, the new Chang'E 5 samples offer the unique opportunity to test the chronology.

Srivastava et al. (2013) investigated a viscous flow in Lowell crater in the Orientale basin, which they interpreted as being volcanic in origin. The flow has a gabbroic/basaltic composition and consists of at least three subunits with variable viscosity. The youngest flow lobe shows only three superposed impact craters which give an inferred age of about 2–10 Ma

(Srivastava et al. 2013). This young age challenges our understanding of volcanic eruptions and the thermal history of the Moon, and, thus, the volcanic origin of the flow has been challenged by Plescia and Spudis (2014), who favor an impact melt origin on the basis of the morphology and the geologic context of the flows.

Hurwitz et al. (2013) found that the age of sinuous rilles is highly correlated with the ages of the surrounding mare units. About 80% of the sinuous rilles were incised into mare units that were emplaced between 3 and 3.75 Ga ago and only 8% were incised into materials younger than 2 Ga. Seven sinuous rilles in the southwestern Aristarchus region were dated by Li et al. (2016). The oldest rille was dated as 3.77 Ga; the youngest rille is only 1.49 Ga old. The remaining rilles exhibit AMAs of 1.65, 3.61, 3.62, 3.69, and 3.73 Ga.

3.1.3. Light plains. Globally distributed, light plains cover ~5% of the lunar surface (Wilhelms and McCauley 1971). Light plains are characterized by mare-like attributes, such as their smoothness, lower crater spatial densities compared to surrounding highlands, and their appearance as crater fill. However, they also show highland-like characteristics such as their geologic and stratigraphic setting and their characteristic high albedos (in comparison to mare basalts). Consequently, their origin has been debated for decades (Wilhelms 1965; Eggleton and Schaber 1972; Trask and McCauley 1972; Chao et al. 1973; Head 1974; Oberbeck et al. 1974; Neukum 1977a,b; Hawke and Head 1978; Schultz and Spudis 1979; Köhler et al. 2000; Hiesinger et al. 2013; Meyer et al. 2013, 2016, 2020). Due to their draping and mantling appearance and a noticeable thickness of the material, light plains were originally interpreted as products of volcanic ash flows (Wilhelms 1965). Alternatively, an origin as lava flows has been proposed because light plains often occur as smooth deposits in crater interiors and other topographic lows, and embay, bury, and cross-cut older landforms (Trask and McCauley 1972). Light plains, i.e., the Cayley Plains were selected as the Apollo 16 landing site from which ~95 kg of samples were returned (Muehlberger et al. 1972). Of those samples, a large number of rocks turned out to be non-volcanic in origin, rather they are light-colored plagioclase-rich breccias, suggesting an impact origin. Consequently, several impact-related models were proposed, including (1) ejecta of large basins, particularly Imbrium and Orientale (e.g., Eggleton and Schaber 1972; Chao et al. 1973; Meyer et al. 2013, 2020), (2) a mixture of material from local and regional craters in addition to basin ejecta (Oberbeck et al. 1974; Oberbeck 1975), and (3) in situ formation combined with impact ejecta from large events (Head 1974). On the basis of their global mapping, Meyer et al. (2020) proposed that about 70% of the light plains are related to the formation of the Orientale and Imbrium basins.

Early CSFD measurements indicated that at least some light plains post-date the Imbrium and Orientale impacts, leading Neukum (1977b) and Köhler et al. (2000) to conclude that these light plains might be endogenic in origin. Models for a volcanic origin of light plains include: (1) unknown form of highland volcanism (e.g., Neukum 1977a), (2) KREEP volcanism (e.g., Hawke and Head 1978; Spudis 1978), and (3) cryptomaria (e.g., Schultz and Spudis 1979; Hawke and Bell 1981; Antonenko et al. 1995; Whitten and Head 2015a,b).

Hiesinger et al. (2013) dated 16 occurrences of light plains in the southern lunar hemisphere, inside and outside the South Pole–Aitken basin. Their CSFD measurements revealed AMAs between 3.71 and 4.01 Ga. These model ages are similar to those established for light plains north of Mare Frigoris, which vary between 3.65 and 4.0 Ga (Köhler et al. 2000), light plains within the SPA basin (3.43–3.81 Ga) (Thiessen et al. 2012), and light plains in the surroundings of the Orientale and Imbrium basins (3.8-4.3 Ga) (Neukum 1977b). Meyer at al. (2016) found AMAs of 3.61–3.83 Ga for light plains NW of the Orientale basin. Pöhler et al. (2019) studied 24 light plains in the northern hemisphere and found a range in AMAs between 3.43 and 3.98 Ga. Thus, it appears that light plains were formed over a wide time range of ~900 Ma from ~3.4–4.3 Ga, which is inconsistent with the hypothesis of a global coeval formation of light plains by either the Nectaris, Imbrium, or Orientale basin.

In addition, many CSFDs of light plains indicate AMAs younger than the Imbrium and Orientale basins and, thus, their origin cannot be related to these basins.

3.2. Basins and craters

3.2.1. Basins. The definition of the lunar chronostratigraphic systems is largely based on the laterally extensive ejecta deposits of Nectaris and Imbrium, and the nature and distribution of the crater ejecta and ray systems of Eratosthenes and Copernicus (e.g., Wilhelms et al. 1987). AMAs were assigned to the chronostratigraphic systems, on the assumptions that specific samples of certain Apollo landing sites represent the ejecta of these basins and craters (e.g., Neukum 1983; Wilhelms et al. 1987; Neukum and Ivanov 1994). However, the link between lunar sample ages and discrete basin forming events is still subject to discussion (e.g., James 1981; Wetherill 1981; Deutsch and Stöffler 1987; Wilhelms et al. 1987; Stadermann et al. 1991; Spudis 1993; Neukum and Ivanov 1994; Stöffler and Ryder 2001; Stöffler et al. 2006; Orgel et al. 2018).

Hiesinger et al. (2011) provide a compilation of literature ages of specific lunar basins. Werner (2014), compiling basin ages from Neukum (1983), Wilhelms et al. (1987), and Fassett et al. (2012) proposed that lunar basins formed between 4.35 and 3.65 Ga. Thus, compared to Mars and Mercury, which have been resurfaced more extensively, the Moon holds the oldest surface record (Werner 2014).

Fassett et al. (2012) measured CSFDs for 30 lunar basins larger than 300 km in diameter. Their results generally confirm the widely used stratigraphic sequence of basins of Wilhelms et al. (1987), although they found 50% higher crater spatial densities than Wilhelms et al. (1987). Compared to the Wilhelms et al. (1987) basin stratigraphy, some of the basins were assigned different positions. For example, in the Fassett et al. (2012) stratigraphy, Serenitatis is older than Nectaris and Humboldtianum is younger than Crisium. Fassett et al. (2012) argued that their data show a transition between two impact crater populations before the mid-Nectarian period, i.e., before the end of the period of rapid cratering and before the putative lunar cataclysm. They also reported that the South Pole–Aitken basin (and many other pre-Nectarian basins) are in saturation equilibrium (Fassett et al. 2012). However, for the South Pole–Aitken (SPA) basin, Hiesinger et al. (2012b), as well as Orgel et al. (2018), demonstrated that this is not the case. On the basis of their CSFD measurements, Hiesinger et al. (2012b) derived a minimum model age of 4.26 Ga for the SPA basin, assuming that craters larger than ~100 km are not in equilibrium. Orgel et al. (2018) published a slightly older model age of 4.31 Ga. On the basis of their study using a buffered non-sparseness correction to reanalyze the Fassett et al. (2012) dataset, Orgel et al. (2018) reordered and dated the basins, and concluded that there is no evidence for two impact crater populations as suggested by Fassett et al. (2012).

Whitten et al. (2011) derived an AMA for the Orientale ejecta (3.68 Ga) and interior melt sheet (3.64 Ga). Cho et al. (2012) reported a CSFD-based AMA for Orientale basin of 3.79 Ga. However, Cho et al.'s (2012) figure 2 indicates that their CSFD measurements might show evidence for resurfacing. Thus, their fitted age might in fact date a younger resurfacing event, rather than the basin forming event. Light plains units, inferred to be associated with the formation of the Orientale basin show AMAs of 3.61 to 3.83 Ga (Meyer et al. 2016).

A new geologic map of the Crisium basin indicates the exposure of potential impact melt remnants of this basin (Spudis and Sliz 2017). Mapping revealed that these fissured, cracked deposits are embayed by subsequent mare basalts, show a lower FeO content than the Crisium basalts, and have orthopyroxene as their major mafic component. However, some of the putative melt remnants appear to be secondary craters, whereas others might be megablocks (van der Bogert et al. 2018a). Their rugged morphology, in combination with their small areal extent only allowed the determination of poorly constrained AMAs (van der Bogert et al. 2018a). The AMA of the largest of these putative impact melts is about 3.94 Ga (van der Bogert et al. (2018a). Neukum (1983) reported an AMA of 3.99 Ga using his 1983

chronology function, while Orgel at al. (2018) proposed an age of 4.07 Ga on the basis of CSFD measurements on the crater rim and ejecta using a buffered non-sparseness correction and the chronology function of Neukum et al. (2001). Updated radiometric ages of Luna 20 samples originally analyzed by Swindle et al. (1991), give ages of 3.88 and 4.10 Ga, the same range as the CSFD-derived ages (van der Bogert et al. 2018a).

3.2.2. Copernicus crater. The Apollo 12 landing site is affected by the deposition of distal ejecta material, most plausibly from Copernicus crater (93 km in diameter) (e.g., Wood et al. 1970; Goles et al. 1971; Hubbard et al. 1971; Schnetzler and Philpotts 1971; Schonfeld and Meyer 1972; Wänke et al. 1972; Huang et al. 2017). On the basis of NAC images, Hiesinger et al. (2012a) found that Copernicus shows an AMA of ~797 Ma and a WAC-derived AMA of 779 Ma. Determining exposure ages of samples 12032 and 12033 collected at Head crater revealed an age of 800–850 Ma (Silver 1971; Eberhardt et al. 1973; Alexander et al. 1976). Support for an age of 800 ± 15 Ma comes from radiometric ages of these samples, including degassing ages of felsite clasts within the ropy glasses (Bogard et al. 1992, 1994; Wentworth et al. 1994). Recent analyses of 21 Apollo 12 regolith samples, including additional analyses of samples 12032 and 12033, yielded degassing ages of 700–800 Ma, which give an estimated 782 ± 21 Ma age for the Copernicus impact event (Barra et al. 2006).

3.2.3. Tycho crater. On the basis of their CSFD measurements on WAC images, Hiesinger et al. (2012a) proposed that 85-km diameter Tycho crater is ~124 Ma old, whereas their CSFD measurements on NAC images indicate a somewhat younger AMA of ~85 Ma, similar to the AMA derived for the landslide at the Apollo 17 landing site, interpreted as being triggered by Tycho secondaries (Wolfe et al. 1975; Lucchitta 1977). Given that the AMAs of the landslide (~85 Ma; Hiesinger et al. 2012a) and the Lee–Lincoln scarp (75–105 Ma; van der Bogert et al. 2012) are very similar, an alternative interpretation of the landslide formation was proposed by van der Bogert et al. (2012) and Schmitt et al. (2017), who argued that the landslide was triggered by the formation of the Lee–Lincoln scarp. Krüger et al. (2016) geologically mapped Tycho crater and derived 17 AMAs for several geologic units, ranging from ~14–82 Ma. They found that the summed CSFDs for the floor of Tycho exhibit an AMA of ~26 Ma. The summed AMA of the ejecta deposit CSFD measurements is ~74 Ma, and the AMAs for the melt pools are 39–47 Ma. This behavior is consistent with target property effects causing a discrepancy between impact melt and ejecta ages (van der Bogert et al. 2010, 2017). From sample exposure ages, Drozd et al. (1977) concluded that Tycho is 109 ± 4 Ma old. This age is identical to that of Guinness and Arvidson (1977) and is similar to an exposure age of 96 ± 5 Ma for the landslide and Central Cluster materials derived by Arvidson et al. (1976).

3.2.5. North Ray crater. Two independent CSFD measurements for 1-km diameter North Ray crater revealed AMAs of 46 and 47 Ma, respectively (Hiesinger et al. 2012a), thus being in excellent agreement with exposure ages of Behrmann et al. (1973; 50.6 Ma), Husain and Schaeffer (1973; 30–50 Ma), Marti et al. (1973; 49 Ma), and Drozd et al. (1974; 50.3 Ma).

3.2.6. Cone crater. The fourth calibration point for the lunar chronology at young ages, i.e., Cone crater (330 m diameter), was investigated by Plescia and Robinson (2011), Robbins (2014), and Hiesinger et al. (2015). Like Plescia and Robinson (2011), Hiesinger et al. (2015) found a significant range in AMAs for the Cone ejecta deposit, ranging from 16–82 Ma. Although this seems to be a worrisome result, exposure ages also show a wide range of 12–95 Ma (Bhandari et al. 1972; Bogard and Nyquist 1972; Burnett et al. 1972; Crozaz et al. 1972; Husain et al. 1972; Lugmair and Marti 1972; York et al. 1972; Stettler et al. 1973; Eugster et al. 1984; Stadermann et al. 1991). The sum of all count areas of Hiesinger et al. (2015) indicates an AMA of 39 Ma; somewhat older than the 25–26 Ma of Moore et al. (1980). The newer CSFD measurements agree in the determination of older AMAs, with the CSFDs of Robbins (2014) and Hiesinger et al. (2015) being basically identical.

3.2.7. Autolycus and Aristillus craters. Rays from Autolycus (39 km in diameter) and Aristillus (55 km in diameter) presumably transported material to the Apollo 15 landing site (e.g., Swann 1986; Wilhelms et al. 1987; Bogard et al. 1990; Ryder et al. 1991), although Russ et al. (1972) did not find evidence of ray material in neutron fluence data. Provided Autolycus and Aristillus materials can be identified and radiometrically dated, this would offer the possibility to add a new calibration point to the lunar chronology when combined with CSFD measurements of these craters (Hiesinger et al. 2016a). Bogard et al. (1990) and Ryder et al. (1991) proposed that the ^{39}Ar–^{40}Ar age of 2.1 Ga derived from three petrologically distinct, shocked Apollo 15 KREEP basalt samples (15434,25, 15434,29, 15358), date Autolycus crater. Aristillus crater is younger than Autolycus crater and a heating event of sample 15405 at 1.29 Ga was interpreted as the age of Aristillus crater (Bernatowicz et al. 1978). This relatively old age is consistent with findings of Hawke et al. (2004) that indicate that the rays of Autolycus and Aristillus are compositional rays and not maturity rays. Aristillus has severely modified Autolycus and its ejecta deposits and on the basis of crater spatial densities, Guinness and Arvidson (1977) argued that Aristillus might even be younger than Copernicus crater. Hiesinger et al. (2016a) dated six regions on the ejecta deposit and the interior of Autolycus crater. The CSFD measurements revealed a wide range of ages between ~0.6 to ~3.80 Ga, which are inconsistent with stratigraphic observations, the AMAs of surrounding basalts, and the sample ages. The CSFDs of Hiesinger et al. (2016a) either imply that the dated samples are not related to Autolycus or that the CSFD measurements are so heavily affected by resurfacing and secondary cratering from Aristillus that they do not represent the formation age of Autolycus. Thus, Hiesinger et al. (2016a) argued that Autolycus should not be used as a calibration point for the lunar chronology function.

The floors of the south polar craters Shackleton (21 km), Faustini (42 km), Haworth (51 km), and Shoemaker (12 km) are permanently shaded regions that contain sequestered volatiles (e.g., Watson et al. 1961; Nozette et al. 1996; Zuber et al. 2012). Tye et al. (2015) dated these craters with CSFD measurements and found that Shackleton crater is ~3.51 Ga old, similar to the age of 3.60/3.69 Ga derived by Zuber et al. (2012). According to Tye et al. (2015), Haworth formed 4.18 Ga ago, Shoemaker formed 4.15 Ga ago, and Faustini crater is 4.10 Ga old. The floors of these craters exhibit ages of 3.46 Ga (Shoemaker), 3.55 Ga (Haworth), 3.50 Ga (Faustini), and 2.63 Ga (Shackleton) (Tye et al. 2015).

Ashley et al. (2012) dated King crater (76 km) to be ~1 Ga old. However, the large Al-Tusi impact melt deposit NW of King crater shows a model age of only 385 Ma. A similar behavior was seen for other lunar craters, i.e., Tycho, Copernicus, Aristarchus, and Jackson craters. CSFD measurements of the Al-Tusi melt deposit NW of King crater as well as Tycho crater revealed characteristic kinks in the cumulative CSFD of craters. At King crater, the CSFD of the smaller craters rolls over to meet the CSFD for the ejecta deposit at larger diameters, once the transition from strength to gravity scaling is apparently completed at diameters of 170–400 m (van der Bogert et al. 2017). Thus, van der Bogert et al. (2017) concluded that the differences in King crater CSFDs most likely result from differences in target properties rather than field and/or self-secondary cratering.

Li et al. (2018) dated two proximal ejecta deposits, four smooth ponds, and one hummocky area of Lalande crater (24 km). The summed AMAs for the ejecta deposits reveal an AMA of 94 Ma, which was interpreted as the formation age of Lalande crater (Li et al. 2018). The summed melt pool AMAs are significantly younger at about 38 Ma, whereas the hummocky terrain shows an AMA of 44 Ma. This behavior is also consistent with target property effects causing a discrepancy between impact melt and ejecta ages (van der Bogert et al. 2017).

Giordano Bruno is a very young 22 km large impact crater that might have formed during historic times (Hartung 1976). Shkuratov et al. (2012) proposed that Giordano Bruno is probably the youngest crater of its size on the Moon and published an age of ~1 Ma.

In addition, it is of particular interest because a ray of this crater affects the Luna 24 landing site (Basilevsky and Head 2012). On the basis of its morphologic prominence, Basilevsky and Head (2012) estimated the age of Giordano Bruno to be "somewhere between 5 and 10 m.y." This age is consistent with a CSFD age of 1–10 Ma (Morota et al. 2009) and the 14.5 ± 1.5 Ma exposure age of cataclastic anorthosite 2460.3–0.05.1, collected at the Luna 24 landing site (Fugzan et al. 1986). Plescia et al. (2010) found a large fraction of small craters superposed on the ejecta of Giordano Bruno to lack ejecta deposits and concluded that they are self-secondaries from the Giordano Bruno impact. They also proposed that if these craters are indeed secondary craters, the age derived by Morota et al. (2009) might be too old and that Giordano Bruno might be a historic crater. However, Basilevsky and Head (2012) pointed out that even if the superposed craters are largely self-secondary craters, this does not require a formation of Giordano Bruno in historic times. On the basis of geochemical data (^{3}He spike, Th content) of lunar meteorites, Fritz (2012) proposed a possible ejection of the meteorites Yamato 82192/82193/86032 by Giordano Bruno about 8.2 Ma ago.

Bell et al. (2012) used Mini-RF data to determine absolute ages of small (< 3 km) craters, which are difficult to date with CSFD measurements because of their small sizes. The investigated craters show radar-bright haloes, which fade with time. On the basis of radar brightness, i.e., the lifetime of the halo, Bell et al. (2012) determined ages of 0.45 to 39 Ma for a total of 8 craters. Individual ages are: 0.45, 4.3, 5.0, 5.0, 7.1, 12.5, 37.0, and 39.0 Ma. For South Ray crater, Bell et al. (2012) reported a radar-brightness age of 1.94 Ma, which compares favorably with the exposure age of 2.01 Ma derived from Apollo 16 samples (Eugster 1999).

Using Diviner thermal radiometer data, Ghent et al. (2014) calculated the rock abundance of nine craters that were previously dated with CSFD measurements (Morota et al. 2009; van der Bogert et al. 2010; Ashley et al. 2012; Hiesinger et al. 2012a) and found a strong correlation between these two parameters (R^2 = 0.96). For North and South Ray, the ages derived by this method compare favorably with exposure ages. In particular, exposure ages indicate an age of 50 Ma for North Ray crater and 2 Ma for South Ray crater (e.g., Arvidson et al. 1975), which are very similar to the ages derived from rock abundance data of 46–80 Ma for North Ray and 7–18 Ma for South Ray crater, respectively (Ghent et al. 2014). Thus, the method of Ghent et al. (2014) might be a new approach in determining surface ages and might be particularly interesting for dating small lunar features that can not be dated with traditional CSFD measurements (Ghent et al. 2014). Cold spot craters are also estimated to represent the population of craters ≲1 Ma. CSFD measurements on the largest cold spot craters (D = 0.8 – 2.3 km), give AMA's 200 ka–1.3 Ma—many of these craters likely represent lunar meteorite source craters based on most meteorite launch ages being < 1.4 Ma. (Williams et al. 2018a,b)

3.3. Volcanic features

In the past decades, several detailed studies on the geologic setting, the composition, morphometry, morphology, and the eruption style of lunar mare and highland domes have been performed (Wagner et al. 1996, 2002; Weitz and Head 1998, 1999; Jolliff et al. 2011; Kiefer 2013; Lawrence et al. 2013; Lena et al. 2013; Hiesinger et al. 2016b; Ivanov et al. 2016a).

3.3.1. Mare domes. Lunar mare domes are generally broad, convex, semi-circular landforms with relatively low topographic relief (e.g., Head and Gifford 1980; Hiesinger et al. 2006b). The Marius Hills consist of more than 100–250 domes and cones (Whitford-Stark and Head 1977; Weitz and Head 1998; Kiefer 2013) and 43 of them have been dated with CSFD measurements by Hiesinger et al. (2016b). The CSFDs of Hiesinger et al. (2016b) exhibit a wide range of AMAs of 1.03 to 3.65 Ga and there is no clear spatial correlation of ages with location of the dated domes/cones, although younger domes appear to occur preferentially in the West whereas older domes are located in the East. Hiesinger et al. (2016b) also performed CSFD measurements for basalts located immediately adjacent to the dated domes.

The 27 dated basalts are 1.20–3.69 Ga old, thus exhibit a similar range than the domes. However, only three of the dated basalts are younger than 3 Ga, whereas most basalts exhibit AMAs of 3–3.5 Ga. Like for the domes, Hiesinger et al. (2016b) did not observe a correlation of AMAs with the geographic position of the dated basalts. Comparing the model ages of the domes with those of the adjacent basalts, Hiesinger et al. (2016b) recognized that most domes post-date the neighboring basalts, supporting an interpretation of the domes as late-stage products of the volcanic activity (e.g., McCauley 1967; Heather et al. 2003) rather than the interpretation that the domes are embayed by the basalts (Weitz and Head 1999). Both data sets indicate that the volcanic activity in the Marius Hills region lasted much longer and is more complex than previously thought (e.g., McCauley 1967; Moore 1967; Whitford-Stark and Head 1977; Heather and Dunkin 2002; Heather et al. 2003; Lawrence et al. 2013) although possible effects of small count area sizes and topography on the determination of AMAs with CSFD measurements must be further explored.

The Mons Rümker region has been visited by the Chinese Chang'E-5 landing mission (Zhao et al. 2017; Qian et al. 2018, 2021a,b; Jia et al. 2020). In the context of characterizing the potential landing site, Zhao et al. (2017) determined AMAs of 7 geologic units on Mons Rümker, including three plateau-forming units, two shallow domes, and two steep-sided domes. On the basis of their study, the AMAs range from 2.91 to 3.71 Ga, with the plateau-forming units exhibiting AMAs of 3.51, 3.58, and 3.71 Ga, the shallow domes showing AMAs of 3.04 and 3.43 Ga, and the steep-sided domes yielding AMAs of 2.91 and 3.04 Ga, respectively. Zhao et al. (2017) proposed that the steep-sided domes might be younger than the shallow domes, but they were careful enough to emphasize that the AMAs of the steep-sided domes might be affected by topography, small count area sizes, and secondary craters differently than the plateau-forming units and the shallow domes. Qian et al. (2018) dated a range of units in the same region and found unit Em4 to be the most extensive (~36,000 km^2) and youngest (~1.21 Ga) mare unit in the area, recommending that this unit be considered for the landing region for the Chang'E-5 sample return mission.

3.3.2. Non-mare domes. Several presumably volcanic features exist on the Moon that have albedos, spectral characteristics, and morphologies that are distinct from mare volcanic deposits. Examples of such non-mare volcanism are the Gruithuisen domes, the Mairan domes and cones, as well as Hansteen Alpha and Helmet. According to CSFD studies by Wagner et al. (1996, 2002), the Gruithuisen domes are contemporaneous with the emplacement of the maria but postdate the formation of post-Imbrium crater Iridum. Contemporaneity with the maria has been interpreted to indicate petrogenetic linkages; one possibility is that mare diapirs stalled at the base of the crust and partially remelted the crust which produced more silicic viscous magmas (e.g., Malin 1974; Head et al. 1998). Ivanov et al. (2016a) proposed that the spatial association of the silicic extrusive Gruithusen domes with highland lava plains might reflect either fractional crystallization in basaltic magma reservoirs or remelting of high-silica crustal materials. Provided the Gruithusen domes were formed by fractional crystallization then the evolved magmas would appear in later stages of volcanic activity whereas if they were formed by remelting, the melts would have formed early in the evolution of the magma (Ivanov et al. 2016a). On the basis of their CSFD measurements, Ivanov et al. (2016a) found the impact melt of Iridum crater to be ~3.9 Ga old, Gruithuisen Gamma and Delta to be ~3.8 Ga old, and the plains surrounding the domes to be ~2.3–3.6 Ga old. Thus, they argued that this sequence of events is more consistent with remelting of crustal material although they realized that this formation mechanism requires preexisting granite-like materials and must account for age differences of hundreds of millions of years between the domes and the adjacent mare basalts (Ivanov et al. 2016a).

A complex stratigraphic relationship of the Mairan middle dome, a lunar red spot of silicic composition, and the surrounding mare basalts was found by Boyce et al. (2017). The dome formed in distinct eruptions between 3.35 and 3.75 Ga, consisting of low FeO, high-

silica eruptions contemporaneous with basaltic eruptions that formed the mare basalts (Boyce et al. 2017). The simultaneous eruption of mare basalts and the Mairan middle dome is rather complex and supports the underplating model for the production of magma that created the red spots (Boyce et al. 2017).

The Compton–Belkovich Volcanic Complex (CBVC) in the northeastern lunar hemisphere exhibits an unusual abundance of Th, which coincides with a broad topographic rise with several superposed domes and cones, high albedo, and a high silica content (e.g., Jolliff et al. 2011; Chauhan et al. 2015; Shirley et al. 2016). Using CSFD measurements, Shirley et al. (2016) proposed that the onset of the volcanism that formed the Compton–Belkovich Volcanic Complex (CBVC) could have occurred as far back as ~3.8 Ga ago. Crater Compton formed about 3.6 Ga ago, followed by a resurfacing event ~3.5 Ga ago and the formation of Hayn crater at about 1 Ga ago. Thus, the CBVC age was bracketed at ~3.5 Ga. For their age determinations, Shirley et al. (2016) used craters larger than ~300 m because smaller craters appear to be in equilibrium.

3.3.3. Pyroclastics. Regional pyroclastic (dark mantle) deposits are extensive (>1000 km) and are often located on the highlands adjacent to younger mare (e.g., Hawke et al. 1979, 1989; Head and Wilson 1980; Gaddis et al. 1985, 2000, 2003; Coombs et al. 1990; Greeley et al. 1993; Weitz et al. 1998; Weitz and Head 1999; Head et al. 2002; Gustafson et al. 2012). In contrast, localized pyroclastic deposits are smaller in extent and are more widely dispersed across the lunar surface (Head 1976; Hawke et al. 1989; Coombs et al. 1990). Pyroclastic deposits are notoriously difficult to date with CSFD measurements because their mantling nature, their subdued crater rims, and their low albedo make it challenging to recognize and measure craters accurately (e.g., van der Bogert et al. 2016). Thus, they are often dated indirectly by deriving AMAs of adjacent geologic units. Lucchitta and Sanchez (1975) investigated dark mantle deposits west of Taurus Littrow and found a paucity of craters <500 m, which they explained by an abnormally high rate of degradation due to the thick, unconsolidated nature of the pyroclastic deposits. Ivanov et al. (2016b) found that pyroclastic deposits in Oppenheimer crater date back to the Nectarian–Lower Imbrian epochs, showing AMAs between 3.66 and 3.98 Ga.

3.3.4. Irregular mare patches. Ina is an enigmatic D-shaped structure that has been known since Apollo 15 high-resolution panoramic camera images became available (e.g., Whitaker 1972; El-Baz 1973; Strain and El-Baz 1980; Schultz et al. 2006; Garry et al. 2012). On the basis of LROC images, Braden et al. (2014) discovered 70 similar features in mare areas on the lunar nearside. Their mare locations, along with their lobate morphology, were used to infer a volcanic origin, hence, they were termed irregular mare patches (IMPs). IMPs have been interpreted as squeezed-up residual lava extruded during magma withdrawal and fragmentation of a solid lava lake surface (Strain and El-Baz 1980; Braden et al. 2014; Head et al. 2016; Stopar et al. 2017), outgassing (Schultz et al. 2006; Stooke 2012), and ancient atypical volcanism (Head et al. 2016). IMPs are relatively small (<5000 m maximum extent) and only three of them, i.e., Ina, Sosigenes, and Cauchy-5 could be dated with CSFD measurements. For these IMPs, Braden et al. (2014) derived extremely young ages of ~18±1 Ma (Sosigenes), ~33±2 Ma (Ina), ~58±4 Ma (Cauchy-5) that challenge our understanding of the thermal history of the Moon and our models of the ascent and eruption of lunar magma.

The young ages have been challenged by Qiao et al. (2017a,b), arguing that very specific target properties might lead to systematically lower AMAs. In particular, Qiao et al. (2017a,b), supported by theoretical studies (Wilson and Head 2017a), proposed that Ina and Sosigenes mounds were composed of ancient extruded magmatic foams developed in the waning stages of pit crater development, and might have porosities of up to 90%. Taking these extreme target properties into account, the Ina and Sosigenes IMPs could be about 3.5 Ga old, thus, being of the same age as the surrounding shield and mare basalts. However, the IMPs are characterized by an extremely sharp and well-preserved lobate morphology that is difficult to explain if they are billions of years old. This characteristic is accounted for in the magmatic foam model (Wilson

and Head 2017a,b) by the physical properties of magmatic foams and their behavior during impact; impact energy partitioning in the foam results in vertical crushing dominating over lateral ejection, accounting both for smaller craters (therefore, producing younger CSFD ages) and significantly impeded lateral transport of ejecta (thus helping to maintain sharp contacts).

Elder et al. (2017) analyzed the thermophysical measurements collected by the LRO Diviner thermal radiometer, and found that (1) the Ina interior is only slightly rockier than the surrounding mature mare regolith, while much less rocky than the ejecta of some ~100 Ma-old craters; furthermore the relatively rocky areas are mainly concentrated along the edges of the interior floor; (2) the surface regolith of the Ina interior is interpreted to be thicker than 10–15 cm; and (3) the Ina interior has slightly lower thermal inertia than the surrounding mare, indicating that the Ina materials are less consolidated or contain fewer small rock fragments than typical regolith; in particular, the largest mound within Ina has the lowest thermal inertia values. These surface physical properties suggest either that Ina is older than its calculated crater retention ages, or that Ina is indeed < 100 Ma old, but its surface accumulates regolith more rapidly than blocky ejecta deposits. Elder et al. (2017) proposed that some form of explosive activity, either pyroclasts deposition (Carter et al. 2013) or another style of outgassing (Schultz et al. 2006) was likely to have been involved in the formation of Ina, though the possibility of lava flow inflation (Garry et al. 2012) or regolith drainage into subsurface void space (Qiao et al. 2017a) could not be precluded; however, the specific formation mechanism and emplacement sequences of the various morphologic units within Ina were not detailed by Elder et al. (2017).

Valantinas et al. (2018) reinvestigated CSFDs of the Nubium and Sosigenes IMPs and derived AMAs of 46 ± 5 Ma for the Nubium IMP and 22 ± 1 Ma for the Sosigenes IMP, similar to the results of Braden et al. (2014). They also performed CSFD measurements for similarly sized close-by mare control areas and several wrinkle ridges and found steep SFDs for all studied areas that indicate that these surfaces are still in production rather than equilibrium as would be expected if the IMPs are indeed several billion years old. In addition, because they all show the same slope, Valantinas et al. (2018) concluded that it is unlikely that the Nubium and Sosigenes IMPs were affected by a unique endogenic process.

3.4 Tectonic features

3.4.1 Lobate scarps. Lobate scarps are compressional tectonic features, which are the surface expression of low angle thrust faults resulting from tidal deformation and interior cooling and contraction of the Moon (Hartmann and Davis 1975; Cameron and Ward 1976; Binder 1982; Watters 2003; Watters et al. 2009, 2010, 2012, 2015; Watters and Johnson 2010; Banks et al. 2012). More than 3,200 lobate scarps have been identified globally on the lunar surface and based on their generally crisp appearance and the absence of superimposed, large-diameter impact craters (> 400 m), lobate scarps are among the youngest landforms on the Moon (< 1 Ga) (Schultz 1976; Binder 1986; Watters et al. 2010; van der Bogert et al. 2012, 2018b; Clark et al. 2014, 2015, 2016, 2017; Senthil Kumar et al. 2016). Using crater degradation measurements on craters transected by or superposed on the scarps, Binder and Gunga (1985) derived ages of 21 lobate scarps, ranging from 60 ± 30 Ma to 680 ± 250 Ma. Similarly, AMAs on the basis of CSFD measurements indicate that the ages of 9 lobate scarps range from 60 to < 600 Ma, implying geologically recent faulting (Clark et al. 2015). This is consistent with the work of Binder and Gunga (1985), Watters et al. (2010), van der Bogert et al. (2012, 2018b), and Clark et al. (2014, 2015). Investigating crater populations of 34 additional lunar scarps revealed model ages of ~24–400 Ma with most scarps forming in the last ~140 Ma (Clark et al. 2017). Combining ages of more than 60 lobate scarps derived by Binder and Gunga (1985), van der Bogert et al. (2012, 2018b), Senthil Kumar et al. (2016) and Clark et al. (2017) indicates that faulting has been active in the last 700 Ma and that the distribution of lobate scarp ages is spatially random across the lunar surface. The majority of derived model ages are relatively closely clustered, implying a short formation period, while a few others exhibited multiple episodes of deformation that lasted several hundred Ma (e.g., Binder and Gunga 1985; Clark et al. 2016).

3.4.2. Wrinkle ridges. Wrinkle ridges are linear to sinuous compressional features that commonly occur in mare basins but rarely also extend into adjacent highlands (e.g., Strom 1972; Bryan 1973; Maxwell et al. 1975; Chicarro and Schultz 1985; Plescia and Golombek 1986; Watters and Johnson 2010). Although it is commonly accepted that wrinkle ridges are tectonic features, the exact mechanism of formation is still debated, including the depth of faulting and whether they reflect thick- or thin-skinned deformation (e.g., Watters 1991; Mangold et al. 1998; Montési and Zuber 2003a,b; Ono et al. 2009; Watters and Johnson 2010; Byrne et al. 2015). In addition, the timing of wrinkle ridge formation has been debated. For example, Fagin et al. (1978) proposed that wrinkle ridges were formed by a late-stage deformation and that ridges in Crisium, Imbrium, Serenitatis, and Tranquillitatis started forming from 3.8–2.5 Ga. Work by Ono et al. (2009) indicates that ridges in Serenitatis formed after 2.84 Ga and Watters and Johnson (2010) suggested that wrinkle ridges formed as recently as 1.2 Ga ago. Daket et al. (2016) studied the timing of tectonic features in the northwestern part of the Imbrium basin and found that lobate scarps, wrinkle ridges, and graben are significantly younger than the basalts on which they are located. Daket et al. (2016) concluded that Copernican features are dominant in their study region and that the formation of such young features cannot be explained by basin loading. Instead, they proposed a reactivation of preexisting zones of weaknesses that were originally formed during the basin impact event (Daket et al. 2016). Applying the buffered crater counts method (Kneissl et al. 2011, 2015), Yue et al. (2017) determined wrinkle ridge model ages for several mare areas, including Oceanus Procellarum, Imbrium, Serenitatis, Crisium, Frigoris, Nubium, Tranquillitatis, Fecunditatis, and Humorum. The results demonstrate that typical lunar wrinkle ridge groups have average ages from the late Imbrian to the early Eratosthenian, i.e., from 3.5 to 3.1 Ga (Yue et al. 2017). Comparing their wrinkle ridge ages with the ages of the surrounding basalts (Hiesinger et al. 2000, 2003, 2006b, 2011), Yue et al. (2017) found that the wrinkle ridges formed 0.1–0.7 Ga after the eruption of the basalts, thus, being consistent with local stress fields induced by loading of the basin with basalt fill. AMAs of wrinkle ridges in Tranquillitatis (2.4 Ga), however, were formed about 1.4 Ga after the basalt emplacement and as such differ from the trend seen elsewhere. This might imply a different stress mechanism having acted in this basin (Yue et al. 2017).

4. IMPLICATIONS FOR LUNAR HISTORY AND EVOLUTION

4.1. Volcanism

CSFD measurements of numerous volcanic units on the Moon indicate a long record of volcanic activity. Early volcanic activity is expressed as cryptomaria (e.g., Schultz and Spudis 1979, 1983; Hawke and Bell 1981; Bell and Hawke 1984; Head and Wilson 1992; Antonenko et al. 1995; Antonenko and Yingst 2002; Whitten and Head 2015a,b), which have ages and stratigraphic relationships that imply that volcanism started prior to the emplacement of the oldest dated basalts at ~4 Ga (Hiesinger et al. 2011; Head and Wilson 2017), indicating that the total duration of active volcanism on the Moon lasted more than ~3 Ga. The lunar meteorite Kalahari 009 might represent a very-low-Ti cryptomare basalt (Terada et al. 2007). Radiometric U–Pb age dating of phosphate grains associated with basaltic clasts in this meteorite revealed that lunar volcanism was already active at least 4.35 Ga ago (Terada et al. 2007). In addition, lunar meteorites Miller Range 13317 and Kalahari 009 show evidence for ancient volcanic activity 4332 ± 2 Ma and 4369 ± 7 Ma ago (Snape et al. 2018).

Young ages of some basalts on the lunar surface are supported by crater degradation ages of Boyce (1976) and Boyce and Johnson (1978), crater counts by Schultz and Spudis (1983), several lunar meteorites that have ages of ~2.7–3.0 Ga (Fagan et al. 2002; Fernandes et al. 2003; Anand et al. 2006; Fernandes and Burgess 2006; Borg et al. 2007; Rankenburg et al. 2007), and geophysical models of the thermal history of the Moon (Ziethe et al. 2009).

For example, the youngest age group of Boyce (1976) and Boyce and Johnson (1978), represents an age of 2.5 ± 0.5 Ga and the Lichtenberg basalt might be as young as 900 Ma (Schultz and Spudis 1983). Young ages often occur in areas elevated in heat-producing elements suggesting a complex and diverse history of the thermal evolution of the interior of the Moon.

The evolution of the near- and farside volcanism is relatively similar in that major volcanic activity occurred between 3.2 Ga and 3.6 Ga and around 2.2 Ga (Hiesinger et al. 2011; Pasckert et al. 2018). The volcanic activity was more abundant and lasted longer on the nearside compared to the farside and this might have multiple reasons. For example, stripping of insulating crust (Ziethe et al. 2009) by the large SPA-forming impact event, in combination with lower amounts of heat producing elements such as Th, might have contributed to the observed asymmetry. In addition, the absence of weaknesses on the farside due to the absence of a sufficiently large impact basin (SPA-sized) on the nearside (Schultz and Crawford 2011) might have also played a role in the reduced and shorter volcanic activity in the SPA basin (Pasckert et al. 2018). Among others, a study by Taguchi et al. (2017) indicated that the minimum crustal thicknesses beneath the lunar basins might have been a dominant factor for magma eruption. Thus, the hemispherically asymmetric distribution of maria might be related to differences in crustal thicknesses as well as differences in produced magma volumes.

The extremely young AMAs of irregular mare patches and their small volumes (Braden et al. 2014) are at odds with our understanding of the thermal evolution of the Moon (e.g., Ziethe et al. 2009) and our understanding of the ascent and eruption mechanism of magma (e.g., Head and Wilson 1992, 2017). To explain the seemingly young AMAs, Qiao et al. (2017a,b) proposed specific physical lava properties (i.e., high porosity) that would affect the crater size and, thus, the derived AMAs.

Age relationships between high- and low-Ti basalts and their implications for the structure, composition, and thermal evolution of the mantle and the source regions of the basalts are discussed in detail in Head et al. (2023, this volume).

Studies of domes and surrounding mare basalts indicate complex stratigraphic relationships (e.g., Lawrence et al. 2013; Hiesinger et al. 2016b). Remote-sensing results indicate that the Marius Hills domes share the same basaltic composition than the surrounding mare basalts and are not silicic in nature (e.g., Weitz and Head 1999; Heather et al. 2003; Besse et al. 2011; Lawrence et al. 2013). Lawrence et al. (2013) interpreted the morphology, morphometry, and mineralogy of the Marius Hills to be consistent with basaltic effusions, and domes being formed by rough, blocky lava flows, with typically thinner and shorter flows interpreted to indicate relatively lower effusion rates and increased late-stage viscosity. In the Marius Hills region, many flows originate at breached cones, which are superposed on domes, implying a synchronous formation of cones and lobate flows during the last stages of Marius Hills volcanism (Lawrence et al. 2013; Head and Wilson 2017). Together with the non-silicic nature of the domes, this was interpreted as evidence against the differentiation hypothesis of McCauley (1967), although CSFD measurements of Hiesinger et al. (2016b) seem to indicate that dome formation lasted longer than the production of mare basalts. In particular, on the basis of their CSFD measurements for 43 low shields, Hiesinger et al. (2016b) determined a wide range of AMAs of 1.03 to 3.65 Ga. They also performed CSFD measurements for 27 basalts occurring immediately adjacent to the dated low shields. The dated basalts showed AMAs of 1.20–3.69 Ga, thus a similar range than for the low shields. However, only three of the dated basalts are younger than 3 Ga, with the remaining 24 basalt units exhibiting AMAs of 3–3.5 Ga.

Pyroclastic deposits were found to often be older than mare basalts in their vicinity (Head 1974; Hiesinger et al. 2000) and this might be consistent with an initial pressure release from overpressurized dikes (e.g., Head and Wilson 1992, 2017; Wilson and Head 2016, 2018) because Wilson and Head (2003a,b) proposed that gas concentrated in a low-pressure micro-environment at the tip of a dike propagating rapidly from a magma reservoir to the surface.

In summary, the wide variety of lunar volcanic deposits in eruption style (effusive and explosive), composition, AMAs, and physical properties are evidence for a complex evolution and history of the Moon. The reader is referred to Head et al. (2023, this volume) for further information on lunar volcanism.

4.2. Tectonism

Several studies revealed that small-scale lobate scarps formed within the last few hundred million years and that their spatial distribution is most consistent with a compressive stress field in response to cooling and shrinking of the Moon as well as tidal deformation. There are at least two competing models of the initial thermal conditions of the Moon (e.g., Clark et al. 2017), both of which make very specific predictions for the timing, duration, and extent of lunar scarp formation. These are (1) the initially totally molten Moon (ITM) (e.g., Runcorn 1977; Runcorn et al. 1977; Binder and Lange 1980) and (2) the lunar magma ocean (LMO) (e.g., Solomon and Chaiken 1976; Solomon and Head 1979). The ITM predicts that after formation, the Moon was in a hot initial state, either near or above the basalt solidus (Pritchard and Stevenson 2000). Thus, the model predicts that lunar thrust faults should be young (< 1 Ga). In this model, trust faults were created by horizontal compressional stresses of up to 350 Mpa in the outer megaregolith, with radial contraction of up to 5 km and increasing thrust faulting with time (Binder 1982; Binder and Gunga 1985). The LMO model predicts that immediately after its formation, the Moon had a hot magma ocean with depths between 300–500 km and a cool interior at 1700–1800 K (Solomon and Chaiken 1976; Solomon and Head 1979). The model predicts that global stresses in the outer crust should today be less than 100 Mpa and insufficient to initiate global scale thrust faulting (Solomon and Head 1979; Turcotte and Schubert 2014). Thrust faulting in this model is localized, mainly around maria, does not occur in the highlands, and is limited to the early lunar geologic history (> 3 Ga) (Solomon and Chaiken 1976). The absence of compressional tectonic features might be explained by the fact that more stress is required for faults to slip in the highlands versus the maria, as the highly brecciated material in the highlands would need to first compact before thrust faulting can occur (Clark et al. 2017). Although these predictions can be tested, the results are somewhat ambiguous. For example, the identification of lobate scarps in the highlands appears to be inconsistent with the LMO. To initiate faulting in the highlands, compressive stresses larger than those produced by the LMO model are required and can be achieved with the ITM model. However, Banks et al. (2012) determined compressional stresses of ~16 Mpa for the highland scarps. Such stress values are too low for the ITM model but are consistent with the LMO model (Clark et al. 2017). Many researchers (e.g., Binder and Gunga 1985; Watters et al. 2010, 2015; van der Bogert et al. 2012, 2018b; Clark et al. 2017), applying various dating techniques, agree that lunar lobate scarps are rather young geologic features, probably less than 700 Ma. Watters et al. (2010, 2012) argued that the low stress levels derived for the young scarps and their sizes are more consistent with thermal models for the early Moon that predict relatively low levels of global compression (< 100 Mpa; radius change of ±1 km in the past 3.8 Ga), i.e., the LMO model.

In summary, although we cannot currently distinguish between the two thermal models on the basis of the available data, the crisp appearance and the young AMAs of lobate scarps are consistent with late-stage horizontal crustal shortening due to tidal stresses and global contraction of the Moon by secular cooling (e.g., Watters et al. 2015). Investigating the timing of tectonic deformation will ultimately allow us to better understand the thermal evolution of the Moon and these studies have been largely overlooked so far. (Nahm et al. 2023, this volume) provides a more detailed discussion of lunar tectonism.

4.3. Cataclysm

Almost 50 years after being first proposed by Tera et al. (1973), the existence of a lunar cataclysm (i.e., an unusually high impact bombardment) is still debated (e.g., Tera et al. 1973,

1974; Baldwin 1974, 1987, 2006; Wasserburg et al. 1974; Hartmann 1975, 2003; Grinspoon 1989; Neukum and Ivanov 1994; Cohen et al. 2000; Stöffler and Ryder 2001; Chapman et al. 2007; Hartmann et al. 2007; Bottke et al. 2012; Morbidelli et al. 2012b; Fernandes et al. 2013; Geiss and Rossi 2013; Norman and Nemchin 2014; Boehnke and Harrison 2016; Frey 2016; Michael et al. 2018; Morbidelli et al. 2018). Tera et al. (1973) compared Apollo 16 Rb–Sr and U–Th–Pb ages to those of Apollo 12, 14, and 15 and found evidence for extensive melting and metamorphism at ~3.95 Ga ago, which they interpreted as (1) the Imbrium ejecta deposit having affected all the studied rocks or (2) a major peak in impact rate. Baldwin (1974) carefully reviewed the arguments for a cataclysm and concluded that the emplacement of the Imbrium basin is responsible for the peak in radiometric ages.

Lunar meteorites are likely to be random samples from the lunar surface and thus provide new information on the cataclysm. If the spike in ages at 3.9–4.0 Ga is also identified in the meteorites, this would support the cataclysm hypothesis whereas the absence of such a spike would argue for a sample bias introduced by the collection of Imbrium ejecta material and thus negate the existence of the cataclysm. Cohen et al. (2000) reexamined several lunar meteorites and although they did not observe a spike, they proposed that the absence of impact melts older than 3.92 Ga supports the cataclysm hypothesis. However, this idea has been questioned, for example, by Michael et al. (2018) who did not find a spike in ages at 3.9–4.0 Ga ago and concluded that studies on lunar meteorites as well as extensive CSFD measurements do not support the classical lunar cataclysm, i.e., an unusual high impact rate between 3.9 and 4.0 Ga ago (e.g., Michael et al. 2018).

On the basis of numerical models and mass accretion arguments, Bottke et al. (2007) and Ryder (2002) argued that the decay of accretional leftovers is inconsistent with the late formation times of lunar basins and a steady decline in impact rate. The so-called "Nice-Model" is an elegant way to explain the putative lunar cataclysm (e.g., Morbidelli et al. 2001, 2005; Gomes et al. 2005; Tsiganis et al. 2005; Bottke et al. 2007). The Nice models assume a migration of the giant planets that would disturb the asteroid belt, resulting in a massive delivery of planetesimals to the inner Solar System that could have caused the cataclysm (e.g., Gomes et al. 2005). Although the numerical calculations strongly depend on the parameters chosen, some Nice models (e.g., Gomes et al. 2005) predict a sharp increase in impact rate caused by a Jupiter–Saturn 2:1 mean motion resonance, consistent with the cataclysm hypothesis.

Recently, Morbidelli et al. (2018) revisited their earlier work (Morbidelli et al. 2012a,b) that attempted to derive a numerical model that is compatible with both the lunar crater record in the 3–4 Ga period and the abundance of highly siderophile elements (HSE) in the lunar mantle. The new study indicates that under the traditional assumption that the HSEs record the total amount of material accreted by the Moon since its formation, only the cataclysm scenario can explain the data. However, Morbidelli et al. (2018) also evaluated a scenario in which the HSEs are sequestered from the mantle during magma ocean crystallization, due to iron sulfide exsolution (O'Neil 1991; Rubie et al. 2015). Assuming that the lunar magma ocean crystallized about 100–150 Ma after Moon formation (Elkins-Tanton et al. 2011), and therefore that HSEs accumulated in the lunar mantle only after this timespan, Morbidelli et al. (2018) showed that the bombardment in the 3–4 Ga period can be explained in the accretion tail scenario. Not only does this scenario not require a cataclysm, it would explain why the Moon appears to be depleted in HSEs relative to the Earth (Morbidelli et al. 2018).

Osinski et al. (2023, this volume) and Cohen et al. (2023, this volume) offer further insight into impact cratering processes, including the cataclysm.

4.4. Recent impact rate

Several studies suggest periodic impact rate variations caused by cometary showers due to perturbation of the Oort cloud by galactic tides, the passage of the Solar System near a molecular

cloud, or an unseen star (e.g., Davis et al. 1984; Rampino and Stothers 1984; Napier 1998; Gardner et al. 2011). In addition, Rampino and Stothers (1984) and Napier (1998) proposed that vertical oscillations of the Sun about the galactic mid-plane with a period of 52–74 Ma would cause variations in the impact rate. However, on the basis of an in-depth study of all available data, Bailer-Jones (2011) did not identify any periodicity, similar to results of Grieve (1991) and Jetsu and Pelt (2000). Bailer-Jones (2011) argued that most studies that claim a periodicity in the impact rate suffer from problems in their methodology, including misinterpretations of statistical probabilities (*p*-values), overestimating the significance of periodogram peaks, or failing to consider a sufficient set of models. On the basis of the four data points for Copernicus, Tycho, North Ray, and Cone craters, Neukum (1983) and Neukum et al. (2001) postulated a constant lunar impact rate for the last 3 Ga. Remeasured CSFDs for these craters (Hiesinger et al. 2012a, 2015) are generally consistent with a constant impact rate, thus supporting the conclusions of Grieve (1991), Jetsu and Pelt (2000), and Bailer-Jones (2011). However, with only four data points it is impossible to exclude short-term episodic variations in the cratering rate between the four anchor points. However, observation of newly formed impact craters since orbit insertion of the Lunar Reconnaissance Orbiter in 2009 (Speyerer et al. 2016) are in general agreement with models of the recent impact rate (e.g., Neukum et al. 2001). Although Speyerer et al. (2016) found 33% more craters larger than 10 m than predicted by the Neukum et al. (2001) production and chronology function, the contemporary crater production rate is within the uncertainties of the Neukum et al. (2001) PF. Speyerer et al. (2016) argued that this finding is consistent with a uniform cratering rate over recent geologic time. Alternatively, it has been argued that the impact flux might have increased at the end of the Paleozoic (e.g., Mazrouei et al. 2019). Further information on the impact rate is provided by (Cohen et al. 2023; Osinski et al. 2023, both this volume).

4.5. Interior/thermal evolution

Basalt ages as young as 1.2 Ga have been identified in the general area of the Procellarum-KREEP-Terrane (PKT). New thermal conduction models suggest that a concentration of heat-producing elements in the lower crust beneath the PKT could result in continued melting of the underlying mantle over much of lunar history (Wieczorek and Phillips 2000; Laneuville et al. 2013). Three-dimensional mantle convection models taking into account the isolating effects of the porous megaregolith with a low thermal conductivity demonstrated that the melting zone could have lasted up to about 2 Ga ago (Ziethe et al. 2009), thus potentially explaining the eruption of the youngest mare basalts. Alternatively, Spohn et al. (2001) proposed that extremely high initial mantle temperatures and/or large amounts of heat-producing elements could maintain a partially molten zone as the source region for the young mare basalts. While thermal models can explain volcanic eruption on the Moon until about 1–2 Ga ago, they fail to explain the young volcanism that is interpreted to have produced the irregular mare patches a few tens of millions years ago (e.g., Braden et al. 2014). Others have pointed out that at this recent point in time, the compressional stress field initiated by secular cooling of the Moon and the thickness of the lunar lithosphere were sufficiently large to terminate any volcanic eruption onto the lunar surface (e.g., Head and Wilson 1992, 2017; Wilson and Head 2017b). For further information, refer to Nahm et al. (2023, this volume).

In conclusion, CSFD measurements and derived AMAs and products provide important insight into the geologic and thermal evolution of the Moon. Upcoming lunar missions with in-situ dating capabilities or sample return will allow us to further test and possibly improve the PF and CF. Thus, we will not only better understand our closest neighbor but from application of these two functions will also learn much more about the timing of geologic processes on other planetary objects.

REFERENCES

Alexander EC Jr, Bates A, Coscio MR Jr, Dragon JC, Murthy VR, Pepin RO, Venkatesan TR (1976) K/Ar dating of lunar soils II. Proc Lunar Planet Sci Conf 7:625–648

Anand M, Taylor LA, Floss C, Neal CR, Terada K, Tanikawa S (2006) Petrology and geochemistry of LaPaz Icefield 02205: A new unique low-Ti mare-basalt meteorite. Geochim Cosmochim Acta 70:246–264

Antonenko I, Yingst RA (2002) Mare and cryptomare deposits in the Schickard region of the Moon: New measurements using Clementine FeO data. Lunar Planet Sci Conf 33:#1438

Antonenko I, Head JW, Mustard JF, Hawke BR (1995) Criteria for the detection of lunar cryptomaria. Earth, Moon Planets 69:141–172

Arthur DWG (1963) The system of lunar craters, quadrant I. Tucson, University of Arizona Press

Arthur DWG, Agnieray AP, Horvath RA, Wood CA, Chapman CR (1965a) The system of lunar craters, quadrant II. Comm Lunar Planet Lab 3:1–2

Arthur DWG, Agnieray AP, Pellicori RA, Wood CA, Weller T (1965b) The systems of lunar craters, quadrant III. Comm Lunar Planet Lab 3:61–62

Arthur DWG, Pellicori RH, Wood CA (1966) The system of lunar craters, quadrant IV. Comm Lunar Planet Lab 5:1–2

Arvidson R, Crozaz B, Drozd RJ, Hohenberg CM, Morgan CJ (1975) Cosmic ray exposure ages of features and events at the Apollo landing sites. The Moon 13:259–276

Arvidson R, Drozd RJ, Guinness E, Hohenberg CM, Morgan CJ, Morrison RH, Oberbeck VR (1976) Cosmic ray exposure ages of Apollo 17 samples and the age of Tycho. Proc Lunar Planet Sci Conf 7:2817–2832

Ashley JW, Robinson MS, Hawke BR, van der Bogert CH, Hiesinger H, Sato H, Speyerer EJ, Enns AC, Wagner RV, Young KE, Burns KN (2012) Geology of the King crater region—New insights into impact melt dynamics on the Moon, J Geophys Res 117:E00H29

Bailer-Jones CAL (2011) Bayesian time series analysis of terrestrial impact cratering. Mon Not R Astron Soc 416:1163–1180

Baldwin RB (1964) Lunar crater counts. Astron J 69:377–392

Baldwin RB (1971) On the history of lunar impact cratering: The absolute time scale and the origin of planetesimals. Icarus 14:36–52

Baldwin RB (1974) Was there a "Terminal Lunar Cataclysm" 3.9–4.0×10^9 years ago? Icarus 23:157–166

Baldwin RB (1987) On the relative and absolute ages of seven lunar front face basins: II. From crater counts. Icarus 71:19–29

Baldwin RB (2006) Was there ever a terminal lunar cataclysm?: With lunar viscosity arguments. Icarus 184:308–318

Bandfield JL, Cahill JTS, Carter LM, Neish CD, Patterson GW, Williams J-P, Paige DA (2017) Distal ejecta from lunar impacts: Extensive regions of rocky deposits. Icarus 283:282–299

Banks ME, Watters TR, Robinson MS, Tornabene LL, Tran T, Ojha L, Williams NR (2012) Morphometric analysis of small-scale lobate scarps on the Moon using data from the Lunar Reconnaissance Orbiter. J Geophys Res 117:E00H11

Barra F, Swindle TD, Korotev RL, Jolliff BL, Zeigler RA, Olson E (2006) $^{40}Ar/^{39}Ar$ dating of Apollo 12 regolith: Implications for the age of Copernicus and the source of nonmare materials. Geochim Cosmochim Acta 70:6016–6031

Basaltic Volcanism Study Project (BVSP) (1981) Basaltic Volcanism on the Terrestrial Planets. Pergamon New York

Basilevsky AT (1976) On the evolution rate of small lunar craters. Proc Lunar Planet Sci Conf 7:1005–1020

Basilevsky AT (2015) Assessment of the absolute age of impact craters of the Moon, Mercury, and Mars by their morphological severity. *In:* Proc. Fourth Int. Symp. on the Study of Solar System "Studies of the Solar System: Space Milestones," Moscow, October 14–18 2013. Zakharov AV (Ed.) p. 213–228, Space Research Institute, Moscow (in Russian)

Basilevsky AT, Head JW (2012) Age of Giordano Bruno crater as deduced from the morphology of its secondaries at the Luna 24 landing site. Planet Space Sci 73:302–309

Basilevsky AT, Kreslavsky MA, Karachevtseva IP, Gusakova EN (2014) Morphometry of small impact craters in the Lunokhod-1 and Lunokhod-2 study areas. Planet Space Sci 92:77–87

Basilevsky AT, Kozlova NA, Zavyalov IY, Karachevtseva IP, Kreslavsky MA (2018) Morphometric studies of the Copernicus and Tycho secondary craters on the Moon: Dependence of crater degradation rate on crater size. Planet Space Sci 162:31–40

Behrmann C, Grozaz G, Drozd R, Hohenberg C, Ralston C, Walker R, Yuhas D (1973) Cosmic-ray exposure history of North Ray and South Ray material. Proc Lunar Sci Conf 4:1957–1974

Bell JF, Hawke BR (1984) Lunar dark-haloed impact craters: Origins and implications for early mare volcanism. J Geophys Res 8:6899–6910

Bell SW, Thomson BJ, Dyar MD, Neish CD, Cahill JTS, Bussey DBJ (2012) Dating small fresh craters with mini-RF radar observations of ejecta blankets. J Geophys Res 117:E00H30

Bernatowicz TJ, Hohenberg CM, Hudson B, Kennedy BM, Podosek FA (1978) Argon ages for lunar breccias 14064 and 15405. Proc Lunar Planet Sci Conf 9:905–919

Besse S, Sunshine JM, Staid MI, Petro NE, Boardman JW, Green RO, Head JW, Isaacson PJ, Mustard JF, Pieters CM (2011) Compositional variability of the Marius Hills complex from the Moon Mineralogy Mapper (M3). J Geophys Res 116:E00G13

Bhandari N, Goswami JN, Gupta SK, Lal D, Tamhane AS, Venkatavaradan VS (1972) Collision controlled radiation history of the lunar regolith. Proc Lunar Planet Sci Conf 3:2811–2829
Bierhaus EB, Chapman CR, Merline WJ (2005) Secondary craters on Europa and implications for cratered surfaces. Nature 437:1125–1127
Bierhaus EB, McEwen AS, Robbins SJ, Singer KN, Dones L, Kirchoff MR, Williams J-P (2018) Secondary craters and ejecta across the solar system: Populations and effects on impact-crater-based chronologies. Meteoritic Planet Sci 53:638–671
Binder AB (1982) Post-Imbrium global lunar tectonics: Evidence for an initially totally molten Moon. The Moon 26:117–133
Binder, AB (1986) The initial thermal state of the Moon. Proc Origin of the Moon Conf:425
Binder AB, Gunga HC (1985) Young thrust-fault scarps in the highlands: Evidence for an initially totally molten Moon. Icarus 63:421–441
Binder AB, Lange MA (1980) On the thermal history, thermal state, and related tectonism of a Moon of fission origin. J Geophys Res 85:3194–3208
Bloch M, Fechtig H, Funkhouser J, Gentner W, Jessberger E, Kirsten T, Müller O, Neukum G, Schneider E, Steinbrunn F, Zähringer J (1971) Meteorite impact craters, crater simulations and the meteoric flux in the early Solar System. Lunar Planet Sci Conf 2:164–165
Boehnke P, Harrison TM (2016) Apparent late heavy bombardments. Annu Meeting Meteor Soc 79:#6039
Bogard DD, Nyquist LE (1972) Noble gas studies on regolith materials from Apollo 14 and 15. Proc Lunar Planet Sci Conf 3:1797–1819
Bogard DD, Ryder G, Garrison D (1990) A major ~2.1 Ga impact event recorded in some Apollo 15 KREEP basalts: Autolycus? Lunar Planet Sci Conf 21:105–106
Bogard DD, Garrison DH, McKay DS, Wentworth SJ (1992) The ages of Copernicus: New evidence for 800±15 million years. Lunar Planet Sci Conf 23:133–134
Bogard DD, Garrison DH, Shih CY, Nyquist LE (1994) ^{40}Ar–^{39}Ar dating of two lunar granites: The age of Copernicus. Geochim Cosmochim Acta 58:3093–3100
Borg LE, Gaffney A, DePaolo D (2007) Rb–Sr and Sm–Nd isotopic systematics of NWA 032. Annu Meteor Soc Meeting 70:#5232
Borisov D, Hiesinger H, Iqbal W, van der Bogert CH (2019) Revised crater size–frequency distribution measurements at the Apollo 14 landing site. Lunar Planet Sci Conf 50:#2323
Bottke J, William F, Durda DD, Nesvorný D, Jedicke R, Morbidelli A, Vokrouhlický D, Levison, HF (2005) Linking the collisional history of the main asteroid belt to its dynamical excitation and depletion. Icarus 179:63–94
Bottke WF, Vokrouhlický D, Nesvorný D (2007) An asteroid breakup 160 Myr ago as the probable source of the K/T impactor. Nature 449:48–53
Bottke WF, Vokrouhlický D, Minton D, Nesvorný D, Morbidelli A, Brasser R, Simonson B, Levison HF (2012) An Archaean heavy bombardment from a destabilized extension of the asteroid belt. Nature 485:78–81
Boyce JM (1976) Ages of flow units in the lunar nearside maria based on Lunar Orbiter IV photographs. Proc Lunar Sci Conf 7:2717–2728
Boyce JM, Dial AL Jr (1975) Relative ages of flow units in Mare Imbrium and Sinus Iridum. Proc Lunar Planet Sci Conf 6:2585–2595
Boyce JM, Johnson DA (1978) Ages of flow units in the far eastern maria and implications for basin-filling history. Proc Lunar Planet Sci Conf 9:3275–3283
Boyce JM, Giguerre T, Mouginis-Mark P, Glotch T, Taylor GJ (2017) Geology of Mairan middle dome. Lunar Planet Sci Conf 48:#1036
Braden SE, Stopar JD, Robinson MS, Lawrence SJ, van der Bogert CH, Hiesinger H (2014) Evidence for basaltic volcanism on the Moon within the past 100 million years. Nat Geosci 7:787–791
Bryan WB (1973) Wrinkle-ridges as deformed surface crust on ponded mare lava. Proc Lunar Planet Sci Conf 4:93–106
Bugiolacchi RP, Guest JE (2008) Compositional and temporal investigation of exposed lunar basalts in the Mare Imbrium region. Icarus 197:1–18
Bugiolacchi RP, Spudis P, Guest JE (2006) Stratigraphy and composition of lava flows in Mare Nubium and Mare Cognitum. Meteoritics 41:285–304
Burgess R, Turner G (1998) Laser ^{40}Ar–^{39}Ar age determinations of Luna 24 mare basalts. Meteoritics 33:921–935
Burnett DS, Huneke JC, Podosek FA, Russ GP, Turner G, Wasserburg GJ (1972) The irradiation history of lunar samples. Lunar Planet Sci Conf 3:105–107
Byrne PK, Klimczak C, McGovern PJ, Mazarico E, James PB, Neumann GA, Zuber MT, Solomon SC (2015) Deep-seated thrust faults bound the Mare Crisium lunar mascon. Earth Planet Sci Lett 427:183–190
Cameron AGW, Ward WR (1976) The origin of the Moon. Lunar Planet Sci Conf 7:120–122
Carter LM, Ghent RR, Bandfield, JL (2013) Measurements of the near-surface column structure of lunar pyroclastic deposits. Am Astro Soc Div Planet Sci Meeting 45:107.01
Chao ECT, Soderblom LA, Boyce JM, Wilhelms DE, Hodges CA (1973) Lunar light plains deposits (Cayley Formation) – A reinterpretation of origin. Lunar Planet Sci Conf 4:127–128
Chapman CR (2015) A critique of methods for analysis of crater size–frequency distributions. Workshop on Issues in Crater Studies and Dating of Planetary Surfaces, LPI Contribution 1841:#9039
Chapman CR, McKinnon WB (1986) Cratering of planetary satellites. *In:* Satellites. Burns JA, Matthews MS (eds) Univ of Arizona Press, Tucson, p 529–533

Chapman CR, Cohen BA, Grinspoon DH (2007) What are the real constraints on the existence and magnitude of the late heavy bombardment? Icarus 189:233–245
Chauhan M, Bhattacharya S, Saran S, Chauhan P, Dagar A (2015) Compton–Belkovich Volcanic Complex (CBVC): An ash flow caldera on the Moon. Icarus 252:115–129
Chicarro AF, Schultz PH (1985) Global and regional ridge patterns on Mars. Icarus 63:153–174
Cho Y, Morota T, Haruyama J, Yasui M, Hirata N, Sugita S (2012) Young mare volcanism in the Orientale region contemporary with Procellarum KREEP Terrane (PKT) volcanism peak period ~2 billion years ago. Geophys Res Lett 39:L11203
Clark JD, Hurtado JM, Hiesinger H, van der Bogert CH (2014) Investigation of lobate scarps: Implications for the tectonic and thermal evolution of the Moon. Lunar Planet Sci Conf 45:#2048
Clark JD, van der Bogert CH, Hiesinger H (2015) How young are lunar lobate scarps? Lunar Planet Sci Conf 46:#1730
Clark JD, van der Bogert CH, Hiesinger H (2016) An in-depth investigation of the Mandel'shtam lobate scarp complex, Lunar Planet Sci Conf 47:#2956
Clark JD, Hurtado JM, José M, Hiesinger H, van der Bogert CH, Bernhardt H (2017) Investigation of newly discovered lobate scarps: Implications for the tectonic and thermal evolution of the Moon. Icarus 298:78–88
Cohen BA, Swindle TD, Kring DA (2000) Support for the lunar cataclysm hypothesis from lunar meteorite impact melt ages. Science 290:1754–1756
Cohen BA, van der Bogert CH, Bottke WF, Curran NM, Fassett CI, Hiesinger H, Joy KH, Mazrouei S, Nemchin A, Neumann GA, Norman MV, Zellner NEB (2023) Impact history of the Moon. Rev Mineral Geochem 89:373–400
Coombs CR, Hawke BR, Peterson CA, Zisk SH (1990) Regional pyroclastic deposits in the north-central portion of the Lunar Nearside. Lunar Planet Sci Conf 21:228–229
Crater Analysis Techniques Working Group (1979) Standard techniques for presentation and analysis of crater size–frequency data. Icarus 37:467–474
Crozaz G, Drozd R, Hohenberg CM, Hoyt HP, Ragan D, Walker RM, Yuhas D (1972) Solar flare and galactic cosmic-ray studies of Apollo 14 and 15 samples. Proc Lunar Planet Sci Conf 3:2917–2931
Ćuk M, Gladman BJ, Stewart ST (2010) Constraints on the source of lunar cataclysm impactors. Icarus 207:590–594
Daket Y, Yamaji A, Sato K, Haruyama J, Morota T, Ohtake M, Matsunaga T (2016) Tectonic evolution of northwestern Imbrium of the Moon that lasted in the Copernican Period. Earth Planet Space 68:157
Dalrymple GB (1991) The Age of the Earth. Stanford University Press
Dasch EJ, Shih C-Y, Bansal BM, Wiesmann H, Nyquist LE (1987) Isotopic analysis of basaltic fragments from lunar breccia 14321: Chronology and petrogenesis of pre-Imbrium mare volcanism. Geochim Cosmochim Acta 51:3241–3254
Davis DR, Chapmann CR, Weidenschilling SJ, Greenberg R (1984) Asteroid collisional evolution studies. Lunar Planet Sci Conf 15:192–193
Deutsch A, Stöffler D (1987) Rb-Sr analyses of Apollo 16 melt rocks and a new age estimate for the Imbrium basin*:* Lunar basin chronology and the early heavy bombardment of the Moon. Geochim Cosmochim Acta 51:1951–1964
Drozd RJ, Hohenberg CM, Morgan CJ, Ralston CE (1974) Cosmic-ray exposure history at the Apollo 16 and other lunar sites: Lunar surface dynamics. Geochim Cosmochim Acta 38:1625–1642
Drozd RJ, Hohenberg CM, Morgan CJ, Podosek FA, Wroge ML (1977) Cosmic ray exposure history at Taurus-Littrow. Proc Lunar Sci Conf 8:3027–3043
Dundas CM, Keszthelyi LP, Bray VJ, McEwen AS (2010) Role of material properties in the cratering record of young platy-ridged lava on Mars. Geophys Res Lett 37:L12203
Eberhardt P, Geiss J, Grögler N, Stettler A (1973) How old is the crater Copernicus? The Moon 8:104–114
Eggleton RE, Schaber GG (1972) Cayley Formation interpreted as basin ejecta. Ap 16 Prelim Sci Rep NASA SP-315:29-7–29-16
El-Baz F (1973) D-Caldera new photographs of a unique feature. Ap 17 Prelim Sci Rep NASA SP-330:30-13–30-17
Elder CM, Hayne PO, Bandfield JL, Ghent RR, Williams J-P, Donaldson-Hanna KL, Paige DA (2017) Young lunar volcanic features: Thermophysical properties and formation. Icarus 290:224–237
Elkins-Tanton LT, Burgess S, Yin Q-Z (2011) The lunar magma ocean: Reconciling the solidification process with lunar petrology and geochronology. Earth Planet Sci Lett 304:326–336
Eugster O (1999) Chronology of dimict breccias and the age of South Ray crater at the Apollo 16 site. Meteoritics 34:385–391
Eugster O, Eberhardt P, Geiss J, Grögler N, Jungck M, Meier F, Mörgeli M, Niederer F (1984) Cosmic ray exposure histories of Apollo 14, Apollo 15, and Apollo 16 rocks. Proc Lunar Planet Sci Conf 14:498–512
Evans AJ, Soderblom JM, Andrews- Hanna JC, Solomon SC, Zuber MT (2016) Identification of buried lunar impact craters from GRAIL data and implications for the nearside maria. Geophys Res Lett 43:2445–2455
Evans AJ, Andrews-Hanna JC, Head III JW, Soderblom JM, Solomon SC, Zuber MT (2018) Reexamination of early lunar chronology with GRAIL data: Terranes, basins, and impact fluxes. J Geophys Res 123:1596–1617
Fa W, Liu T, Zhu M-H, Haruyama J (2014) Regolith thickness over Sinus Iridum: Results from morphology and size–frequency distribution of small impact craters. J Geophys Res 119:1914–1935
Fagan TJ, Taylor GJ, Keil K, Bunch TE, Wittke JH, Korotev RL, Jolliff BL, Gillis JJ, Haskin LA, Jarosewich E, Clayton RN, Mayeda TK, Fernandes VA, Burgess R, Turner G, Eugster O, Lorenzetti S (2002) Northwest Africa 032: Product of lunar volcanism. Meteoritics 37:371–394

Fagin SW, Worrall DM, Muehlberger WR (1978) Lunar mare ridge orientation—Implications for lunar tectonic models. Proc Lunar Planet Sci Conf 9:3473–3479
Fassett CI (2013) Crater degradation of kilometer-sized craters on the lunar maria: Initial observations and modeling. Lunar Planet Sci Conf 44:#2016
Fassett CI, Thomson BJ (2014) Crater degradation on the lunar maria: Topographic diffusion and the rate of erosion on the Moon. J Geophys Res 119:2255–2271
Fassett CI, Kadish SJ, Head JW, Solomon SC, Strom RG (2011) The global population of large craters on Mercury and comparison with the Moon. Geophys Res Lett 38:L10202
Fassett CI, Head JW, Kadish SJ, Mazarico E, Neumann GA, Smith DE, Zuber MT (2012) Lunar impact basins: Stratigraphy, sequence and ages from superposed impact crater populations measured from Lunar Orbiter Laser Altimeter (LOLA) data. J Geophys Res 117:E00H06
Fassett CI, Minton DA, Thomson BJ, Hirabayashi M, Watters WA (2018) Reanalysis of observations of crater degradation on the lunar maria accounting for anomalous diffusion. Lunar Planet Sci Conf 49:#1502
Fernandes VA, Burgess R (2006) Lunar volcanism during the Erastothenian II: NWA479. Annu Meteorit Soc Meeting 69:5312
Fernandes VA, Burgess R, Turner G (2003) ^{40}Ar–^{39}Ar chronology of lunar meteorites Northwest Africa 032 and 773. Meteoritics 38:555–564
Fernandes VA, Fritz J, Weiss BP, Garrick-Bethell I, Shuster DL (2013) The bombardment history of the Moon as recorded by ^{40}Ar–^{39}Ar chronology. Meteoritics 48:241–269
Frey HV (2016) Comparing the early and late heavy bombardments on the Moon. Lunar Planet Sci Conf 47:#1238
Fritz J (2012) Impact ejection of lunar meteorites and the age of Giordano Bruno. Icarus 221:1183–1186
Fugzan MM, Minh DV, Tarasov LS, Kolesov GM, Shukolyukov YA (1986) ^{40}Ar–^{39}Ar-dating of lunar rocks from Mare Crisium. Geokhimiya 4:469–479
Gaddis LR, Pieters CM, Hawke BR (1985) Remote sensing of lunar pyroclastic mantling deposits. Icarus 61:461–489
Gaddis LR, Hawke BR, Robinson MS, Coombs C (2000) Compositional analyses of small lunar pyroclastic deposits using Clementine multispectral data. J Geophys Res 105:4245–4262
Gaddis LR, Staid MI, Tyburczy JA, Hawke BR, Petro N (2003) Compositional analyses of lunar pyroclastic deposits. Icarus 161:262–280
Gaffney AM, Borg LE, Depaolo DJ, Irving AJ (2008) Age and isotope systematics of Northwest Africa 4898, a new type of highly depleted mare basalt. Lunar Planet Sci 34:#1877
Gallant J, Gladman B (2006) Lunar cratering asymmetries. Lunar Planet Sci Conf 37:#2336
Gallant J, Gladman B, Ćuk M (2009) Current bombardment of the Earth–Moon system: Emphasis on cratering asymmetries. Icarus 202:371–382
Gardner E, Nurmi P, Mikkola S (2011) The effect of the solar motion on the flux of long-period comets. Month Not R Astron Soc 411:947–954
Garry WB, Robinson MS, Zimbelman JR, Bleacher JE, Hawke BR, Crumpler LS, Braden SE, Sato H (2012) The origin of Ina: Evidence for inflated lava flows on the Moon, J Geophys Res 117:E00H31
Gault DE (1970) Saturation and equilibrium conditions for impact cratering on the lunar surface: Criteria and implications. Radio Sci 5:273–291
Gebbing T, Hiesinger H, Iqbal W, van der Bogert CH (2019) New crater size–frequency distribution measurements of the Apollo 16 landing site. Lunar Planet Sci 50:#2337
Gebbing T, Hiesinger H, Iqbal W, van der Bogert CH (2020) Crater size–frequency distribution at the North Ray and South Ray Craters. Lunar Planet Sci 51:#1871
Geiss J, Rossi AP (2013) On the chronology of lunar origin and evolution. Astron Astrophys Rev 21:68
Ghent RR, Hayne PO, Bandfield JL, Campbell BA, Allen CC, Carter LM, Paige DA (2014) Constraints on the recent rate of lunar ejecta breakdown and implications for crater ages. Geology 42:1059–1062
Goles GG, Duncan AR, Lindstrom DJ, Martin MR, Beyer RL, Osawa M, Randle K, Meek LT, Steinborn TL, McKay SM (1971) Analyses of Apollo 12 specimens: Compositional variations, differentiation processes, and lunar soil mixing models. Proc Lunar planet Sci Conf 2:1063–1081
Gomes R, Levison HF, Tsiganis K, Morbidelli A (2005) Origin of the cataclysmic late heavy bombardment period of the terrestrial planets. Science 435:466–469
Grange ML, Nemchin AA, Pidgeon RT (2009) Zircons from the Apollo 17 breccias: Implications for the early history of the Moon. Geochim Cosmochim Acta 73:459
Greeley R, Gault DE (1970) Precision size–frequency distributions for craters for 12 selected areas of the lunar surface. The Moon 2:10–77
Greeley R, Kadel SD, Williams DA, Gaddis LR, Head JW, McEwen AS, Murchie SL, Nagel E, Neukum G, Pieters CM, Sunshine JM, Wagner R, Belton MJS (1993) Galileo imaging observations of lunar maria and related deposits. J Geophys Res 98:17183–17206
Grier JA, McEwen AS, Lucey PG, Milazzo M, Strom RG (1999) The optical maturity of ejecta from large rayed craters: Preliminary results and implications. In Workshop on New Views of the Moon II: Understanding the Moon Through the Integration of Diverse Datasets. LPI Contribution No. 980 19
Grieve RA (1991) Terrestrial impact—The record in the rocks. Meteoritics 26:175–194

Grinspoon DH (1989) Large impact events and atmospheric evolution on the terrestrial planets. PhD thesis, Univ Arizona, Tucson
Guggisberg S, Eberhardt P, Geiss J, Grögler N, Stettler A, Brown GM, Peckett A (1979) Classification of the Apollo 11 mare basalts according to Ar^{39}–Ar^{40} ages and petrological properties. Proc Lunar Planet Sci Conf 10:1–39
Guinness EA, Arvidson RE (1977) On the constancy of the lunar cratering flux over the past 3.3 billion yr. Proc Lunar Sci Conf 8:3475–3494
Gustafson JO, Bell JF, Gaddis LR, Hawke BR, Giguerre TA (2012) Characterization of previously unidentified lunar pyroclastic deposits using Lunar Reconnaissance Orbiter Camera data. J Geophys Res 117:E00H25
Hackwill T (2010) Stratigraphy, evolution, and volume of basalts in Mare Serenitatis. Meteoritics 45:210–219
Hartmann WK (1964) On the distribution of lunar crater diameters. Comm Lunar Planet Lab 2:197–204
Hartmann WK (1965) Terrestrial and lunar flux of meteorites in the last two billion years. Icarus 4:157–165
Hartmann WK (1966) Early lunar cratering. Icarus 5:406–418
Hartmann WK (1969) Terrestrial, lunar, and interplanetary rock fragmentation. Icarus 10:201–213
Hartmann WK (1970a) Lunar cratering chronology. Icarus 13:299–301
Hartmann WK (1970b) Preliminary note on lunar cratering rates and absolute time-scales. Icarus 12:131
Hartmann WK (1971) Martian cratering 3:Theory of crater obliteration. Icarus 15, 410–428
Hartmann WK (1972) Paleocratering of the Moon: Review of post-Apollo data. Astrophys Space Sci 17:48–64
Hartmann WK (1975) Lunar "cataclysm": A misconception? Icarus 24:181–187
Hartmann WK (1984) Does crater "saturation equilibrium" occur in the solar system? Icarus 60:56–74
Hartmann WK (1999) Martian cratering VI. Crater count isochrons and evidence for recent volcanism from Mars Global Surveyor. Meteoritics 34:167–177
Hartmann WK (2003) Megaregolith evolution and cratering cataclysm models--Lunar cataclysm as a misconception (28 years later) Meteoritics 38:579–593
Hartmann WK (2005) Martian cratering 8: Isochron refinement and the chronology of Mars. Icarus 174:294–320
Hartmann WK, Davis DR (1975) Satellite-sized planetesimals and lunar origin. Icarus 24:504–515
Hartmann WK, Gaskell RW (1997) Planetary cratering 2: Studies of saturation equilibrium. Meteoritics 32:109–121
Hartmann WK, Neukum G (2001) Crater chronology and the evolution of Mars. *In:* Chronology and Evolution of Mars. Kallenbach R et al. (eds), Kluwer Dordrecht, p 165–194
Hartmann WK, Strom RG, Weidenschilling SJ, Balsius KR, Woronow A, Dence MR, Grieve RAF, Diaz J, Chapman CR, Shoemaker EM, Jones KL (1981) Chronology of planetary volcanism by comparative studies of planetary craters. *In:* Basaltic Volcanism on the Terrestrial Planets. Pergamon Press, New York, p 1049–1128
Hartmann WK, Quantin C, Mangold N (2007) Possible long-term decline in impact rates. Part 2: Lunar impact-melt data regarding impact history. Icarus 186:11–23
Hartmann WK, Neukum G, Werner S (2008) Confirmation and utilization of the "production function" size–frequency distributions of Martian impact craters. Geophys Res Lett:L02205
Hartung JB (1976) Was the formation of a 20-km-diameter impact crater on the Moon observed on June 18, 1178? Meteoritics 11:187–194
Haruyama J, Othake M, Matsunaga T, Honda C, Yokota Y, Abe M, Ogawa Y, Miyamoto H, Iwasaki A, Pieters CM, Asada N, Demura H, Hirata N, Terazono J, Sasaki S, Saiki K, Yamaji A, Torii M, Josset J-L (2009) Long-lived volcanism on the lunar farside revealed by SELENE Terrain Camera. Science 323:905–908
Hawke BR, Bell JF (1981) Remote sensing studies of lunar dark-halo impact craters: Preliminary results and implications for early volcanism. Proc Lunar Planet Sci Conf 12:665–678
Hawke BR, Head JW (1978) Lunar KREEP volcanism—Geologic evidence for history and mode of emplacement. Proc Lunar Planet Sci 9:3285–3309
Hawke BR, MacLaskey D, McCord TB, Adams JB, Head JW, Pieters CM, Zisk S (1979) Multispectral mapping of lunar pyroclastic deposits. Bull Am Astron Soc 11:582
Hawke BR, Coombs CR, Gaddis LR, Lucey PG, Owensby PD (1989) Remote sensing and geologic studies of localized dark mantle deposits on the Moon. Proc Lunar Planet Sci Conf 19:255–268
Hawke BR, Blewett DT, Lucey PG, Smith GA, Bell JF, Campbell BA, Robinson MS (2004) The origin of lunar crater rays. Icarus 170:1–16
Head JW (1974) Lunar dark-mantle deposits: Possible clues to the distribution of early mare deposits. Proc Lunar Sci Conf 5:207–222
Head JW (1975) Processes of lunar crater degradation: Changes in style with geologic time. The Moon 12:299–329
Head JW (1976) The significance of substrate characteristics in determining morphology and morphometry of lunar craters. Proc Lunar Planet Sci Conf 7:2913–2929
Head JW, Gifford A (1980) Lunar mare domes: Classification and modes of origin. Moon and Planets 22:235–258
Head JW, Wilson L (1980) The formation of eroded depressions around the sources of lunar sinuous rilles: Observations. Lunar Planet Sci Conf 11:426–427
Head JW, Wilson L (1992) Lunar mare volcanism: Stratigraphy, eruption conditions, and the evolution of secondary crusts. Geochim Cosmochim Acta 55:2155–2175
Head JW, Wilson L (2017) Generation, ascent and eruption of magma on the Moon: New insights into source depths, magma supply, intrusions and effusive/explosive eruptions (Part 2: Predicted emplacement processes and observations) Icarus 283:176–223

Head JW, Reed JS, Weitz C (1998) Lunar Rima Parry IV: Dike emplacement processes and consequent volcanism. Lunar Planet Sci Conf 29:#1914
Head JN, Melosh HJ, Ivanov BA (2002) Martian meteorite launch: High-speed ejecta from small craters. Science 298:1752–1756
Head JW, Fassett CI, Kadish SJ, Smith DE, Zuber MT, Neumann GA, Mazarico E (2010) Global distribution of large lunar craters: Implications for resurfacing and impactor populations. Science 329:1504–1507
Head JW, Wilson L, Qiao L, Xiao L (2016) Eruption of magmatic foams and unusual regolith properties: Anomalously young crater retention ages and the case of Ina. Annual Meeting Lunar Exploration Analysis Group, LPI Contribution 1960:#5069
Head III JW, Wilson L, Hiesinger H, van der Bogert C, Chen Y, Dickson JL, Gaddis LR, Haruyama J, Jawin ER, Jozwiak LM, Li C, Liu J, Morota T, Needham DH, Ostrach LR, Pieters CM, Prissel TC, Qian Y, Qiao L, Rutherford MR, Scott DR, Whitten JL, Xiao L, Zhang F, Ziyuan O (2023) Lunar mare basaltic volcanism: Volcanic features and emplacement processes. Rev Mineral Geochem 89:453–507
Heather DJ, Dunkin SK (2002) A stratigraphic study of southern Oceanus Procellarum using Clementine multispectral data. Planet Space Sci 50:1299–1309
Heather DJ, Dunkin SK, Wilson L (2003) Volcanism on the Marius Hills plateau: Observational analyses using Clementine multispectral data. J Geophys Res 108(E3):5017
Herrick RR, Sharpton VL, Malin MC, Lyons SN, Feely K (1997) Morphology and morphometry of impact craters. *In:* Venus II: Geology, Geophysics, Atmosphere, and Solar Wind Environment. SW Bougher, DM Hunten, RJ Philips (eds) Tucson, University of Arizona Press, p 1015–1046
Hiesinger H, Head JW (2006b) New views in lunar geoscience: An introduction and overview. Rev Mineral Geochem 60:1–81
Hiesinger H, Jaumann R, Neukum G, Head JW (2000) Ages of mare basalts on the lunar nearside. J Geophys Res105:29239–29275
Hiesinger H, Head JW, Wolf U, Neukum G (2001) Lunar mare basalts: Mineralogical variations with time. Lunar Planet Sci 32:#1826
Hiesinger H, Head JW, Wolf U, Jaumann R, Neukum G (2003) Ages and stratigraphy of mare basalts in Oceanus Procellarum, Mare Nubium, Mare Cognitum, and Mare Insularum. J Geophys Res 108(E7):5065
Hiesinger H, Head JW, Wolf U, Jaumann R, Neukum G (2006) New ages for basalts in Mare Fecunditatis based on crater size–frequency measurements. Lunar Planet Sci 9:382–384
Hiesinger H, Head JW, Wolf U, Jaumann R, Neukum G (2010) Ages and stratigraphy of lunar mare basalts in Mare Frigoris and other nearside maria based on crater size–frequency distribution measurements. J Geophys Res 115:E03003
Hiesinger H, Head JW, Wolf U, Jaumann R, Neukum G (2011) Ages and stratigraphy of lunar mare basalts: A synthesis. Geol Soc Am Spec Pap 477:1–51
Hiesinger H, van der Bogert CH, Pasckert JH, Funcke L, Giacomini L, Ostrach LR, Robinson MS (2012a) How old are young lunar craters? J Geophys Res 117:E00H10
Hiesinger H, van der Bogert CH, Pasckert JH, Schmedemann N (2012b) New crater size–frequency distribution measurements of the South Pole–Aitken basin. Lunar Planet Sci Conf 43:#2863
Hiesinger H, van der Bogert CH, Thiessen F, Robinson MS (2013) Absolute model ages of light plains in the southern lunar hemisphere. Lunar Planet Sci Conf 44:#2827
Hiesinger H, Simon I, van der Bogert CH, Robinson MS, Plescia JB (2015) New crater size–frequency distribution measurements for Cone crater at the Apollo 14 Landing Site. Lunar Planet Sci Conf 46:#1834
Hiesinger H, Pasckert JH, van der Bogert CH, Robinson MS (2016a) New crater size–frequency distribution measurements for Autolycus crater, Moon. Lunar Planet Sci Conf 47:#1879
Hiesinger H, Gebbhart J, van der Bogert CH, Pasckert JH, Weinauer J, Lawrence SJ, Stopar JD, Robinson MS (2016b) Stratigraphy of low shields and mare basalts of the Marius Hills region, Moon. Lunar Planet Sci Conf 47:#1877
Hiesinger H, Marchi S, Schmedemann N, Schenk P, Pasckert JH, Neesemann A, O'Brien DP, Kneissl T, Ermakov AI, Fu RR, Bland MT, Nathues A, Platz T, Williams DA, Jaumann1 R, Castillo-Rogez JC, Ruesch O, Schmidt B, Park RS, Preusker F, Buczkowski DL, Russell CT, Raymond CA (2016c) Cratering on Ceres: Implications for its crust and evolution. Science 353:6303
Hirabayashi M, Minton DA, Fassett CI (2017) An analytical model of crater count equilibrium. Icarus 289:134–143
Huang Y-H, Minton DA, Hirabayashi M, Elliott JR, Richardson JE, Fassett CI, Zellner NEB (2017) Heterogeneous impact transport on the Moon. J Geophys Res 122:1158–1180
Hubbard NJ, Meyer C, Gast PW, Wiesmann H (1971) The composition and derivation of Apollo 12 soils. Earth Planet Sci Lett 10:341–350
Hurwitz DM, Head JW, Hiesinger H (2013) Lunar sinuous rilles: Distribution, characteristics, and implications for their origin. Planet Space Sci 79–80:1–38
Husain L (1974) ^{40}Ar–^{39}Ar chronology and cosmic ray exposure ages of the Apollo 15 samples. J Geophys Res 79:2588–2606
Husain L, Schaeffer OA (1973) ^{40}Ar–^{39}Ar crystallization ages and ^{38}Ar–^{37}Ar cosmic ray exposure ages of samples from the vicinity of the Apollo16 landing site. Lunar Planet Sci Conf 4:406–408

Husain L, Schaeffer OA, Funkhouser J, Sutter J (1972) The ages of lunar material from Fra Mauro, Hadley Rille, and Spur crater. Proc Lunar Planet Sci Conf 3:1557–1567
Iqbal W, Hiesinger H, van der Bogert CH (2019a) Geological mapping and chronology of lunar landing sites: Apollo 11. Icarus. 333: 528–547
Iqbal W, Hiesinger H, van der Bogert CH (2019b) New geological maps and crater size–frequency distribution measurements of the Apollo 17 landing site. Lunar Planet Sci Conf 50:#1005
Iqbal W, Hiesinger H, van der Bogert CH (2020a) Geological mapping and chronology of lunar landing sites: Apollo 12. Icarus. 333: 528–547
Iqbal W, Hiesinger H, van der Bogert CH (2020b) New geological map and model ages for the Apollo 15 landing site. Lunar Planet Sci Conf 51:#1073
Ito T, Malhotra R (2010) Asymmetric impacts of near-Earth asteroids on the Moon. Astron Astrophys 519:A63
Ivanov BA (2001) Mars/Moon cratering rate ratio estimates, Space Sci Rev 96:87–104
Ivanov BA (2006) Earth/Moon impact rate comparison: Searching constraints for lunar secondary/primary cratering proportions. Icarus 183:504–507
Ivanov BA (2018) Size-frequency distribution of small lunar craters: Widening with degradation and crater lifetime. Sol Sys Res 52:1–25
Ivanov BA, Hartmann WK (2007) Exogenic dynamics, cratering and surface ages. Treat Geophys 10:207–242
Ivanov MA, Head JW, Bystrov A (2016a) The lunar Gruithuisen silicic extrusive domes: Topographic configuration, morphology, ages, and internal structure. Icarus 273:262–283
Ivanov MA, van der Bogert CH, Hiesinger H (2016b) Bracketing the age of lunar pyroclastic deposits in Oppenheimer crater. Lunar Planet Sci Conf 47:#1070
James OB (1981) Petrologic and age relations of the Apollo 16 rocks: Implications for the subsurface geology and the age of the Nectaris basin. Proc Lunar Planet Sci Conf 12:209–233
Jessberger EK, Huneke JC, Podosek FA, Wasserburg GJ (1974) High resolution argon analysis of neutron irradiated Apollo rocks and separated minerals. Proc Lunar Planet Sci Conf 5:1419–1449
Jessberger EK, Kirsten T, Staudacher T (1977) One rock and many ages—Further data on consortium breccia 73215. Proc Lunar Planet Sci Conf 8:2567–2580
Jetsu L, Pelt J (2000) Spurious periods in the terrestrial impact crater record. Astron Astrophys 353:409–418
Jia M, Yue Z, Di K, Liu B, Liu J, Michael G (2020) A catalogue of impact craters larger than 200 m and surface age analysis in the Chang'e-5 landing area. Earth Planet Sci Lett 541:116272
Jolliff BL, Wiseman SA, Lawrence SJ, Tran TN, Robinson MS, Sato H, Hawke BR, Scholten F, Oberst J, Hiesinger H, van der Bogert CH, Greenhagen BT, Gloch TD, Paige DA (2011) Non-mare silicic volcanism on the lunar farside at Compton–Belkovich. Nat Geosci 4:566–571
Kadel SD, Greeley R, Neukum G, Wagner R (1993) The history of mare volcanism in the Orientale Basin*:* Mare deposit ages, compositions and morphologies. Lunar Planet Sci Conf 24:745–746
Kato S, Morota T, Yamaguchi Y, Watanabe S, Otake H, Ohtake M (2017) Magma source transition of lunar mare volcanism at 2.3 Ga. Meteoritics 52:1899–1915
Kawamura T, Morota T, Kobayashi N, Tanaka S (2011) Cratering asymmetry on the Moon: New insight from the Apollo Passive Seismic Experiment. Geophys Res Lett 38:L15201
Kiefer WS (2013) Gravity constraints on the subsurface structure of the Marius Hills: The magmatic plumbing of the largest lunar volcanic dome complex. J Geophys Res 118:733–745
Kirchoff MR (2018) Can spatial statistics help decipher impact crater saturation? Meteorit Planet Sci 53:874–890
Kneissl T, van Gasselt S, Neukum G (2011) Map projection-independent crater size–frequency determination in GIS environments—New software tool for ArcGIS. Planet Space Sci 59:1243–1254
Kneissl T, Michael GG, Platz T, Walter SHG (2015) Age determination of linear surface features using the Buffered Crater Counting approach—Case studies of the Sirenum and Fortuna Fossae graben systems on Mars. Icarus 250:384–394
Kodama S, Yamaguchi Y (2003) Lunar mare volcanism in the eastern nearside region derived from Clementine UV/VIS data. Meteoritics 38:1461–1484
Köhler U, Head JW, Neukum G, Wolf U (2000) Lunar light plains in the northern latitudes: Latest results on age distributions, surface composition, nature, and possible origin. Lunar Planet Sci Conf 31:#1822
König B (1977) Investigations of primary and secondary impact structures on the Moon and laboratory experiments to study the ejecta of secondary particles, PhD Dissertation (in German), Rupprecht Karl Univ. Heidelberg, Germany
Krüger T, van der Bogert CH, Hiesinger H (2016) Geomorphologic mapping of the lunar crater Tycho and its impact deposits. Icarus 273:164–181
Laneuville M, Wieczorek MA, Breuer D, Tosi N (2013) Asymmetric thermal evolution of the Moon. J Geophys Res 118:1435–1452
Lawrence SJ, Stopar JD, Hawke BR, Greenhagen BT, Cahill JTS, Bandfield JL, Jolliff BL, Denevi BW, Robinson MS, Glotch TD, Bussey DBJ, Spudis PD, Giguerre TA, Garry WB (2013) LRO observations of morphology and surface roughness of volcanic cones and lobate lava flows in the Marius Hills. J Geophys Res 118:615–634
Lena R, Wöhler C, Phillips J, Chiocchetta MT (2013) Lunar domes—Properties and formation processes. Springer

Le Feuvre M, Wieczorek MA (2011) Nonuniform cratering of the Moon and a revised crater chronology of the inner Solar System. Icarus 214:1–20
Li B, Wang X, Zhang J, Ling Z, Chen J, Wu Z, Ni Y (2016) The relative and absolute age determination of rilles in southwest Aristarchus region. Planet Space Sci 124:84–93
Li B, Ling Z, Zhang J, Chen J, Liu CQ, Bi X (2018) Geologic mapping of lunar highland crater Lalande: Topographic configuration, morphology, and cratering process. Planet Space Sci 151:85–96
Lucchitta BK (1977) Crater clusters and light mantle at the Apollo 17 site: A result of secondary impact from Tycho. Icarus 30:80–96
Lucchitta BK, Sanchez AG (1975) Crater studies in the Apollo 17 region. Proc Lunar Planet Sci Conf 6:2427–2441
Lucey PG, Blewett DT, Taylor GJ, Hawke BR (2000) Imaging of lunar surface maturity. J Geophys Res 105:20377–20386
Lugmair GW, Marti K (1972) Exposure ages and neutron capture record in lunar samples from Fra Mauro. Proc Lunar Planet Sci Conf 3:1891–1897
Mahanti P, Robinson MS, Thompson TJ, Henriksen MR (2018) Small lunar craters at the Apollo 16 and 17 landing sites—Morphology and degradation. Icarus 299:475–501
Malin MC (1974) Lunar red spots: Possible pre-mare materials. Earth Planet Sci Lett 21:331–341
Malin MC, Edgett K, Posiolova L, McColley S, Noe Dobrea E (2006) Present-day impact cratering rate and contemporary gully activity on Mars. Science 314:1573–1577
Mangold N, Allemand P, Thomas PG (1998) Wrinkle ridges of Mars: Structural analysis and evidence for shallow deformation controlled by ice-rich décollements. Planet Space Sci 46:345–356
Marchi S, Mottola S, Cremonese G, Massironi M, Martellato E (2009) A new chronology for the Moon and Mercury. Astron J 137:4936–4948
Marchi S, Bottke WF, Kring DA, Morbidelli A (2012) The onset of the lunar cataclysm as recorded in its ancient crater populations. Earth Planet Sci Lett 325:27–38
Marti K, Lightner BD, Osborn TW (1973) Krypton and xenon in some lunar samples and the age of North Ray crater. Proc Lunar Sci Conf 4:2037–2048
Maurer P, Eberhardt P, Geiss J, Grögler N, Stettler A, Brown GM, Peckett A, Krähenbühl U (1978) Pre-Imbrian craters and basins ages, compositions, and excavation depths of Apollo 16 breccias. Geochim Cosmochim Acta 42:1687–1720
Maxwell TA, Ward SH, El-Baz F (1975) Distribution, morphology, and origin of ridges and arches in Mare Serenitatis. Geol Soc Bull 86:1273–1278
Mazrouei S, Ghent RR, Bottke WF, Parker AH, Gernon TM (2019) Earth and Moon impact flux increased at the end of the Paleozoic. Science 363:253–257
McCauley JH (1967) Geologic map of the Hevelius Region of the Moon. USGS Misc Inv Map I-491
McEwen AS, Bierhaus EB (2006) The importance of secondary cratering to age constraints on planetary surfaces. Annu Rev Earth Planet Sci 34:535–567
McEwen AS, Preblich BS, Turtle EP, Artemieva NA, Golombek MP, Hurst M, Kirk RL, Burr DM, Christensen PR (2005) The rayed crater Zunil and interpretations of small impact craters on Mars. Icarus 176:351–381
McGill GE (1977) Craters as "fossils": The remote dating of planetary surface materials. Geol Soc Am Bull 88:1102–1110
Melosh HJ (1989) Impact Cratering: A Geological Process. Oxford University Press
Merle RE, Nemchin AA, Grange ML, Whitehouse MJ, Pidgeon RT (2014) High resolution U–Pb ages of Ca-phosphates in Apollo 14 breccias: Implications for the age of the Imbrium impact. Meteoritics Planet Sci 49:2241–2251
Meyer HM, Denevi BW, Boyd AK, Robinson MS (2013) The distribution and origin of lunar light plains around Orientale basin. Lunar Planet Sci Conf 44:#1539
Meyer HM, Denevi BW, Boyd AK, Robinson MS (2016) The distribution and origin of lunar light plains around Orientale basin. Icarus 273:135–145
Meyer HM, Denevi BW, Boyd AK, Robinson MS (2020) The global distribution of lunar light plains from the Lunar Reconnaissance Orbiter Camera. Icarus 125:e2019JE006073
Michael GG, Neukum G (2010) Planetary surface dating from crater size–frequency distribution measurements: Partial resurfacing events and statistical age uncertainty. Earth Planet Sci Lett 294:223–229
Michael GG, Platz T, Kneissl T, Schmedemann N (2012) Planetary surface dating from crater size–frequency distribution measurements: Spatial randomness and clustering. Icarus 218:169–177
Michael GG, Kneissl T, Neesemann A (2016) Planetary surface dating from crater size–frequency measurements: Poisson timing analysis. Icarus 277:279–285
Michael GG, Basilevsky A, Neukum G (2018) On the history of the early meteoritic bombardment of the Moon: Was there a terminal lunar cataclysm? Icarus 302:80–103
Montési LGJ, Zuber MT (2003a) Spacing of faults at the scale of the lithosphere and localization instability: 1. Theory. J Geophys Res 108(B2):2110
Montési LGJ, Zuber MT (2003b) Spacing of faults at the scale of the lithosphere and localization instability: 2. Application to the Central Indian Basin. J Geophys Res 108(B2):2111
Moore HJ (1967) Geologic map of the Seleucus quadrangle of the Moon. I-527 (LAC-38) U.S. Geol Surv Washington D.C.
Moore HJ, Boyce JM, Hahn DA (1980) Small impact craters in the lunar regolith—Their morphologies, relative ages, and rates of formation. The Moon 23:231–252

Morbidelli A, Petit J-M, Gladman B, Chambers J (2001) A plausible cause of the late heavy bombardment. Meteoritics 36:371–380
Morbidelli A, Levison HF, Tsiganis K, Gomes R (2005) Chaotic capture of Jupiter's Trojan asteroids in the early Solar System. Nature 435:462–465
Morbidelli A, Lunine JI, O'Brien DP, Raymond SN, Walsh KJ (2012a) Building terrestrial planets. Annu Rev Earth Planet Sci 40:251–275
Morbidelli A, Marchi S, Bottke WF, Kring DA (2012b) A sawtooth-like timeline for the first billion years of lunar bombardment. Earth Planet Sci Lett 355:144–151
Morbidelli A, Nesvorný D, Laurenz V, Marchi S, Rubie DC, Elkins-Tanton L, Wieczorek M, Jacobson S (2018) The timeline of the lunar bombardment: Revisited. Icarus 305:262–276
Morota T, Furumota M (2003) Asymmetrical distribution of rayed craters on the Moon. Earth Planet Sci Lett 206:315–323
Morota T, Haruyama J, Honda C, Othake M, Yokota Y, Limura J, Matsunaga T, Ogawa Y, Hirata N, Demura H, Iwasaki A, Miyamoto H, Nakamura R, Takeda H, Ishihara Y, Sasaki S (2009) Mare volcanism in the lunar farside Moscoviense region: Implication for lateral variation in magma production of the Moon. Geophys Res Lett 36:L21202
Morota T, Haruyama J, Othake M, Matsunaga T, Honda C, Yakota Y, Kimura J, Ogawa Y, Hirata N, Demura H, Iwasaki A, Sugihara T, Saiki K, Nakamura R, Kobayashi S, Ishihara Y, Takeda H, Hiesinger H (2011a) Timing and characteristics of the latest mare eruption on the Moon. Earth Planet Sci Lett 302:255–266
Morota, T, Haruyama J, Ohtake M, Matsunaga T, Kawamura T, Yokota Y, Honda C, Kimura J, Hirata N, Demura H, Iwasaki A, Sugihara T (2011b) Timing and duration of mare volcanism in the central region of the northern farside of the Moon. Earth Planets Space 63:5–13
Muehlberger WR, Batson RM, Boudette EL, Duke CM, Eggleton RE, Elston DP, Head JW (1972) Preliminary geologic investigation of the Apollo 16 landing site, Apollo 16 Prelim Sci Rep NASA Spec Publ 315:6-1–6-81
Nahm AL, Watters TR, Johnson CL, Banks ME, van der Bogert CH, Weber RC, Andrews-Hanna JC (2023) Tectonics of the Moon. Rev Mineral Geochem 89:691–727
Napier WM (1998) NEOs and impacts: The galactic connection. Celest Mech Dyn Astron 69:59–75
Nesvorný D, Vokrouhlický D, Bottke WF, Gladman B, Häggström T (2007) Express delivery of fossil meteorites from the inner asteroid belt to Sweden. Icarus 188:400–413
Neukum G (1971) Untersuchungen über Einschlagskrater auf dem Mond. Dissertation an der Ruprecht-Karl-Universität, Heidelberg
Neukum G (1977a) Different ages of lunar light plains. The Moon 17:383–393
Neukum G (1977b) Lunar cratering. Phil Trans R Soc Lond A 285:267–272
Neukum G (1983) Meteoritenbombardement und Datierung planetarer Oberflächen. Habilitationsschrift, Univ. Munich, Munich, Germany
Neukum G, Horn P (1976) Effects of lava flows on lunar crater populations. The Moon 15:205–222
Neukum G, Ivanov BA (1994) Crater size distributions and impact probabilities on Earth from lunar, terrestrial-planet, and asteroid cratering data. *In:* Hazard Due to Comets and Asteroids. Gehrels T (ed) Univ. of Ariz. Press, p 359–416
Neukum G, Wilhelms DE (1972) Ancient lunar impact record. Lunar Planet Sci Conf 13:590–591
Neukum G, Wise DU (1976) Mars—A standard crater curve and possible new time scale. Science 194:1381–1387
Neukum G, Schneider E, Mehl A, Storzer D, Wagner GA, Fechtig H, Bloch MR (1972) Lunar craters and exposure ages derived from crater statistics and solar flare tracks. Proc Lunar Sci Conf 3:2793–2810
Neukum G, König B, Arkani-Hamed J (1975a) A study of lunar impact crater size-distributions. The Moon 12:201–229
Neukum G, Koenig B, Fechtig H, Storzer D (1975b) Cratering in the Earth–Moon system: Consequences for age determination by crater counting. Proc Lunar Planet Sci Conf 6:2597–2620
Neukum G, Ivanov BA, Hartmann WK (2001) Cratering records in the inner solar system in relation to the lunar reference system. Space Sci Rev 96:55–86
Neukum G, Werner SC, Ivanov BA (2006) The characteristics of the impact crater production size–frequency distributions on the Solar System planetary bodies, their relationships to asteroidal and cometary impacts, and the question of secondary-cratering contributions. Workshop on surface ages and histories: Issues in planetary chronology, LPI Contribution 1320:38–39
Neumann GA, Zuber MT, Wieczorek MA, Head III JW, Baker DMH, Solomon SC, Smith DE, Lemoine FG, Mazarico E, Sabaka TJ, Goossens S, Melosh HJ, Phillips RJ, Asmar SW, Konopliv AS, Williams J, Sori MM, Soderblom JM, Miljković K, Andrews-Hanna JC, Nimmo F, Kiefer WS (2015) Lunar impact basins revealed by Gravity Recovery and Interior Laboratory measurements. Sci Adv 1:e1500852
Norman MD, Nemchin AA (2014) A 4.2 billion year old impact basin on the Moon: U–Pb dating of zirconolite and apatite in lunar melt rock 67955. Earth Planet Sci lett 388:387–398
Nozette S, Lichtenberg CL, Spudis P, Bonner R, Ortr W, Malaret E, Robinson M, Shoemaker EM (1996) The Clementine bistatic radar experiment. Science 274:1495–1498
Nunes PD, Tatsumoto M, Unruh DM (1974) U–Th–Pb systematics of some Apollo 17 lunar samples and implications for a lunar basin excavation chronology. Proc Lunar Planet Sci Conf 5:1487–1514
Nyquist LE, Shih C-Y (1992) The isotopic record of lunar volcanism. Geochim Cosmochim Acta 56:2213–2234
Nyquist LE, Bogard DD, Shih C-Y (2001) Radiometric chronology of the Moon and Mars. *In:* The Century of Space Science. Bleeker JA, Geiss J, Huber M (eds) Kluwer Academic Publishers, p 1325–1376

O'Brien DP, Greenberg R (2003) Steady-state size distributions for collisional populations: Analytical solution with size-dependent strength. Icarus 164:334–345
O'Neil HSC (1991) The origin of the Moon and the early history of the Earth; a chemical model; Part 1, The Moon. Geochim Cosmochim Acta 55:1135–1157
Oberbeck VR (1975) The role of ballistic erosion and sedimentation in lunar stratigraphy. Rev Geophys Space Phys 13:337–362
Oberbeck VR, Quaide WL, Gault DE, Morrison RH, Hörz F (1974) Smooth plains and continuous deposits of craters and basins. Proc Lunar Planet Sci Conf 5:111–136
Ono T, Kumamoto A, Nakagawa H, Yamaguchi Y, Oshigami S, Yamaji A, Kobayashi T, Kasahara Y, Oya H (2009) Lunar radar sounder observations of subsurface layers under the nearside maria of the Moon. Science 323:909–912
Öpik EJ (1960) The lunar surface as an impact counter. Month Not R Astron Soc 120:404
Orgel C, Michael GG, Fassett CI, van der Bogert CH, Riedel C, Kneissl T, Hiesinger H (2018) Ancient bombardment of the inner Solar System - Reinvestigation of the "fingerprints" of different impactor populations on the lunar surface. J Geophys Res 123:748–762
Osinski GR, Melosh HJ, Andrews-Hanna J, Baker D, Denevi B, Dhingra D, Ghent R, Hayne PO, Hill P, James PB, Jaret S, Johnson B, Kenkmann T, Kring D, Mahanti P, Minton D, Neish CD, Neumann G, Plescia J, Potter RWK, Richardson J, Silber EA, Soderblom JM, Zanetti M, Zellner N (2023) Lunar impact features and processes. Rev Mineral Geochem 89:339–371
Papanastassiou DA, Wasserburg GJ (1971) Lunar chronology and evolution from Rb–Sr studies of Apollo 11 and 12 samples. Earth Planet Sci Lett 11:37–62
Pasckert JH, Hiesinger H, van der Bogert CH (2015) Small-scale lunar farside volcanism. Icarus 257:336–354
Pasckert JH, Hiesinger H, van der Bogert CH (2018) Lunar farside volcanism in and around the South Pole–Aitken basin. Icarus 299:538–562
Plescia JB, Golombek MP (1986) Origin of planetary wrinkle ridges based on the study of terrestrial analogs. Geol Soc Am Bull 97:1289–1299
Plescia JB, Robinson MS (2011) New constraints on the absolute lunar crater chronology. Lunar Planet Sci Conf 42:#1839
Plescia JB, Spudis PD (2014) Impact melt flows at Lowell crater. Planet Space Sci 103:219–227
Plescia JB. Robinson MS, Paige DA (2010) Giordano Bruno: The young and the restless, Lunar Planet Sci Conf 41:#2038
Pohn HA, Offield TW (1970) Lunar crater morphology and relative age determination of lunar geologic units—Part 1. Classification, U.S. Geol Surv Prof Pap 700-C:C153–C162
Pöhler CM, van der Bogert CH, Hiesinger H (2019) Light plains on the lunar northern hemisphere. Lunar Planet Sci 50:#2310
Povilaitis RZ, Robinson MS, van der Bogert CH, Hiesinger H, Meyer HM, Ostrach LR (2018) Crater density differences: Exploring regional resurfacing, secondary crater populations, and crater saturation equilibrium on the Moon. Planet Space Sci 162:41–51
Pritchard ME, Stevenson DJ (2000) The thermochemical history of the Moon: Constraints and major questions. Lunar Planet Sci 31:#1878
Qian YQ, Xiao L, Zhao SY, Zhao JN, Huang J, Flahaut J, Martinot M, Head III JW, Hiesinger H, Wang GX (2018) Geology and scientific significance of the Rümker region in northern Oceanus Procellarum: China's Chang'e-5 landing region, J Geophys Res 123:1407–1430
Qian YQ, Xiao L, Head JW, van der Bogert CH, Hiesinger H, Wilson L (2021a) Young lunar mare basalts in the Chang'e 5 sample return region, northern Oceanus Procellarum. Earth Planet Sci Lett 555:116702
Qian YQ, Xiao L, Wang Q, Head JW, Yang R, Kang Y, van der Bogert CH, Hiesinger H, Lai X, Wang G, Pang Y, Zhang N, Yuan Y, He Q, Huang J, Zhao J, Wang J, Zhao S (2021b) China's Chang'e-5 landing site: Geology, stratigraphy, and provenance of materials. Earth Planet Sci Lett 561:116855
Qiao L, Xiao L, Zhao J, Huang Q, Haruyama J (2014) Geological features and evolution history of Sinus Iridum, the Moon. Planet Space Sci 101:37–52
Qiao L, Head J, Wilson L, Xiao L, Kreslavsky M, Dufek J (2017a) Ina pit crater on the Moon: Extrusion of waning-stage lava lake magmatic foam results in extremely young crater retention ages. Geology 45:455–458
Qiao L, Head J, Xiao L, Wilson L, Dufek J (2017b) Sosigenes lunar irregular mare patch (IMP): Morphology, topography, sub-resolution roughness, and implications for origin. Lunar Planet Sci Conf 47:#2002
Rajmon D, Spudis P (2004) Distribution and stratigraphy of basaltic units in Mare Tranquillitatis and Fecunditatis: A Clementine perspective. Meteoritics 39:1699–1720
Rampino MR, Stothers PB (1984) Terrestrial mass extinctions, cometary impacts and the Sun's motion perpendicular to the galactic plane. Nature 308:709–712
Rankenburg K, Brandon AD, Norman MD (2007) A Rb–Sr and Sm–Nd isotope geochronology and trace element study of lunar meteorite LaPaz Icefield 02205. Geochim Cosmochim Acta 71:2120–2135
Richardson JE (2009) Cratering saturation and equilibrium: A new model looks at an old problem. Icarus 204:697–715
Robbins SJ (2014) New crater calibrations for the lunar crater-age chronology. Earth Planet Sci Lett 403:188–198
Robbins SJ (2019) A new global database of lunar impact craters > 1–2 km: 1. Crater locations and sizes, comparisons with published databases, and global analysis. J Geophys Res 124:871–892

Robbins SJ, Riggs JD, Weaver BP, Bierhaus EB, Chapman CC, Kirchoff MR, Singer KN, Gaddis LR (2018) Revised recommended methods for analyzing crater size–frequency distributions. Meteoritics 53:891–931
Robinson MS, Brylow SM, Tschimmel M, Humm D, Lawrence SJ, Thomas PC, Denevi BW, Bowman-Cisneros E, Zerr J, Ravine MA, Caplinger MA, Ghaemi FT, Schaffner JA, Malin MC, Mahanti P, Bartels A, Anderson J, Tran TN, Eliason EM, McEwen AS, Turtle E, Jolliff BL, Hiesinger H (2010) Lunar Reconnaissance Orbiter Camera (LROC) instrument overview. Space Sci Rev 150:81–124
Robinson MS, Thomas PC, Plescia JB, Denevi BW, Burns KN, Bowman-Cisneros E, Henriksen MR, van der Bogert CH, Hiesinger H, Mahanti P, Stelling RW, Povilaitis RZ (2016) An exceptional grouping of lunar highland smooth plains: Geography, morphology, and possible origins. Icarus 273:121–134
Rolf T, Zhu M-H, Wünnemann K, Werner SC (2017) The role of impact bombardment history in lunar evolution. Icarus 286:138–152
Rubie DC, Jacobson SA, Morbidelli A, O'Brien DP, Young ED, de Vries J, Nimmo F, Palme H, Frost DJ (2015) Accretion and differentiation of the terrestrial planets with implications for the compositions of early-formed Solar System bodies and accretion of water. Icarus 248:89–108
Runcorn SK (1977) Early melting of the Moon. Proc Lunar Planet Sci Conf 8:463–469
Runcorn SK, Libby LM, Libby WF (1977) Primeval melting of the Moon. Nature 270:676–681
Russ GP, Burnett DS, Wasserburg GJ (1972) Lunar neutron stratigraphy. Earth Planet Sci Lett 15:172–186
Ryder G (2002) Mass flux in the ancient Earth–Moon system and benign implications for the origin of life on Earth. J Geophys Res 107(E4):5022
Ryder G, Spudis PD (1980) Volcanic rocks in the lunar highlands. *In:* Proc Conf Lunar Highlands Crust. Pergamon Press, p 353–375
Ryder G, Spudis PD (1987) Chemical composition and origin of Apollo 15 impact melts. J Geophys Res 92:432–446
Ryder G, Bogard D, Garrison D (1991) Probable age of Autolycus and calibration of lunar stratigraphy. Geology 19:143–146
Salamuniccar G, Loncaric S, Pinta P, Bandeira L, Saraiva J (2011) MA130301GT catalogue of Martian impact craters and advanced evaluation of crater detection algorithms using diverse topography and image datasets. Planet Space Sci 59:111–131
Sato H, Robinson MS, Lawrence SJ, Denevi BW, Hapke B, Jolliff BL, Hiesinger H (2017) Lunar mare TiO_2 abundances estimated from UV/Vis reflectance. Icarus 296:216–238
Schaefer OA, Husain L (1974) Chronology of lunar basin formation and ages of lunar anorthositic rocks. Lunar Planet Sci V:663–665
Schmitt HH, Petro NE, Wells RA, Robinson MS, Weiss BP, Mercer CM (2017) Revisiting the field geology of Taurus-Littrow. Icarus 298:2–33
Schnetzler CC, Philpotts JA (1971) Alkali, alkaline earth and rare-earth element concentrations in some Apollo 12 soils, rocks, and separated phases. Proc Lunar Planet Sci Conf 2:1101–1122
Schonfeld E, Meyer C jr (1972) The abundances of components of the lunar soils by a least-squares mixing model and the formation age of KREEP. Proc Lunar Planet Sci Conf 3:1397–1420
Schultz PH (1976) Floor-fractured lunar craters. The Moon 15:241–273
Schultz PH, Crawford DA (2011) Origin of nearside structural and geochemical anomalies on the Moon. Geol Soc Am Spec Pap 477:141–159
Schultz PH, Spudis PD (1979) Evidence for ancient mare volcanism. Proc Lunar Planet Sci Conf 10:2899–2918
Schultz PH, Spudis PD (1983) Beginning and end of lunar mare volcanism. Nature 302:233–236
Schultz PH, Gault D, Greeley R (1977) Interpreting statistics of small lunar craters. Proc Lunar Planet Sci Conf 8: 3539–3564
Schultz PH, Staid MI, Pieters CM (2006) Lunar activity from recent gas release. Nature 444:184–186
Senthil Kumar P, Sruthi U, Lakshmi KJP, Menon R, Amitabh, Krishna BG, Kring DA, Head JW, Goswami JN, Kumar ASK (2016) Recent shallow moonquakes and impact-triggered boulder falls on the Moon: New insights from the Schrödinger basin, J Geophys Res 121:147–197
Shirley KA, Zanetti M, Jolliff B, van der Bogert CH, Hiesinger H (2016) Crater size–frequency distribution measurements and age of the Compton–Belkovich Volcanic Complex. Icarus 273:214–223
Shkuratov Y, Kaydash V, Videen G (2012) The lunar crater Giordano Bruno as seen with optical roughness imagery. Icarus 218:525–533
Shoemaker EM (1962) Interpretation of lunar craters, *In:* Physics and Astronomy of the Moon. Kopal Y (ed), Academic Press, New York, p. 283–359
Shoemaker EM (1965) 2. Preliminary analysis of the fine structure of the lunar surface in Mare Cognitum. Int Astron U Colloq 5:23–77
Shoemaker EM, Batson RM, Bean AL, Conrad C jr., Dahlem D, Goddard EN, Hait MT, Larson KB, Schaber GG, Schleicher DL, Sutton RL, Swann GA, Waters AC (1970) Preliminary geologic investigation of the Apollo 12 landing site. Part A Geology of the Apollo 12 landing site. *In:* Apollo 12 Prelim Sci Rep NASA SP-235, p 113–182
Silver LT (1971) U–Th–Pb isotope systems in Apollo 11 and 12 regolithic materials and a possible age for the Copernican impact. Eos Trans AGU 52:534

Smith DE, Zuber MT, Neumann GA, Lemoine FG, Mazarico E, Torrence MH, McGarry JF, Rowlands DD, Head III JW, Duxbury TH, Aharonson O, Lucey PG, Robinson MS, Barnouin OS, Cavanaugh JF, Sun X, Liiva P, Mao D, Smith JC, Bartels AE (2010) Initial observations from the Lunar Orbiter Laser Altimeter (LOLA) Geophys Res Lett 37, L18204

Snape JF, Curran NM, Whitehouse MJ, Nemchin AA, Joy KH, Hopkinson T, Mahesh A, Bellucci JJ, Kenny GG (2018) Ancient volcanism on the Moon: Insights from Pb isotopes in the MIL 13317 and Kalahari 009 meteorites. Earth Planet Sci Lett 502:84–95

Snape JF, Nemchin AA, Curran NM, Whitehouse MJ, Merle RE, Hopkinson T, Mahesh A (2019) The timing of basaltic volcanism at the Apollo landing sites. Geochimica et Cosmochimica Acta 266:29–53

Snyder GA, Borg LE, Nyquist LE, Taylor LA (2000) Chronology and isotopic constraints on lunar evolution. *In:* The Origin of the Earth and the Moon, Univ. Arizona Press, Tucson, p 361–395

Soderblom LA (1970) A model for small-impact erosion applied to the lunar surface. J Geophys Res 75:2655–2661

Soderblom LA (1972) The process of crater removal in the lunar maria. *In:* Apollo 15 Prelim Sci Rep NASA SP-289:25-87–25-91

Soderblom LA, Boyce JM (1972) Relative ages of some near-side and far-side terra plains based on Apollo 16 metric photography. *In:* Apollo 16 Prelim Sci Rep NASA SP-315:29-3–29-6

Soderblom LA, Lebofsky LA (1972) Technique for rapid determination of relative ages of lunar areas from orbital photography. J Geophys Res 77:279–296

Soderblom LA, Condit CD, West RA, Herman BM, Kreidler TJ (1974) Martian planetwide crater distributions: Implications for geologic history and surface processes. Icarus 22:239–263

Solomon SC, Chaiken J (1976) Thermal expansion and thermal stress in the Moon and terrestrial planets: Clues to early thermal history. Proc Lunar Planet Sci Conf 7:3229–3243

Solomon SC, Head JW (1979) Vertical movement in mare basins: Relation to mare emplacement, basin tectonics, and lunar thermal history. J Geophys Res 84:1667–1682

Spangler RR,Warasila R, Delano LW (1984) ^{40}Ar–^{39}Ar ages for the Apollo 15 green and yellow volcanic glasses. Proc Lunar Planet Sci Conf 14:487–497

Speyerer EJ, Povilaitis RZ, Robinson MS, Thomas PC, Wagner RV (2016) Quantifying crater production and regolith overturn on the Moon with temporal imaging. Nature 538:215–218

Spohn T, Konrad W, Breuer D, Ziethe R (2001) The longevity of lunar volcanism: Implications of thermal evolution calculations with 2D and 3D mantle convection models. Icarus 149:54–65

Spudis PD (1978) Composition and origin of the Apennine Bench Formation. Lunar Planet Sci IX:1086–1088

Spudis PD (1993) The Geology of Multi-Ring Impact Basins, Cambridge Planet. Sci Ser. 8, Cambridge Univ. Press

Spudis PD, Sliz MU (2017) Impact melt of the lunar Crisium multiring basin. Geophys Res Lett 44:1260–1265

Squyres SW, Howell C, Liu MC, Lissauer JJ (1997) Investigation of crater ”saturation” using spatial statistics. Icarus 125:67–82

Srivastava N, Kumar D, Gupta RP (2013) Young viscous flows in the Lowell crater of Orientale basin, Moon: Impact melts or volcanic eruptions? Planet Space Sci 87:37–45

Sruthi U, Senthil Kumar P (2014) Volcanism on farside of the Moon: New evidence from Antoniadi in South Pole–Aitken basin. Icarus 242:249–268

Stadermann AC, Zanetti MR, Jolliff BL, Hiesinger H, van der Bogert CH, Hamilton CW (2018) The age of lunar mare basalts south of the Aristarchus plateau and effects of secondary craters formed by the Aristarchus event. Icarus 309:45–60

Stadermann FJ, Heusser E, Jessberger EK, Lingner S, Stöffler D (1991) The case for a younger Imbrium basin—New Ar-40–Ar-39 ages of Apollo 14 rocks. Geochim Cosmochim Acta 55:2339–2349

Staid MI, Pieters CM, Head JW (1996) Mare Tranquillitatis: Basalt emplacement history and relation to lunar samples. J Geophys Res 101:23213–23228

Stettler A, Eberhardt P, Geiss J, Grögler N, Maurer P (1973) Ar^{39}–Ar^{40} ages and Ar^{37}–Ar^{38} exposure ages of lunar rocks. Proc Lunar Planet Sci Conf 4:1865–1888

Stöffler D, Ryder, G (2001) Stratigraphy and isotope ages of lunar geologic units: Chronological standard for the inner solar system. *In:* Chronology and Evolution of Mars. Kallenbach R, Geiss J, Hartmann WK (eds), Space Science Series of ISSI, Kluwer Academic Publishers, Dordrecht, Space Sci Rev 96:9–54

Stöffler D, Bischoff A, Borchardt R, Burghele A, Deutsch A, Jessberger EK, Ostertag R, Palme H, Spettel B, Reimold WU (1985) Composition and evolution of the lunar crust in the Descartes highlands, Apollo 16. J Geophys Res 90:C449–C506

Stöffler D, Ryder G, Ivanov BA, Artemieva NA, Cintala MJ, Grieve RA (2006) Cratering history and lunar chronology. Rev Mineral Geochem 60:519–596

Stooke PJ (2012) Lunar meniscus hollows. Lunar Planet Sci Conf 43:#1011

Stopar JD, Robinson MS, van der Bogert CH, Hiesinger H, Ostrach LR, Giguerre TA, Lawrence SJ (2017) Young lunar volcanism: Irregular mare patches as drained lava ponds and inflated flows. Lunar Planet Sci Conf 48:#1792

Strain PL, El-Baz F (1980) The geology and morphology of Ina. Proc Lunar Planet Sci Conf 11:2437–2446

Strom RG (1972) Lunar mare ridges, rings and volcanic ring complexes. The Moon 47:187–215

Strom RG, Neukum G (1988) The cratering record on Mercury and the origin of impacting objects. *In:* Mercury. Vilas F, Chapman CR, Matthews MS (eds) University of Arizona Press, p 336–373

Strom RG, Croft SK, Barlow NG (1992) The Martian impact cratering record. *In:* Kieffer HH, Jakovsky BM, Snyder CW, Matthews MS (eds) Mars, Tucson, AZ: University of Arizona Press, p 383–423
Strom RG, Malhotra R, Ito T, Yoshida F, Kring DA (2005) The origin of planetary impactors in the inner Solar System. Science 309:1847–1850
Swann GA (1986) Some observations on the geology of the Apollo 15 landing site. *In:* Workshop on the Geology and Petrology of the Apollo 15 Landing Site:108–112
Swindle TD, Spudis PD, Taylor GJ, Korotev RL, Nichols RH, Olinger CT (1991) Searching for Crisium basin ejecta: Chemistry and ages of Luna 20 impact melts. Proc Lunar Planet Sci Conf 21:167–181
Taguchi M, Morota T, Kato S (2017) Lateral heterogeneity of lunar volcanic activity according to volumes of mare basalts in the farside basins. J Geophys Res 122:1505–1521
Taylor LA, Shervais JW, Hunter RH, Shih C-Y, Bansal BM, Wooden J, Nyquist LE, Laul LC (1983) Pre-4.2 AE mare-basalt volcanism in the lunar highlands. Earth Planet Sci. Lett 66:33–47
Tera F, Wasserburg GJ (1974) The evolution and history of mare basalts as inferred from U–Th–Pb systematics. Lunar Planet Sci Conf 6:807–809
Tera F, Papanastassiou DA, Wasserburg GJ (1973) A lunar cataclysm at ~3.95 AE and the structure of the lunar crust. Lunar Planet Sci Conf 4:723–724
Tera F, Papanastassiou DA, Wasserburg GJ (1974) Isotopic evidence for a terminal lunar cataclysm. Earth Planet Sci Lett 22:1–21
Terada K, Anand M, Sokol A, Bischoff A, Sano Y (2007) Cryptomare magmatism 4.35 Gyr ago recorded in lunar meteorite Kalahari 009. Nature 450:849–852
Thaisen KG, Head JW, Taylor LA, Kramer GY, Isaacson P, Nettles J, Petro N, Pieters CM (2011) Geology of the Moscoviense Basin. J Geophys Res 116:E00G07
Thiessen F, Hiesinger H, van der Bogert CH, Pasckert JH, Robinson MS (2012) Surface ages and mineralogy of lunar light plains in the South Pole–Aitken basin. Lunar Planet Sci Conf 43:#1659
Trang D, Gillis-Davis JJ, Boyce JM (2015) Absolute model ages to crater degradation. J Geophys Res 120:725–738
Trask NJ (1971) Geologic maps of early Apollo landing sites of set C. NASA Cont Rep NASA CR-116408
Trask NJ (1966) Size and spatial distribution of craters estimated from Ranger photographs. *In:* Ranger VIII and IX —Part II, Experimenters' Analyses and Interpretations, Shoemaker E et al. (eds). Jet Propulsion Lab, Calif Inst Technol Rept 32-800:252–263
Trask NJ, McCauley JF (1972) Differentiation and volcanism in the lunar highlands: Photogeologic evidence and Apollo 16 implications. Earth Planet Sci Lett 14:201–206
Tsiganis K, Gomes R, Morbidelli A, Levison HF (2005) Origin of the orbital architecture of the giant planets of the Solar System. Science 435:459–461
Turcotte D, Schubert G (2014) Geodynamics. Cambridge University Press
Tye AR, Fassett CI, Head JW, Mazarico E, Basilevsky AT, Neumann GA, Smith DE, Zuber MT (2015) The age of lunar south circumpolar craters Haworth, Shoemaker, Faustini, and Shackleton: Implications for regional geology, surface processes, and volatile sequestration. Icarus 255:70–77
Valantinas A, Kinch KM, Bridzius A (2018) Low crater frequencies and low model ages in lunar maria: Recent endogenic activity or degradation effects? Meteoritics Planet Sci 53:826–838
van der Bogert CH, Hiesinger H (2020) Which samples are needed for improved calibration of the lunar cratering chronology? Lunar Planet Sci Conf 51:#2088
van der Bogert CH, Hiesinger H, McEwen AS, Dundas C, Bray V, Robinson MS, Plescia JB, Reiss D, Klemm K, and the LROC Team (2010) Discrepancies between crater size–frequency distributions on ejecta and impact melt pools at lunar craters: An effect of differing target properties? Lunar Planet Sci Conf 41:#2165
van der Bogert CH, Hiesinger H, Banks ME, Watters TR, Robinson MS (2012) Derivation of absolute model ages for lunar lobate scarps. Lunar Planet Sci Conf 43:#1847
van der Bogert CH, Gaddis L, Hiesinger H, Ivanov M, Jolliff B, Mahanti P, Pasckert JH (2016) Revisiting the CSFDs of the Taurus Littrow dark mantle deposit: Implications for age determinations of pyroclastic deposits. Lunar Planet Sci Conf 47:#1616
van der Bogert CH, Hiesinger H, Dundas C, Krüger T, McEwen AS, Zanetti M, Robinson MS (2017) Origin of discrepancies between crater size–frequency distributions of coeval lunar geologic units via target property contrasts. Icarus 298:49–63
van der Bogert CH, Hiesinger H, Spudis P, Fernandes VA, Runyon KD, Denevi BW (2018a) Constraining the age of the Crisium impact basin. Eur Lunar Symp 6:#111
van der Bogert CH, Clark JD, Hiesinger H, Banks ME, Watters TR, Robinson MS (2018b) How old are lunar lobate scarps? 1. Seismic resetting of crater size–frequency distributions. Icarus 306:225–242
Wagner RJ, Head JW, Wolf U, Neukum G (1996) Age relations of geologic units in the Gruithuisen region of the Moon based on crater size–frequency measurements. Lunar Planet Sci 28:1367–1368
Wagner R, Head JW, Wolf U, Neukum G (2002) Stratigraphic sequence and ages of volcanic units in the Gruithuisen region of the Moon. J Geophys Res 107(E11):5104
Wagner R, Head JW, Wolf U, Neukum G (2010) Lunar red spots: Stratigraphic sequence and ages of domes and plains in the Hansteen and Helmet regions on the lunar near-side. J Geophys Res 115:10.1029/2009JE003359
Wang J, Cheng W, Zhou C (2015) A Chang'E-1 global catalog of lunar impact craters. Planet Space Sci 112:42–45

Wänke H, Baddenhausen H, Balacescu A, Teschke F, Spettel B, Dreibus G, Palme H, Quijano-Rico M, Kruse H, Wlotzka F, Begemann F (1972) Multielement analyses of lunar samples and some implications of the results. Proc Lunar Planet Sci Conf 3:1251–1268
Wasserburg GJ, Huneke JC, Papanastassiou DA, Rajan RS, Tera F (1974) A summary of the lunar time scale and implications for the chronology of the Solar System. The Moon 11:408–409
Watson K, Murray BC, Brown H (1961) The behavior of volatiles on the lunar surface. J Geophys Res 66:3033–3045
Watters TR (1991) Origin of periodically spaced wrinkle ridges on the Tharsis Plateau of Mars. J Geophys Res 96:15,599–15,616
Watters TR (2003) Thrust faults along the dichotomy boundary in the eastern hemisphere of Mars. J Geophys Res 108(E4):5054
Watters TR, Johnson CL (2010) Lunar tectonics. *In:* Planetary Tectonics. Watters TR, Schultz RA (eds), New York, Cambridge University Press, p 121–182
Watters TR, Solomon SC, Robinson MS, Head JW, André SL, Hauck SA, Murchie SL (2009) The tectonics of Mercury: The view after MESSENGER's first flyby. Earth Planet Sci Lett 285:283–296
Watters TR, Robinson MS, Beyer RA, Banks ME, Bell JF, Pritchard ME, Hiesinger H, van der Bogert CH, Thomas PC, Turtle E, Williams NR (2010) Evidence of recent thrust faulting on the Moon revealed by the Lunar Reconnaissance Orbiter Camera. Science 329:936–940
Watters TR, Robinson MS, Banks ME, Tran T, Denevi BW (2012) Recent extensional tectonics on the Moon revealed by the Lunar Reconnaissance Orbiter Camera. Nat Geosci 5:181–185
Watters TR, Robinson MS, Collins GC, Banks ME, Daud K, Williams NR, Selvans MM (2015) Global thrust faulting on the Moon and the influence of tidal stresses. Geology 43:851–854
Weitz C, Head JW (1998) Diversity of lunar volcanic eruptions at the Marius Hills complex. Lunar Planet Sci Conf 29:#1229
Weitz C, Head JW (1999) Spectral properties of the Marius Hills volcanic complex and implications for the formation of lunar domes and cones. J Geophys Res 104:18933–18956
Weitz CM, Head JW, Pieters CM (1998) Lunar regional dark mantle deposits: Geologic, multispectral, and modeling studies. J Geophys Res 103:22725–22760
Wentworth SJ, McKay DS, Lindstrom DJ, Basu A, Martinez RR, Bogard DD, Garrison DH (1994) Apollo 12 ropy glasses revisited. Meteoritics Planet Sci 29:323–333
Werner SC (2006) Mayor aspects of the chronostratigraphy and geologic evolutionary history of Mars, PhD Dissertation, Freie Universität Berlin, Germany
Werner SC (2014) Moon, Mars, Mercury: Basin formation ages and implications for the maximum surface age and the migration of gaseous planets. Earth Planet Sci Lett 400:54–65
Werner SC, Ivanov BA (2015) Exogenic dynamics, cratering, and surface ages. Treat Geophys:327–365
Werner SC, Medvedev S (2010) The lunar rayed-crater population—Characteristics of the spatial distribution and ray retention. Earth Planet Sci Lett 295:147–158
Wetherill GW (1981) Nature and origin of basin-forming projectiles. *In:* Multi-Ring Basins. Schultz PH and Merrill RB (eds), Proc Lunar Planet Sci Conf 12:1–18
Whitaker EA (1972) Lunar color boundaries and their relationship to topographic features: A preliminary survey. The Moon 4:348–355
Whitford-Stark JL, Head JW (1977) The Procellarum volcanic complexes: Contrasting styles of volcanism. Proc Lunar Sci Conf 8:2705–2724
Whitford-Stark JL, Head JW (1980) Stratigraphy of Oceanus Procellarum basalts: Sources and styles of emplacement. J Geophys Res 85(B11):6579–6609
Whitford-Stark JL (1979) Charting the southern seas: The evolution of the lunar Mare Australe. Proc Lunar Planet Sci Conf 10:2975–2994
Whitten J, Head JW, Staid M, Pieters CM, Mustard J, Clark R, Taylor L (2011) Lunar mare deposits associated with the Orientale impact basin. New insights into mineralogy, history, mode of emplacement, and relation to Orientale Basin evolution from Moon Mineralogy Mapper (M3) data from Chandrayaan-1. J Geophys Res 116:E00G09
Whitten JL, Head III JW (2015a) Lunar cryptomaria: Physical characteristics, distribution, and implications for ancient volcanism. Icarus 247:150–171
Whitten JL, Head III JW (2015b) Lunar cryptomaria: Mineralogy and composition of ancient volcanic deposits, Planet Space Sci 106:67–81
Wieczorek MA, Phillips RJ (2000) The Procellarum KREEP Terrane: implications for mare volcanism and lunar evolution. J Geophys Res 105:20,417–20,430
Wilhelms DE (1965) Fra Mauro and Cayley Formation in the Mare Vaporum and Julius Cesar quadrangles. Astr. Stud. Ann. Prog. Rep U.S. Geol Survey:13–28
Wilhelms DE, McCauley JF (1971) Geologic map of the near side of the Moon. I-703. U.S. Geol Surv Washington D.C.
Wilhelms DE, John F, Trask NJ (1987) The geologic history of the Moon. U.S. Geol Sur Prof Pap 1348
Williams J-P, van der Bogert CH, Pathare AV, Michael GG, Kirchoff MR, Hiesinger H (2018a) Dating very young planetary surfaces from crater statistics: A review of issues and challenges. Meteoritics 53:554–582

Williams J-P, Bandfield JL, Paige DA, Powell T, Greenhagen BT, Taylor S, Hayne PO, Speyerer EJ, Ghent RR, Costello ES (2018b) Lunar cold spots and crater production on the Moon. J Geophys Res 123:2380–2392
Wilson L, Head JW (2003a) Deep generation of magmatic gas on the Moon and implications for pyroclastic eruptions. Geophys Res Lett 30:1605
Wilson L, Head JW (2003b) Lunar Gruithuisen and Mairan domes: Rheology and mode of emplacement. J Geophys Res 108(E2):5012
Wilson L, Head JW (2016) Explosive volcanism associated with the silicic Compton–Belkovich Volcanic Complex: Implications for magma water content. Lunar planet Sci Conf 47:#1564
Wilson L, Head III JW (2017a) Eruption of magmatic foams on the Moon: Formation in the waning stages of dike emplacement events as an explanation of "irregular mare patches". J Volcan Geotherm Res 335:113–127
Wilson L, Head III JW (2017b) Generation, ascent and eruption of magma on the Moon: New insights into source depths, magma supply, intrusions and effusive/explosive eruptions (Part 1: Theory) Icarus 283:146–175
Wilson L, Head III JW (2018) Controls on lunar basaltic volcanic eruption structure and morphology: Gas release patterns in sequential eruption phases. Geophys Res Lett 45:5852–5859
Wolfe EW, Lucchitta BK, Reed VS, Ulrich GE, Sanchez AG (1975) Geology of the Taurus–Littrow valley floor. Proc Lunar Sci Conf 6:2463–2482
Wood JA, Dickey JS, Marvin UB, Powell BN (1970) Lunar anorthosites and a geophysical model of the Moon. Proc Apollo 11 Sci Conf 965–988
Woronow A (1977) Crater saturation and equilibrium: A Monte Carlo simulation. J Geophys Res 82:2447–2456
Woronow A (1978) A general cratering-history model and its implications for the lunar highlands. Icarus 34:76–88
Woronow A, Strom RG, Gurnis M (1982) Interpreting the cratering record—Mercury to Ganymede and Callisto. *In:* Satellites of Jupiter Vol. 1 U Arizona Press, p 237–276
Wu B, Huang J, Li Y, Wang Y, Peng J (2018) Rock abundance and crater density in the candidate Chang'e-5 landing region on the Moon. J Geophys Res 123:3256–3272
Wünnemann K, Marchi S, Nowka D, Michel P (2012) The effect of target properties on impact crater scaling and the lunar crater chronology. Lunar Planet Sci Conf 43:#1805
Xiao Z, Werner SC (2015) Size-frequency distribution of crater populations in equilibrium on the Moon. J Geophys Res 120:2277–2292
Xie M, Zhu M-H, Xiao Z, Wu Y, Xu A (2017) Effects of topography degradation on crater size–frequency distributions: Implications for populations of small craters and age dating. Geophys Res Lett 44:10171–10179
Xie M, Xiao Z, Xu A (2019) Time-dependent production functions of lunar simple craters on layered targets with consideration of topographic degradation. Geophys Res Lett 46:10987–10996
Yasui M, Matsumoto E, Arakawa M (2015) Experimental study on impact-induced seismic wave propagation through granular materials. Icarus 260:320–331
York D, Kenyon WJ, Doyle RJ (1972) ^{40}Ar–^{39}Ar ages of Apollo 14 and 15 samples. Proc Lunar Planet Sci Conf 3:1613–1622
Young RA (1975) Mare crater size–frequency distributions: Implications for relative surface ages and regolith development. Proc Lunar Sci Conf 6:2645–2662
Yue Z, Michael GG, Di K, Liu J (2017) Global survey of lunar wrinkle ridge formation times. Earth Planet Sci Lett 477:14–20
Zhao J-N, Huang J, Xiao L, Qiao L, Wang J, Hu S-Y (2013) Crater size–frequency distribution measurements and age determination of Sinus Iridum. Earth Sci J China Univ Geosci 38:351–361
Zhao J, Xiao L, Qiao L, Glotch TD, Huang Q (2017) The Mons Rümker volcanic complex of the Moon: A candidate landing site for the Chang'E-5 mission. J Geophys Res 122:1419–1442
Ziethe R, Seiferlein K, Hiesinger H (2009) Duration and extent of lunar volcanism: Comparison of 3D convection models to mare basalt ages. Planet Space Sci 57:784–796
Zuber MT, Head JW, Smith DE, Neumann GA, Mazarico E, Torrence MH, Aharonson O, Tye AR, Fassett CI, Rosenburg MA, Melosh HJ (2012) Constraints on the volatile distribution within Shackleton crater at the lunar south pole. Nature 486:378–382
Zuber MT, Smith DE, Watkins MM, Asmar SW, Konopliv AS, Lemoine FG, Melosh HJ, Neumann GA, Phillips RJ, Solomon SC, Wieczorek MA, Williams JG, Goossens SJ, Kruizinga G, Mazarico E, Park RS, Yuan D-N (2013) Gravity field of the Moon from the Gravity Recovery and Interior Laboratory (GRAIL) mission. Science 339:668–671